NUREG/IA-0100

International Agreement Report

Assessment of CCFL Model of RELAP5/MOD3 Against Simple Vertical Tubes and Rod Bundle Tests

Prepared by
S. Cho, N. Arne, Korea Electric Power Corporation, Research Center
B. D. Chung, H. J. Kim, Korea Institute of Nuclear Safety

Korea Electric Power Corporation, Research Center
117-15 Yongjeon-Dong
Dong-Gu
Taejon, Korea

Korea Institute of Nuclear Safety
P.O. Box 16
Daeduk-Danji
Taejon, Korea 305-353

Office of Nuclear Regulatory Research
U.S. Nuclear Regulatory Commission
Washington, DC 20555

June 1993

Prepared as part of
The Agreement on Research Participation and Technical Exchange
under the International Thermal-Hydraulic Code Assessment
and Application Program (ICAP)

Published by
U.S. Nuclear Regulatory Commission

NOTICE

This report was prepared under an international cooperative agreement for the exchange of technical information. Neither the United States Government nor any agency thereof, or any of their employees, makes any warranty, expressed or implied, or assumes any legal liability or responsibility for any third party's use, or the results of such use, of any information, apparatus product or process disclosed in this report, or represents that its use by such third party would not infringe privately owned rights.

Available from

Superintendent of Documents
U.S. Government Printing Office
P.O. Box 37082
Washington, D.C. 20013-7082

and

National Technical Information Service
Springfield, VA 22161

NUREG/IA-0100

International Agreement Report

Assessment of CCFL Model of RELAP5/MOD3 Against Simple Vertical Tubes and Rod Bundle Tests

Prepared by
S. Cho, N. Arne, Korea Electric Power Corporation, Research Center
B. D. Chung, H. J. Kim, Korea Institute of Nuclear Safety

Korea Electric Power Corporation, Research Center
117-15 Yongjeon-Dong
Dong-Gu
Taejon, Korea

Korea Institute of Nuclear Safety
P.O. Box 16
Daeduk-Danji
Taejon, Korea 305-353

Office of Nuclear Regulatory Research
U.S. Nuclear Regulatory Commission
Washington, DC 20555

June 1993

Prepared as part of
The Agreement on Research Participation and Technical Exchange
under the International Thermal-Hydraulic Code Assessment
and Application Program (ICAP)

Published by
U.S. Nuclear Regulatory Commission

NOTICE

This report is based on work performed under the sponsorship of The Korea Advanced Energy Institute of Korea. The information in this report has been provided to the USNRC under the terms of an information exchange agreement between the United States and Korea (Agreement on Thermal-Hydraulic Research between the United States Nuclear Regulatory Commission and The Korea Advanced Energy Research Institute, May 1, 1986). Korea has consented to the publication of this report as a USNRC document in order that it may receive the widest possible circulation among the reactor safety community. Neither the United States Government nor Korea or any agency thereof, or any of their employees, makes any warranty, expressed or implied, or assumes any legal liability of responsibility for any third party's use, or the results of such use, or any information, apparatus, product or process disclosed in this report or represents that its use by such third party would not infringe privately owned rights.

Assessment of CCFL Model of RELAP5/MOD3 Against Simple Vertical Tubes and Rod Bundle Tests

Sungjae Cho and Namsung Arne
Korea Electric Power Corporation, Research Center
117-15 Yongjeon-Dong, Dong-Gu, Taejon, Korea,

Bub Dong Chung and Hho Jung Kim
Korea Institute of Nuclear Safety
P.O.Box 16, Daeduk-Danji,Taejon, Korea, 305-353

Abstract

The CCFL model used in RELAP5/MOD3 version 5m5 has been assessed against simple vertical tubes and rod bundle tests performed at a facility of Korea Atomic Energy Research Institute.

The effect of changes in tube diameter and nodalization of tube section were investigated. The roles of interfacial drags on the flooding characteristics are discussed. Differences between the calculation and the experiment are also discussed.

A comparison between model assessment results and the test data showed that the calculated value lay well on the experimental flooding curve specified by user, but the pressure jump before onset of flooding was not calculated.

Acknowledgement

We are grateful to Dr. Sang-Hoon Lee, the president of the Korea Institute of Nuclear Safety, for organizing the project. We would like to express our special appreciation to Dr. Jong-Hee Cha and Soon-yun Won for their help in constructing the test facility and for kind advice during the experiment.

Nomenclatures

ρ_f= Density of Liquid

ρ_g= Density of Gas

μ_f= Dynamic Viscosity of Liquid

μ_g= Dynamic Viscosity of Gas

σ = Surface Tension of Liquid

g = Universal Acceleration Constant

D_H= Equivalent Hydraulic Diameter = 4A/P

D^*= Nondimensional Diameter = $D_H/[\sigma/\{g(\rho_f-\rho_g)\}]^{1/2}$

K_g^* = Kutateladze Number of Gas Flux = $\rho_g^{0.5}\alpha_g V_g/[g\sigma(\rho_f-\rho_g)]^{0.25}$

K_f^* = Kutateladze Number of Liquid = $\rho_f^{0.5}\alpha_f V_f/[g\sigma(\rho_f-\rho_g)]^{0.25}$

j_g^* = Nondimensional Gas Flux = $\rho_g\alpha_g V_g/[gD_H(\rho_f-\rho_g)]^{0.5}$

j_f^* = Nondimensional Liquid Flux = $\rho_f\alpha_f V_f/[gD_H(\rho_f-\rho_g)]^{0.5}$

P^* = Nondimensional Pressure Gradient = $|dP/dz|/[g(\rho_f-\rho_g)]$

Re_Γ = Film Reynolds Number = $4\Gamma/\mu_f$ where Γ denotes film mass flowrate per unit width

Contents

Abstract ---------- iii
Acknowledgement ---------- v
Nomenclature ---------- vii
List of Tables ---------- x
List of Figures ---------- xi
1. Introduction ---------- 1
2. Sample Problem and Description of Test Facility ---------- 2
2.1 Sample Problems ---------- 2
2.2 Rod Bundle Tests ---------- 3
3. Code and Input Model Description ---------- 8
3.1 The Code Features ---------- 8
3.2 The Calculation Input Model ---------- 9
4. The Base Case Calculation ---------- 17
4.1 Simple Vertical Tubes ---------- 17
4.2 Rod Bundle Tests ---------- 19
5. Sensitivity Results and Discussion ---------- 41
5.1 Tube Diameter ---------- 41
5.2 Nodalization ---------- 44
6. Run Statistics ---------- 63
7. Conclusion ---------- 64
References ---------- 66
Appendices
A. Experimental Data for Rod Bundle CCFL Test ---------- A.1
B. Input Decks for Calculations ---------- B.1

List of Tables

Table 5.1 Test Cases for the simple vertical tubes ---------- 41
Table 6.1 CPU time required in the simulation ---------- 63

List of Figures

Fig. 2.1 Schematic Diagram of Air-Water Counter-current Flooding Test Loop with 3x3 Tube Bundle ---------- 6
Fig. 2.2 Three Type of 3x3 Tube Bundle Test Section ---------- 7
Fig. 3.1 RELAP5 Nodalization for Air/Water Test Problem -------- 13
Fig. 3.2 RELAP5 Nodalization for Type-1 Test Bundle ---------- 14
Fig. 3.3 RELAP5 Nodalization for Type-2 Test Bundle ---------- 15
Fig. 3.4 RELAP5 Nodalization for Type-3 Test Bundle ---------- 16
Fig. 4.1 Air Inlet Flowrate at the Junction 4000000 ---------- 24
Fig. 4.2 Downward Liquid Flowrate at Junction 4000000 ---------- 24
Fig. 4.3 Flow Regime Change at the Test Section Junction ------- 25
Fig. 4.4 Gas Void Fraction at the Test Section Junction -------- 25
Fig. 4.5 Interfacial Drag Coefficient at the Test Section Junction - 26
Fig. 4.6 Pressure Drop in the Test Section ---------- 26
Fig. 4.7 Mass Flux through the Junction 4000000 ---------- 27
Fig. 4.8 Calculated Flooding Data at the Junction 4000000 -------- 27
Fig. 4.9 Air Inlet Flowrate at the Junction 4000000 ---------- 28
Fig. 4.10 Downward Liquid Flowrate at Junction 4000000 ---------- 28
Fig. 4.11 Flow Regime Change at the Test Section Junction ------- 29
Fig. 4.12 Gas Void Fraction at the Test Section Junction -------- 29
Fig. 4.13 Interfacial Drag Coefficient at the Test Section Junction - 30
Fig. 4.14 Pressure Drop in the Test Section ---------- 30
Fig. 4.15 Mass Flux through the Junction 4000000 ---------- 31
Fig. 4.16 Calculated Flooding Data at the Junction 4000000 -------- 31
Fig. 4.17 Air Inlet Flowrate at the Junction 4000000 ---------- 32
Fig. 4.18 Downward Liquid Flowrate at Junction 4000000 ---------- 32
Fig. 4.19 Calculated Flooding Data at the Junction 4000000 ------ 33
Fig. 4.20 Pressure Drop in the Test Section ---------- 33
Fig. 4.21 Flow Regime Change at the Test Section Junction ------- 34
Fig. 4.22 Gas Void Fraction at the Test Section Junction -------- 34
Fig. 4.23 Interfacial Drag Coefficient at the Test Section Junction - 35

Fig. 4.24 Air Inlet Flowrate at the Junction 4000000 ---------- 35
Fig. 4.25 Downward Liquid Flowrate at Junction 4000000 --------- 36
Fig. 4.26 Calculated Flooding Data at the Junction 4000000 ------- 36
Fig. 4.27 Pressure Drop in the Test Section ---------- 37
Fig. 4.28 Flow Regime Change at the Test Section Junction ------ 37
Fig. 4.29 Gas Void Fraction at the Test Section Junction --------- 38
Fig. 4.30 Interfacial Drag Coefficient at the Test Section Junction -38
Fig. 4.31 Calculated Flooding Data at the Junction 3030000 ------- 39
Fig. 4.32 Pressure Drop in the Test Section ---------- 39
Fig. 4.33 Calculated Flooding Data at the Junction 3010000 ------- 40
Fig. 4.34 Pressure Drop in the Test Section ---------- 40
Fig. 5.1 Calculated Flooding Data without CCFL option (D = 0.5 cm)
Fig. 5.2 Pressure Drop in the Test Section (D = 0.5 cm) ------ 45
Fig. 5.3 Calculated Flooding Data with CCFL option (D = 0.5cm) - 46
Fig. 5.4 Pressure Drop in the Test Section (D = 0.5 cm) ------ 46
Fig. 5.5 Calculated Flooding Data with CCFL option (D = 1.0cm) - 47
Fig. 5.6 Pressure Drop in the Test Section (D = 1.0 cm) ------ 47
Fig. 5.7 Calculated Flooding Data with CCFL option (D = 1.0cm) - 48
Fig. 5.8 Pressure Drop in the Test Section (D = 1.0 cm) ------ 48
Fig. 5.9 Calculated Flooding Data without CCFL option (D=3.0cm) 49
Fig. 5.10 Pressure Drop in the Test Section (D = 3.0 cm) ------ 49
Fig. 5.11 Calculated Flooding Data with CCFL option (D = 3.0cm) - 50
Fig. 5.12 Pressure Drop in the Test Section (D = 3.0 cm) ------ 50
Fig. 5.13 Calculated Flooding Data without CCFL option (D=5.0cm) 51
Fig. 5.14 Pressure Drop in the Test Section (D = 5.0 cm) ------ 51
Fig. 5.15 Calculated Flooding Data with CCFL option (D = 5.0cm) - 52
Fig. 5.16 Pressure Drop in the Test Section (D = 5.0 cm) ------ 52
Fig. 5.17 Calculated Flooding Data without CCFL option (D=10.cm) 53
Fig. 5.18 Pressure Drop in the Test Section (D = 10. cm) ------ 53
Fig. 5.19 Calculated Flooding Data with CCFL option (D = 10.cm) - 54
Fig. 5.20 Pressure Drop in the Test Section (D = 10. cm) ------ 54
Fig. 5.21 RELAP5 Fine Nodaiization for Air/Water Test Probiem --- 55

Fig. 5.22 RELAP5 Fine Nodalization for Type-1 Test Bundle ----- 56
Fig. 5.23 Calculated Flooding Data with Fine Nodalization ------- 57
Fig. 5.24 Pressure Drop with Fine Nodalization ---------- 57
Fig. 5.25 Flow Regime Change at the Test Section Junction ----- 58
Fig. 5.26 Interfacial Drag Coefficient at the Test Section Junction 58
Fig. 5.27 Gas Void Fraction at the Test Section Junction ------- 59
Fig. 5.28 Mass Flux through the junction 4000000 ---------- 59
Fig. 5.29 Calculated Flooding Data with Fine Nodalization ------- 60
Fig. 5.30 Pressure Drop with Fine Nodalization ---------- 60
Fig. 5.31 Flow Regime Change at the Test Section Junction ----- 61
Fig. 5.32 Interfacial Drag Coefficient at the Test Section Junction61
Fig. 5.33 Gas Void Fraction at the Test Section Junction ------- 62

1. Introduction

RELAP5/MOD2 [1] is an advanced computer code developed at the Idaho National Engineering Laboratory (INEL) for thermal-hydraulic analyses of Pressurized Water Reactor (PWR) system transients. It was produced by improving and extending the modeling base that had been established with the release of RELAP5/MOD1 [2] in December 1980, and was released as a 'frozen' code in April 1985. Numerous assessments have been carried out worldwide under the International Code Assessment and Application Program (ICAP), and a number of deficiencies in the code [3] have been identified. Evaluation of these deficiencies and their regulatory significance was providing the basis for improvements for a new version of RELAP5, namely RELAP5/MOD3. The RELAP5/MOD3 code was frozen at version 5m5 and released in May 1990. The code improvements were made in many areas including a CCFL model [4] and a new interphase drag model [5].

In the present study the CCFL model of RELAP5/MOD3/5m5 is assessed against a simple tube as a sample problem. It is also assessed against the rod bundle tests which were carried out in a test facility at the Korea Atomic Energy Research Institute (KAERI) to check interactions between the CCFL model and interphase drag model under countercurrent condition in rod bundle.

Descriptions of sample problems and test facility are provided in Chapter 2. A description of code and input model is given in Chapter 3. Various assessments against the sample problems and rod bundle tests are provided in Chapter 4. Sensitivity studies including fine nodalization model and RELAP5/MOD2 calculation are discussed in Chapter 5. Run statistics are given in Chapter 6. General conclusions are drawn in Chapter 7.

Appendix A contains the time averaged data for the rod bundle CCFL experiments at KAERI. Appendix B contains the complete set of input lists.

2. Sample Problems and Description of Test Facility

The phenomenon of Counter Current Flow Limitation (CCFL) has been extensively studied experimentally. Considering the geometries and layouts of the nuclear reactor, there could be some different CCFL conditions which need careful examinations to identify the limiting condition. They are at steam generator tubes, at the portion of the hot legs, at annulus of the vessel downcomer, at the upper tie plate of core and the fuel bundle. Most of experimental works have been performed in simple tubes using air/water flow, thus simple tube tests were selected as sample problems. The rod bundle CCFL tests have been completed by Korea Institute of Nuclear Safety (KINS) under contract to Korea Electric Power Co. (KEPCO) at the end of 1989. The tests were also selected as assessment tests to check the CCFL model and interphase drag model under countercurrent flow condition in rod bundles.

2.1 Sample Problems

An extensive experiment was performed by Wallis and Makkenchery [6] with various diameter pipes. In the experiments the liquid was drained into the the test tube with various liquid entry design and the air was introduced by a surge tank into the test tube. The experimental results can be correlated by the well known Wallis correlation.

$$j_g^{*\,1/2} + m\, j_f^{*\,1/2} = C \qquad (2.1)$$

The experimental constant varied due to the channel inlet shape, length or viscosity effect. For most cases, m has a value between 0.8 to 1.0 and C ranges from 0.7 to 1.0. Simple vertical tubes were chosen as sample problems to assess the RELAP5 model.

The inside diameter of tube is varied from 0.5 cm to 10 cm to check applicability of RELAP5 CCFL model.

2.2 Rod Bundle Tests

The rod bundle CCFL tests have been completed by Korea Institute of Nuclear Safety (KINS) under contract to Korea Electric Power Co. (KEPCO) at the end of 1989. The tests were also selected as assessment tests to check the CCFL model and interphase drag model under countercurrent flow condition in rod bundles.

The test were performed using air and water flow under the atmospheric pressure condition. The test facility consists of test section, water and air supply system, associated sensors and devices to measure flowrates of water and air, differential pressure, water levels, and data recording systems as shown in Fig. 2.1.

The major components of the test section, as shown in Fig.2.2, are (1) a lower plenum, (2) 4x4 cm square channel (145 cm in height) made of transparent lucite to allow visual observations, and (3) an upper plenum. The lower plenum has two inlets, one for water and the other for air. The two inlets are designed in such a way that direct interaction between the incoming air and water and the effects of entrance and entrainment at the inlet can be avoided. The 3x3 stainless steel tube bundle is placed vertically at the center of the lucite square channel. The tube array has the same geometrical dimensions of the typical 17x17 PWR fuel bundle. The outside diameter of each tube and pitch are 0.95 cm and 1.26 cm, respectively.

In order to obtain experimental data on the effects of spacer grids and multi-channel flow interactions on the CCFL, three tube-bundle types were used as shown in Fig.2.2 : The first type

is a 3x3 tube bundle with no spacer grid, the second type is a 3x3 tube bundle with one spacer grid attached at 68.3 cm axially from the top (at "B" in Fig.2.2), and the third type is a 3x3 tube bundle with two spacer grids attached at 17.5 cm and 68.3 cm from the top respectively. For convenience in discussion, these bundles are designated here as type-1 (no spacer-grid), type-2 (one-spacer grid), and type-3 (two spacer grids), respectively.

The grid assembly consists of individual slotted straps interlocked and brazed in an egg-crate arrangement to join the straps permanently. The test section was equipped with two pressure taps. An air-water separator for measuring the entrainment rate and two water level gauges for measuring the film downflow and entrainment rates were also provided.

The water is first introduced into the inlet located at the bottom of the lower plenum, then it rises up to the top of the tube bundle flowing inside of each tube. The water flowing out of the nine tubes at the top (point "A" in Fig.2.2) is then directed, via a nozzle, to flow in reverse direction downward by gravity over the outer surface of the 9-tubes forming a continuous annular water film. The nozzle is placed 30 cm above the top inlet (point "B" in Fig.2.2) of the test channel to form a fully developed flow. The more detailed description for the test facility is given in Reference [7] and [8].

The flooding data were obtained by varying the air flow rate while the water flow rate was fixed. Major quantities measured for each test were (1) liquid penetration rate, (2) liquid carry-over rate, (3) air inlet flow rate, and (4) test channel pressure drop. Actually, to obtain a single CCFL data point with a given test bundle, from 9 to 19 runs were made increasing the air velocity in step until the downward water film flow rate becomes zero (i.e., the zero penetration rate of water) while maintaining a constant water input rate. Although most of data have oscillatory behavior, the time averaged value during 100 seconds

are given in Appendix A. The measurement uncertainties consists of the error of pressure sensor, A/D (Analog to Digital) conversion error, and calibration error. The calculated error of channel pressure drop is about 5 mm H_2O. The estimated error for air flow measurement is about 650 cc/sec and for water flow it is about 1.7 % of liquid injection flow.

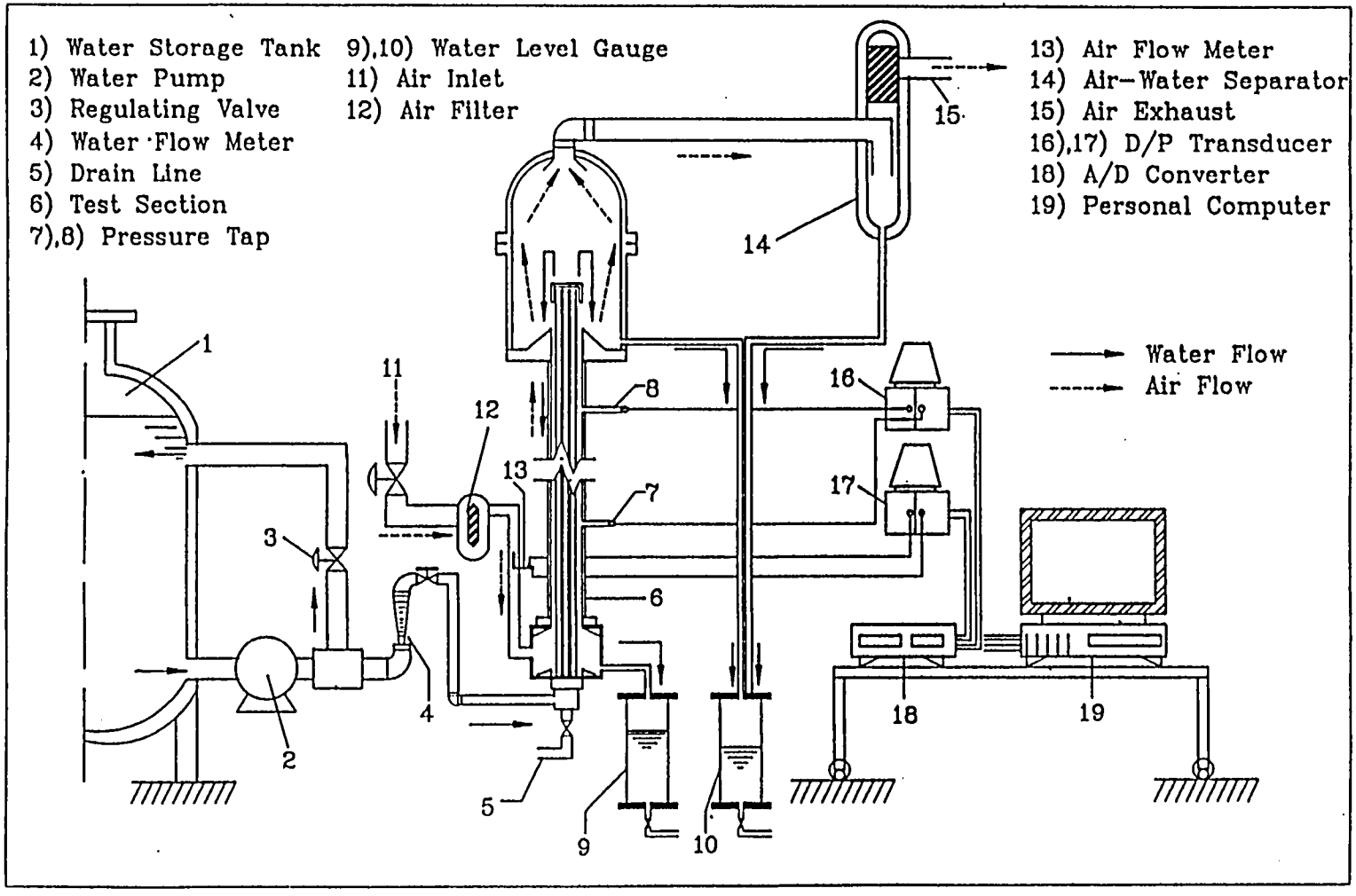

Fig. 2.1 Schematic Diagram of Air-Water Counter-current Flooding Test Loop with 3x3 Tube Bundle

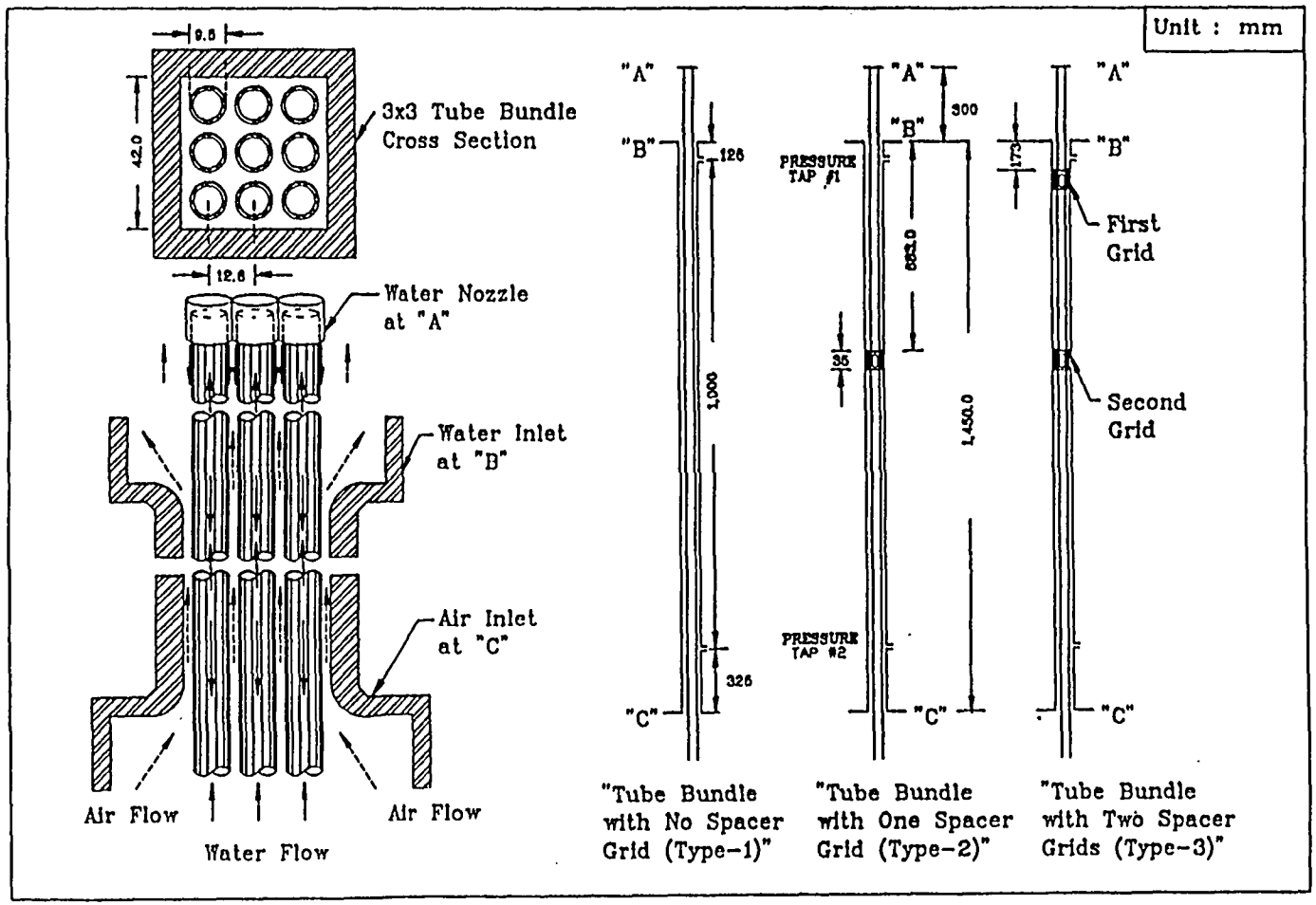

Fig. 2.2 Three Type of 3x3 Tube Bundle Test Section

3. Code and Input Model Description

The assessment calculation for sample problems and rod bundle CCFL experiment was done using RELAP5/MOD3/5m5, code received at the beginning of May 1990. The descriptive document available for this code at the time of preparing this report are scheduled to be released later. However document of a CCFL model and a new interphase drag model tested in this assessment are available in reference [4] and [5].

3.1 Code Model Description

A general CCFL model, which was proposed by Bankoff [9], was implemented in the 5m5 version of RELAP5/MOD3 that allows the user to select the Wallis form, the Kutateladze form, or a form in between Wallis and Kutateladze forms. The general form using dimensionless flux is given by :

$$H_g^{1/2} + m\, H_f^{1/2} = C \qquad (3.1)$$

$$H_g = \alpha_g V_g [\rho_g / g w (\rho_f - \rho_g)]^{1/2}$$

$$H_f = \alpha_f V_f [\rho_f / g w (\rho_f - \rho_g)]^{1/2}$$

where

$$w = D_j^{1-\beta} l^{\beta}$$

$$l = [\sigma / g(\rho_f - \rho_g)]^{1/2}$$

In the above equation, β can be a number from 0 to 1. For β=0, the Wallis form of CCFL equation is obtained, and for β=1, the Kutateladze form of CCFL equation is obtained. The user should make a decision for the input values of m,C,and β using the appropriate experimental results.

With regard to the solution method, if the CCFL model is

requested by the user, the coding checks if counter current flow exits and if the liquid downflow exceeds the limit imposed by eq.(2.2). If this is true, the sum momentum equation and flooding equation (2.2) are applied as the phasic momentum equations. Thus the difference equation, which contains the interfacial friction, is replaced with flooding limit equation (2.2).

Although the RELAP5/MOD3 has a user controlled junction flooding model for flooding at a singularity in the channel geometry, the counter current flow is much related to interfacial drag model. As a part of UK's contribution to the code improvement, the interfacial friction model suggested by CEGB [5] was implemented in a released version of RELAP5/MOD3. The new interfacial friction model was developed for the vertical bubbly and slug flow regimes, and a CCFL correlation appropriate for a straight uniform flow channel was also adopted for the calculation of drift flux used for interfacial friction models.

3.2 The Calculation Input Model

3.2.1 The Sample Problems

The sample problems used in the present calculation is closely related to the test facilities used in many previous experiment for a vertical single tube. The specific nodalization is given by Fig.3.1.

Most experiments were performed using air and water. The water was drained into the test section from the top plenum, forming downward film flow. Air was introduced by a surge tank, flowing up into the test tube. The liquid inlet was modeled as a time dependent junction to specify the constant liquid injection. The air inlet junction from a surge tank was modeled as single junction with a smooth option to avoid the inlet contraction

effect of phasic momentum equation. However, Most experimental data show that the flooding occurs at the air inlet junction due to its geometric singularity, and thus the CCFL option was used at the air inlet junction (JUN-4000000). The air inlet flow was modeled as a time dependent junction. For most experiments the experimental data have oscillatory behavior during the flooding process, and thus the flooding data are presented as the time averaged value during a test period for a given air and liquid injection flow. A steady state calculation for a given air and liquid injection flow will be very time consuming work because there are many different flooding points. Therefore as test sample problems, the liquid flow was fixed and the air flow was increased slowly until the flooding is completed. After some trial and error calculations, we find a 200 second duration is enough to neglect the transient effect of increasing air flow.

For sample problems, the code input of the flooding curve was specified as follows ; the simple Wallis form.

$$j_g^{*1/2} + j_f^{*1/2} = 1 \qquad (3.2)$$

In view of the geometries and layout of nuclear reactor, the specific flooding location for a single tube may be steam generator U-tubes. A typical inside diameter of the PWR tubes is about 1.7 cm. Thus a flooding test in 2 cm diameter tubes was selected as a base test case, and calculations for 5 different tube diameters (0.5 cm, 1 cm, 3 cm, 5 cm, and 10 cm) have been performed as sensitivity studies. The results were discussed in Section 5.1.

The test section pipe was modeled as 6 uniform volumes and liquid drain tank was modeled as a relatively large single volume.

In order to compare calculated values with flooding curves specified by user, the liquid velocity and air velocity at the specific junction were converted to nondimensional gas flux using

junction void fraction and velocity as "control variables" as shown below ;

$$j_g^* = \rho_g^{1/2}\alpha_g V_g/[gD(\rho_f-\rho_g)]^{1/2} \cong 0.0112\ D^{-1/2}\alpha_{gj}V_{gj} \qquad (3.3)$$
$$j_f^* = \rho_f^{1/2}\ \alpha_f V_f/[gD(\rho_f-\rho_g)]^{1/2} \cong 0.3195\ D^{-1/2}\alpha_{fj}V_{fj}$$

The physical properties of each phase were calculated at the experimental condition : 1 atm and 280 K.

3.2.2 Rod Bundle Tests

The specific nodalization and modeling were much similar to the sample problems as shown in Fig. 3.2. But the rod bundle form of the new interfacial friction model was activated by specifying the third flag (b) of an extended volume control flag, bfe, to be unity in the pipe volume of test section. The model geometry and elevation were related to the test facilities described in section 2.2. In the rod bundle CCFL experiment, three test bundles were used, and it was found experimentally that the flooding location is "air inlet" for type-1 test, "spacer grid" for type-2 test, and "first spacer grid" for type-3 test. Therefore three different locations for CCFL junction were examined as shown in Fig. 3.2, 3.3, and 3.4 corresponding to each type of test section.

For moderate high liquid flux, the experimental flooding curves of Kutateladze form are as follows;

$$K_g^{*\ 1/2} + K_f^{*\ 1/2} = D^{*\ 1/4}(\ = 1.44) \quad \text{for type-1} \qquad (3.4)$$
$$K_g^{*\ 1/2} + K_f^{*\ 1/2} = 1.38 \quad \text{for type-2}$$
$$K_g^{*\ 1/2} + K_f^{*\ 1/2} = 1.23 \quad \text{for type-3}$$

Therefore the code input value for flooding curve was specified

as above equations (Eq.3.4) for each type of tests.

In order to compare the calculated values with flooding curves specified by user, the liquid velocity and air velocity at the specific junction were converted to nondimensional gas flux using junction void fraction and velocity as "control variables" as shown below;

$$K_g^* = \rho_g^{1/2}\alpha_g V_g/[g\sigma(\rho_f-\rho_g)]^{1/4} \cong 0.214\ \alpha_{gj}V_{gj} \qquad (3.5)$$

$$K_f^* = \rho_f^{1/2}\ \alpha_f V_f/[g\sigma(\rho_f-\rho_g)]^{1/4} \cong 6.1\ \ \alpha_{fj}V_{fj}$$

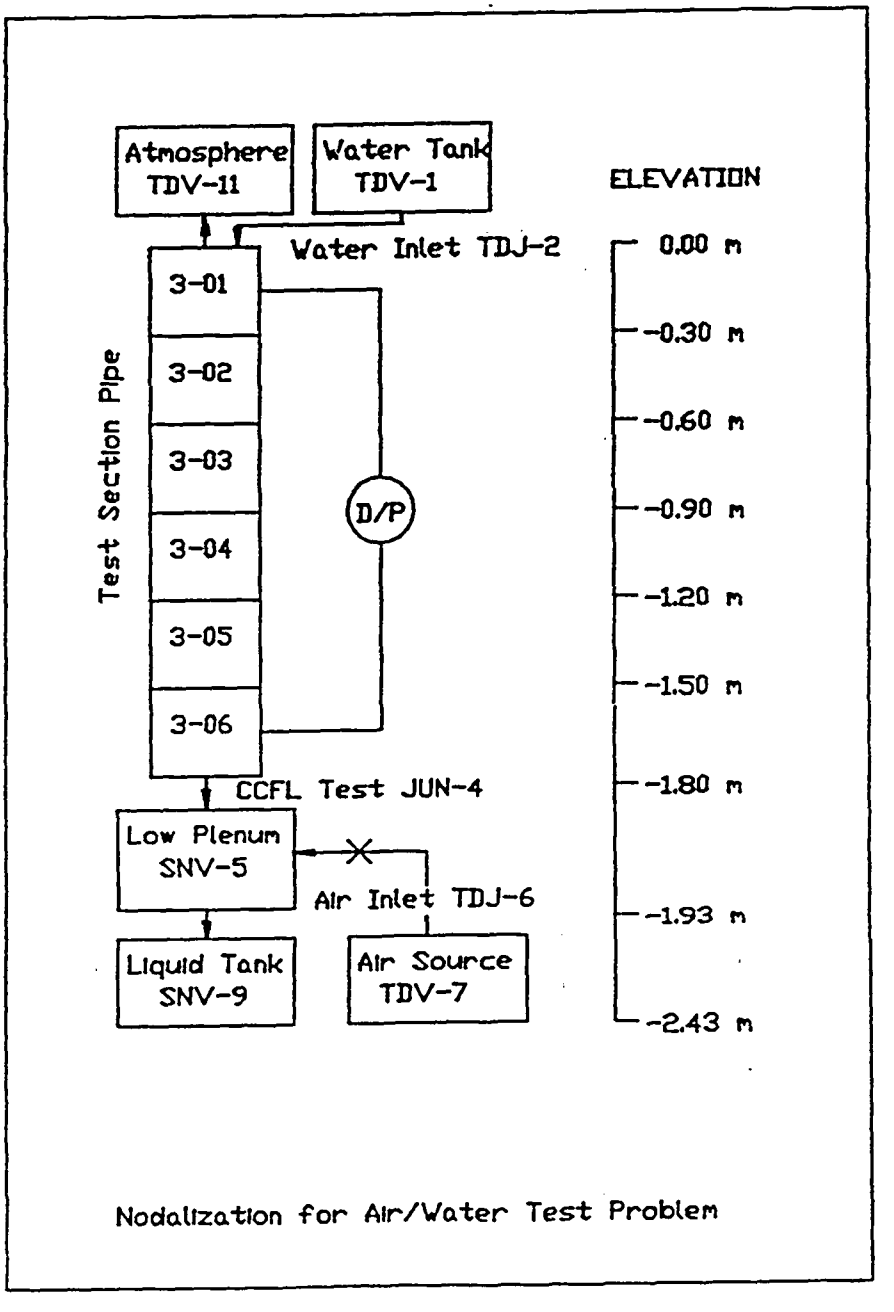

Fig. 3.1 RELAP5 Nodalization for Air/Water Test Problem

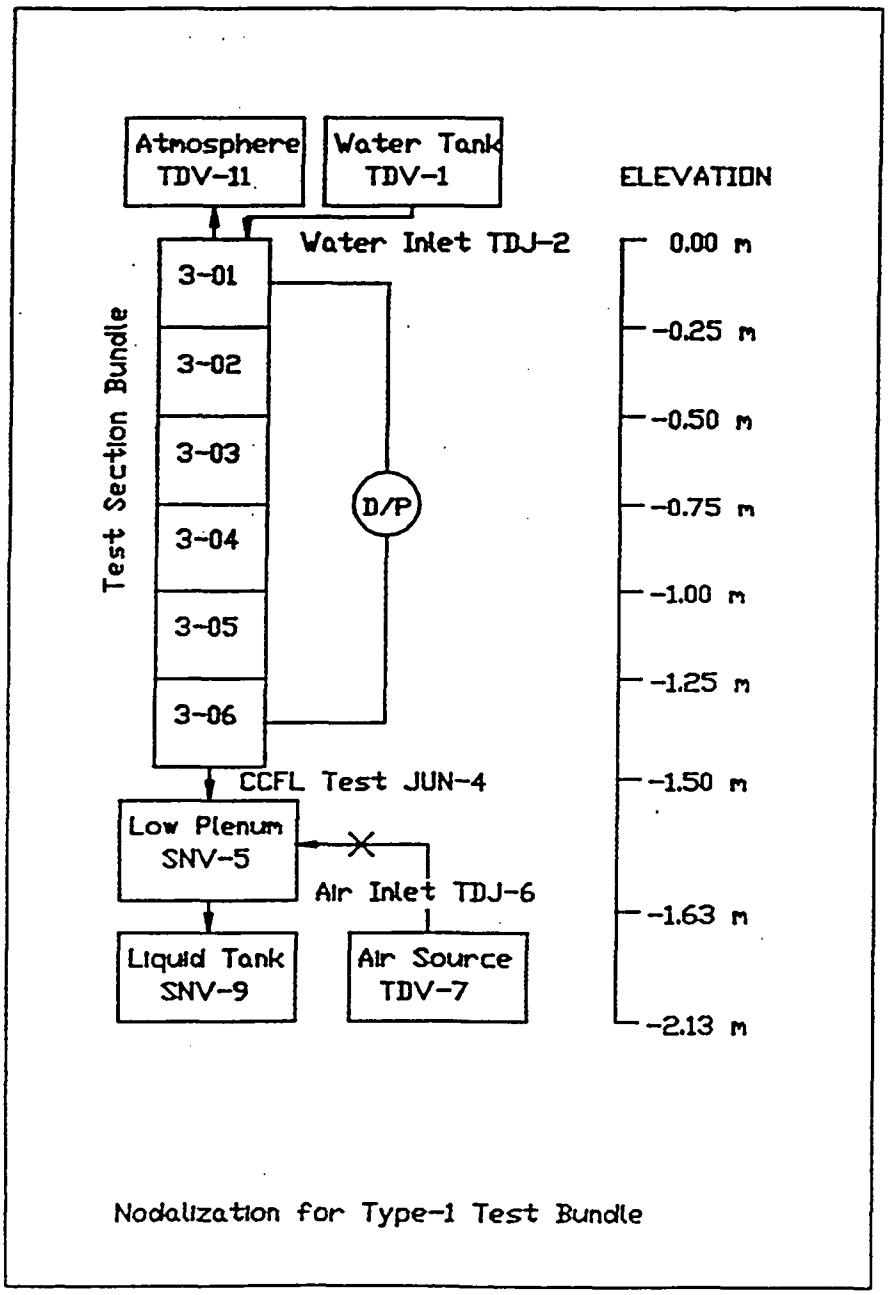

Fig. 3.2 RELAP5 Nodalization for Type-1 Test Bundle

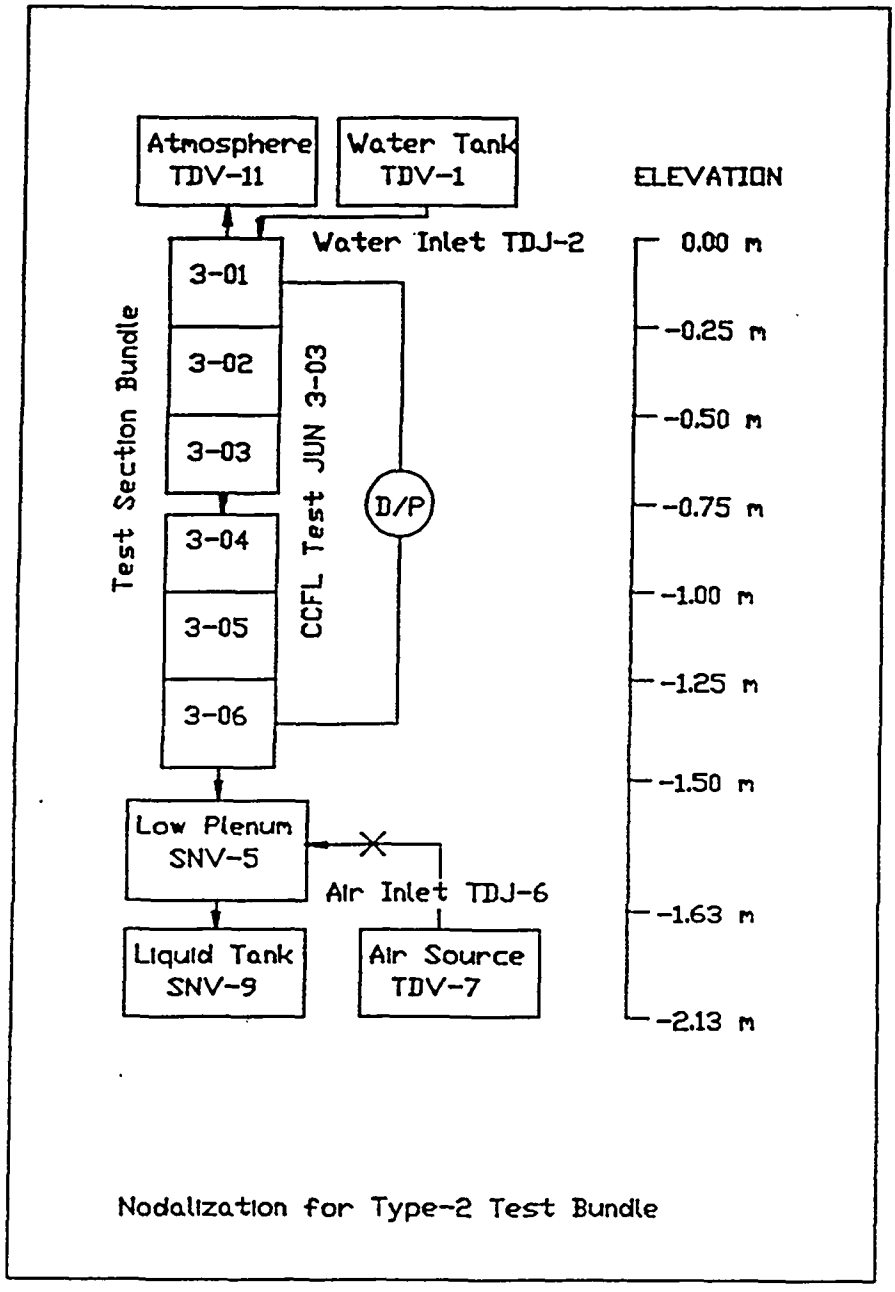

Fig. 3.3 RELAP5 Nodalization for Type-2 Test Bundle

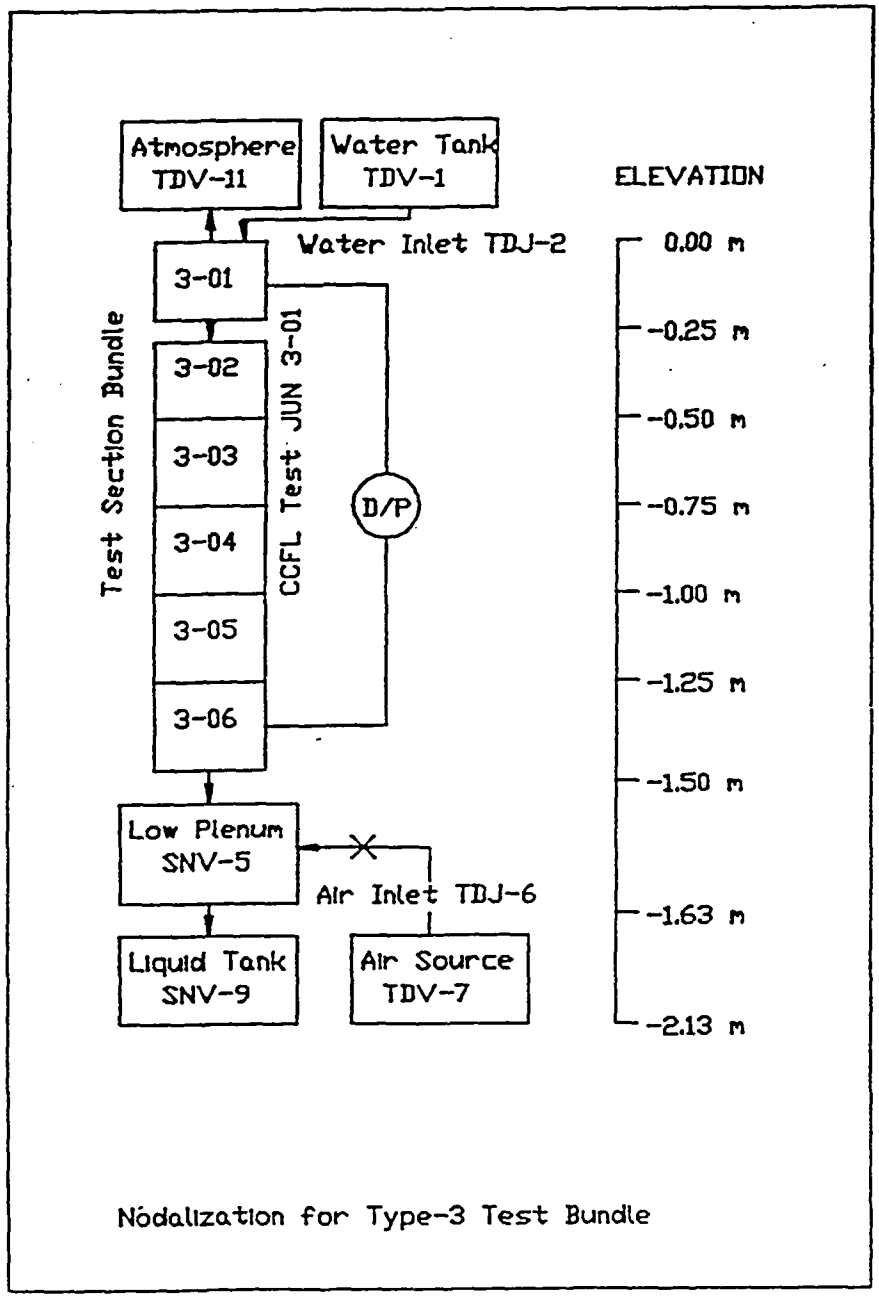

Fig. 3.4 RELAP5 Nodalization for Type-3 Test Bundle

4. The Base Case Calculation

4.1 Simple Vertical Tubes

As discussed in section 3.2.1, the air/water countercurrent flow in a tube of 2 cm inside diameter was simulated with RELAP5/MOD3/5m5. Two calculations were performed with and without a CCFL junction option. Two results were compared in terms of air inlet flow and liquid downward flow at a CCFL junction, flooding curve, total mass flux, gas void fraction, flow regime, interfacial friction,and pressure drop in the test section. The time step size was fixed as 0.01 second during the whole transient. If the time step size became larger than 0.01 seconds, it was experienced that the calculation was unstable or failed in some cases.

Fig. 4.1 shows the gas flowrate at junction 4000000 with no CCFL option. The negative value means the upward direction as shown in Fig. 3.1. The gas flow was increased slowly during 200 seconds until the flooding was completed. During the first 10 seconds, the steady state calculation was performed to get the fully developed free falling annular film flow at zero air inlet flow. Although the air inlet flow through junction 6000000 was set to increase monotonously, the air flow into the test section through junction 4000000 had a little fluctuation at the start of restriction of liquid down flow (~ 120 sec.) and at the end of the flooding (~ 170 sec.). Fig 4.2 shows the restriction of the downward liquid flow. This restriction comes from the increase of the interfacial drag as air flow increases. As shown in Fig.4.3, the junction flow regime is annular-mist(regime 6) over the whole flooding range and becomes dispersed flow regime (regime 7) as the gas void fraction becomes nearly to unity (> 0.9999). The gas void fraction is shown in Fig.4.4. As shown in Fig.4.4 the liquid film thickness increase with increasing air flow, and then

decrease after the flooding occurs. The liquid sweep from the bottom to top section was calculated. The trends of the interfacial friction, shown in Fig. 4.5, has the same trends of liquid void fraction, because the interfacial friction factor, which is described by a Bharathan correlation [10], increases with increasing film thickness. The channel pressure drop trend is similar to that of liquid void fraction, as shown in Fig. 4.6. The new interfacial friction which is based on drift flux ,V_{gj},may not be applied because the mass flux is lower than 50 kg/m^2.sec over most of the flooding range as shown in Fig. 4.7. If we draw a flooding curve using the upward gas flux and the downward liquid flux values calculated during the test transient, it is possible to compare the calculation with the experimental results obtained in single tube tests. Most experimental results can be correlated by the well known Wallis correlation as discussed in section 2.2. The experimental constant in Eq.(2.1) varied due to the channel inlet shape, length or viscosity effect. For most cases, the slope (m) has a value between 0.8 to 1.0 and the constant (C) ranges from 0.7 to 1.0. However the slope of calculated flooding curve (m) is about 0.5, although the CCFL point (C) is about 1.0, as shown in Fig.4.8. Thus the flooding occurs at much higher air velocity ($j_g^* = 0.7$) than the most experimental data. It may be due to lack of CCFL model applicability at the geometric singularity in test section.

Therefore the CCFL option was applied at the junction 4000000 (air inlet). A simple Wallis form (Eq.3.2) was selected as a input value for the flooding curve.

The inlet air flow and downward liquid flow are fluctuated continuously after the flooding was reached (~ 70 seconds) as shown in Fig.4.9 and 4.10. The flow regime in the test section changes between annular-mist (regime 6) and slug (regime 5) during the flooding process, and becomes the dispersed flow regime (regime 7) as the gas void fraction becomes near unity (>

0.9999). The gas void fraction in the test channel is shown in Fig.4.12. The bottom junction restricts the downward flow after 70 seconds by the CCFL curve provided by user, and thus the liquid fraction in upper junctions increases to nearly 0.2. The increased liquid fraction results the change of flow regime; slug regime from annular mist flow. The interfacial friction, as shown in Fig. 4.13, increases sharply in slug flow regime. Thus the liquid carry-over occurs through the whole test channel. It reduces the liquid void fraction again, and the above cycling process is continued until the flooding is completed. The channel pressure drop, shown in Fig. 4.14, increases sharply after the onset of flooding (70 sec.) and decreases slowly during the flooding process. These oscillatory behavior and pressure trends are much similar to the observed phenomena in most CCFL experiments. The total inlet mass flux also oscillates during the flooding. Although the air inlet flow and the downward liquid flow oscillate, their oscillations lie near the CCFL curve specified by user to satisfy the difference momentum equation of RELAP5, as shown in Fig. 4.16.

4.2 Rod Bundle Tests

As described in section 3.2.2, the calculations for each test type were performed and compared with the experimental data. The input data for calculations were prepared based on the specific experimental condition. The liquid injection flow rate was fixed to 2600 cc/min. The corresponding mass flux is about 35 kg/m^2sec in the case of no air flow. The gas flow was increased slowly enough to neglect the transient effect of increasing the air flow.

4.2.1 Type-1 Test Bundle

For test type-1, two calculations were performed with or without CCFL option. Two calculation results were compared with experimental data obtained from the test facility described in section 2.2.

The air inlet flow was increased during 200 seconds until the flooding is completed, as shown in Fig. 4.17. The downward liquid film flow was restricted at 110 seconds by the increased interphase drag force (Fig. 4.18). A little fluctuation occurs at the early stage of the flooding. The calculated flooding curve using the above air flow and liquid flow at junction 4000000 was presented in Fig. 4.19 as a Kutateladze form. The calculated flooding occurs at much higher air velocity than the experimental data (more than 20 %). The complete flooding occurs at $K_g^* = 3.6$, although it was not presented in figure. The channel pressure drop was presented in Fig. 4.20, with respect to the nondimensional air velocity (K_g^*) in order to compare the experimental data. As shown in the figure, the pressure continuously increases with increasing air flow, while the experimental data shows the sudden jump after the onset of flooding. The flow regime changes from annular mist flow (mode 6) to slug flow (mode 5) as shown in Fig. 4.21. The gas void fraction decreases with increasing air flow rate and maintained nearly constant during the flooding process (Fig. 4.22). The interfacial friction factor increases somewhat slowly, not dramatically (Fig. 4.23). However the interphase drag force was sufficient to carry over the water flow due to the high air velocity. All discrepancies may be resulted from the lack of applicability of CCFL model at the geometric singularity in test section.

In the experiment of type-1 test, the flooding occurs at the air inlet junction. Therefore the experimental flooding curve ,Eq. (3.4), was specified as code input value at the air inlet junction. The calculated air inlet flow and the downward liquid

flow at junction 4000000 are shown in Fig. 4.24 and 4.25. These calculated values were used to generate the flooding curve, i.e. the Fig. 4.26. The calculated flooding values lie well on the specified CCFL curve which was obtained from the experimental data. The pressure drop in the test channel is shown in Fig. 4.27. The experimental data of the liquid injection 2600 cc/min are also presented in the figure. In the experiment, it was shown that the static pressure drop in the channel is nearly proportional to the liquid void fraction. The pressure drop increased suddenly before the onset of flooding and oscillated continuously. After the liquid carry over, the pressure decreased again with decreasing liquid fraction. There are two discrepancies between calculation results and experimental results. First, a sudden jump occurred at a higher gas velocity compared with experiment. In the experiment, the liquid downward flow was restricted by the singularity at the air inlet with K_g^*= 0.9, and the liquid fraction increased. Although the liquid flow oscillated due to flow restriction, the total time averaged liquid flow remained constant. Sometimes it was called "the onset of liquid mixing". It resulted a sudden increase of pressure drop before onset of flooding. In the simulation a sudden pressure drop occured after "the onset of flooding" (K_g^*=1.1), because the liquid holdup in the channel is possible after "the onset of flooding". Second, the peak pressure drop was lower than the experimental results and increased with the air flow. It may be resulted from the interphase drag for rod bundle. The transition to slug flow (mode 5) from annular mist flow (mode 6) occurred after the onset of flooding, as shown in Fig. 4.28, and thus a sharp increase of interfacial friction coefficient was also calculated (Fig. 4.29). The liquid film thickness increased with increasing air flow and jumped suddenly at the point of flooding due to restriction of the downward liquid flow at the air inlet junction (Fig. 4.30). Although the liquid fraction decreased

slowly during the flooding process, the calculated pressure drop increased due to increase of interphase drag force with increase of air flow as shown in Fig. 4.27.

4.2.2. Type-2 and Type-3 Test Bundle

In the experiment for the other type of test bundle, the main characteristics of flooding phenomena are almost identical to the characteristics of type-1 test bundle. However the flooding locations due to the singularity of geometry were quite different. Thus a different location of CCFL junction was examined as presented by the nodalizations shown in Fig. 3.3 and 3.4, following the experimental observation. The flooding curve was specified according to the equation (3.4) which was determined by the experiments. The calculated flooding curve at the location of the spacer grid (junction 3-030000) was compared for type-2 test bundle in Fig. 4.31. The calculated values lie well on the curve specified by user and the channel pressure drop during flooding process agrees well with the experimental data, as shown in Fig. 4.32. But a sudden jump of pressure occurs just after the onset of flooding due to the same reason described in the previous section.

The calculated flooding curve at the location of the first spacer grid (junction 3-010000) was compared with experimental data for type-3 test bundle also. The calculation results lie well on the curve specified by user, but the results of CCFL at a higher air velocity than the complete flooding point are somewhat curious (Fig. 4.33). It may be resulted from a wrong implementation or coding error of flooding model in 5m5 version of RELAP5/MOD3 code. Thus no further discussions for the curious results are given here. The pressure drop agreed well with experimental data, except for the point of sudden jump, as shown in Fig. 4.34. The curious pressure increase after the complete

flooding was considered to be a result of coding error of 5m5 version also.

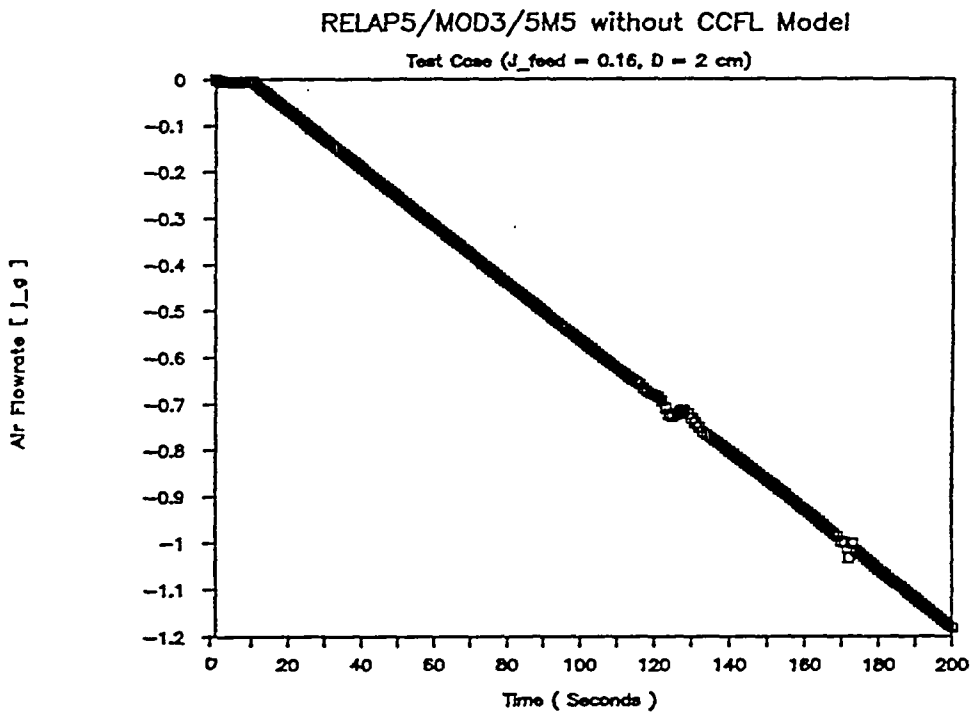

Fig. 4.1 Air Inlet Flowrate at the Junction 4000000

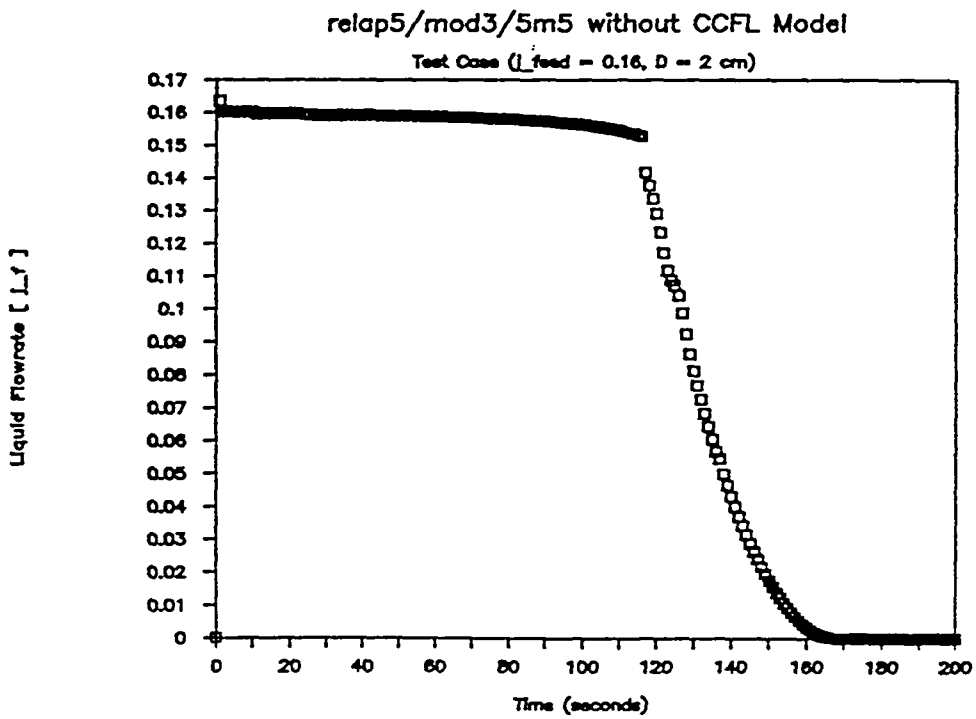

Fig. 4.2 Downward Liquid Flowrate at Junction 4000000

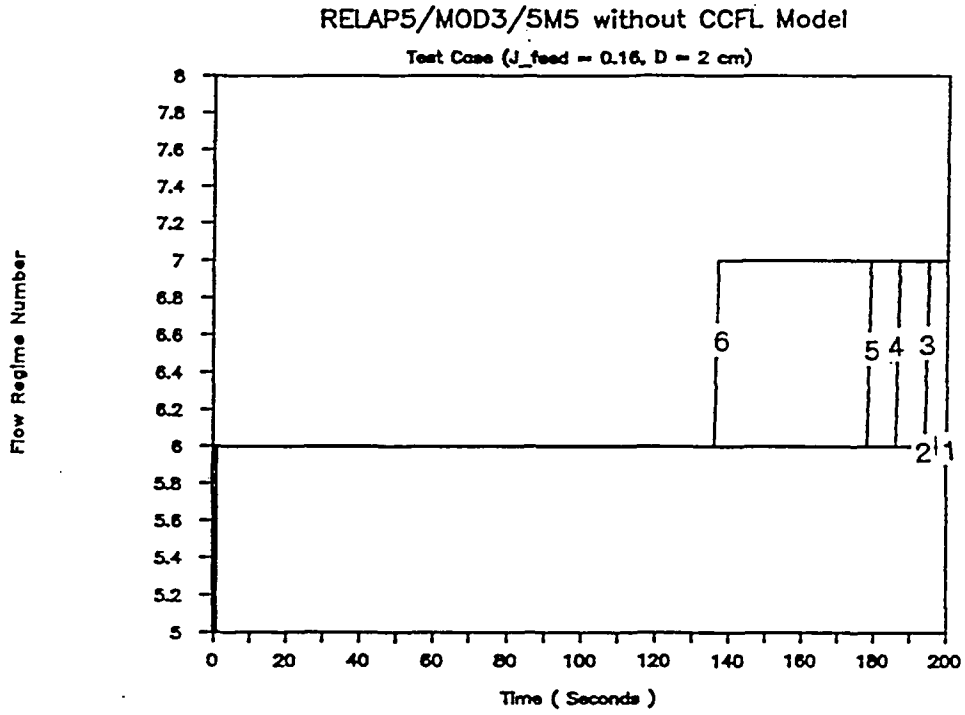

Fig. 4.3 Flow Regime Change at the Test Section Junction
(1 - jun.3010000 : 2 - jun.3020000 : 3 - jun.3030000
4 - jun.3040000 : 5 - jun.3050000 : 6 - jun.4000000)

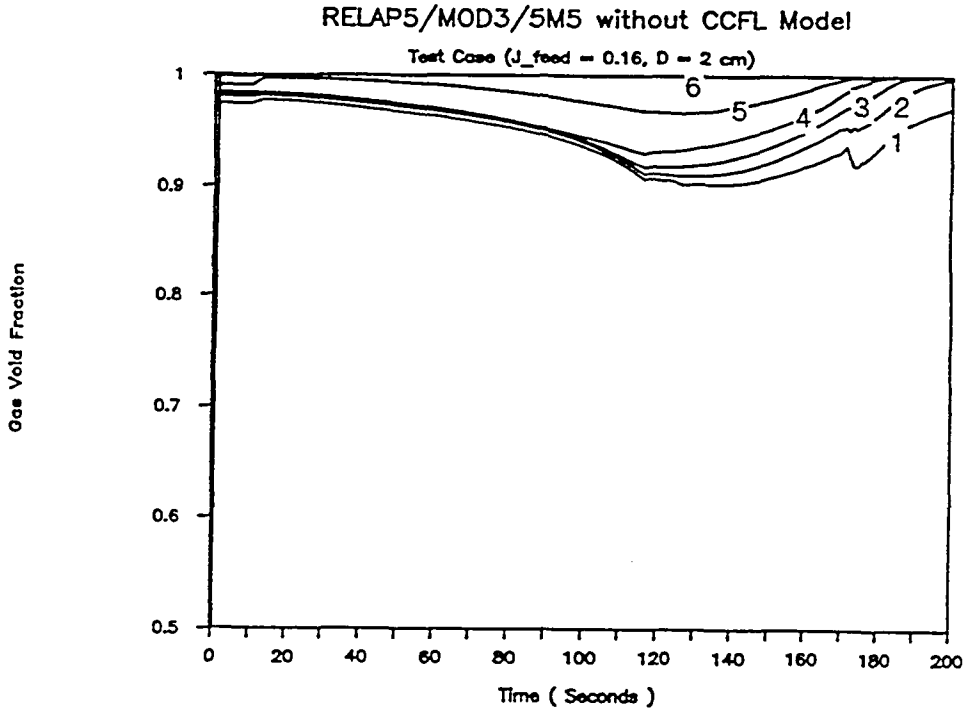

Fig. 4.4 Gas Void Fraction at the Test Section Junction
(1 - jun.3010000 : 2 - jun.3020000 : 3 - jun.3030000
4 - jun.3040000 : 5 - jun.3050000 : 6 - jun.4000000)

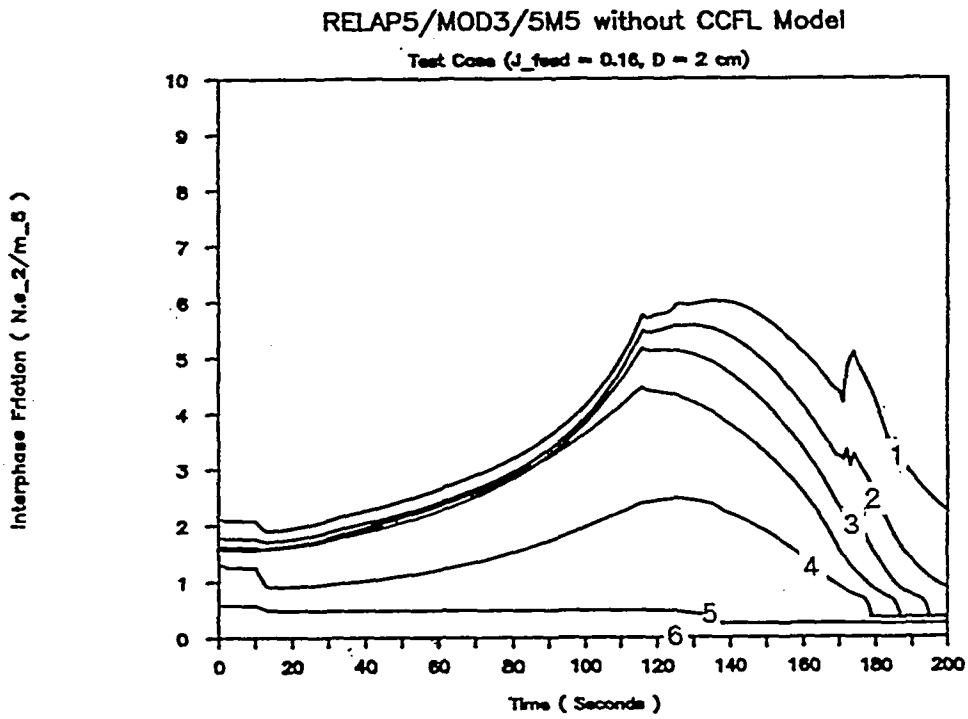

Fig. 4.5 Interfacial Drag Coefficient at the Test Section Junction
(1 - jun.3010000 : 2 - jun.3020000 : 3 - jun.3030000
4 - jun.3040000 : 5 - jun.3050000 : 6 - jun.4000000)

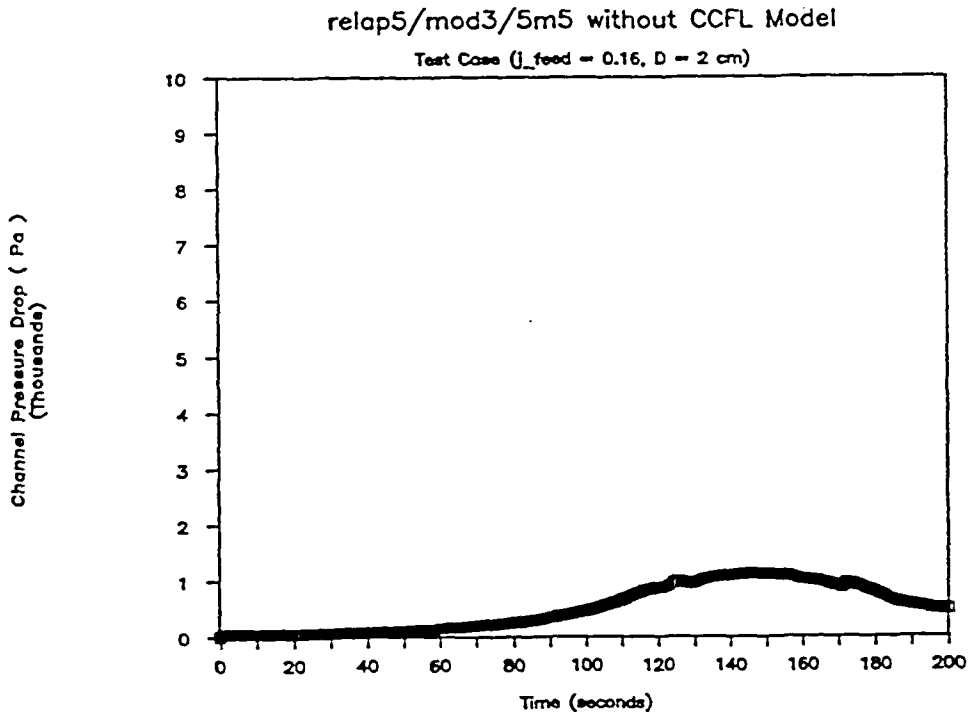

Fig. 4.6 Pressure Drop in the Test Section

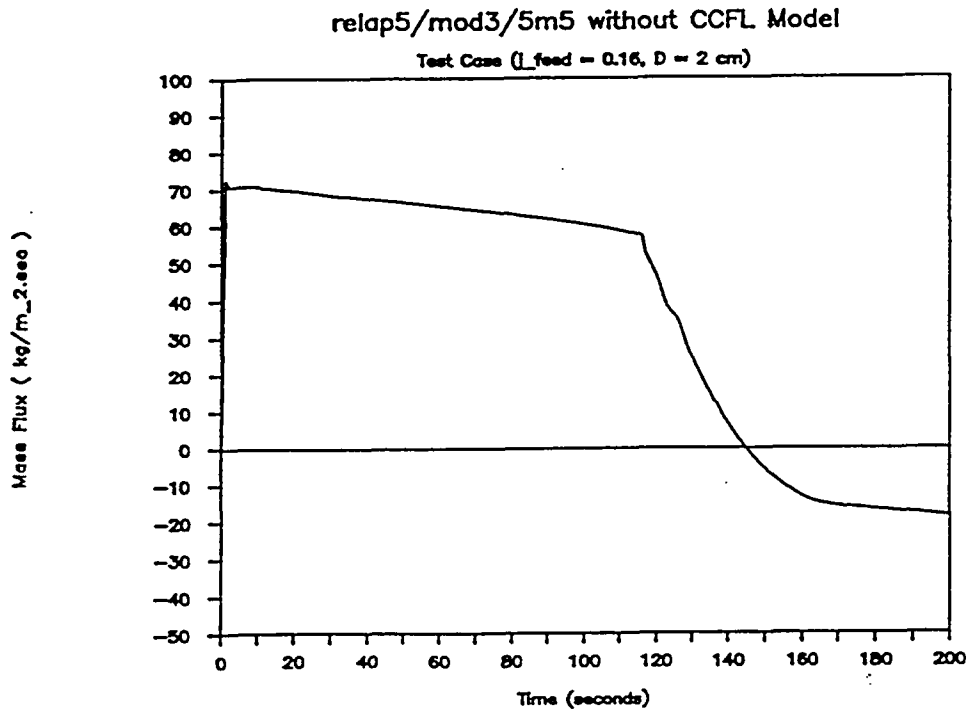

Fig. 4.7 Mass Flux through the Junction 4000000

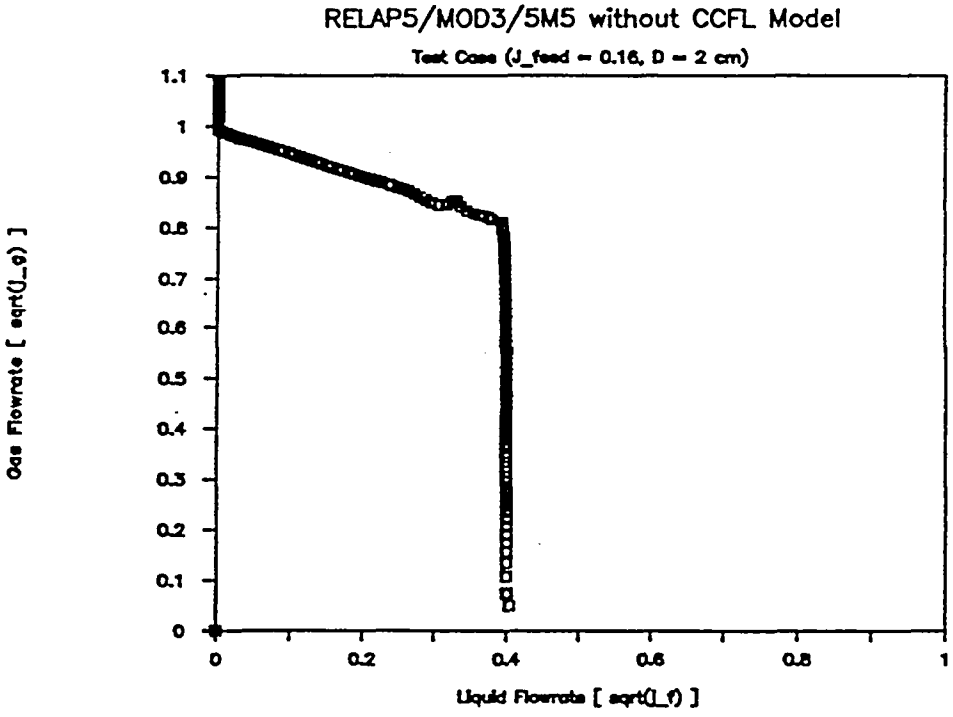

Fig. 4.8 Calculated Flooding Data at the Junction 4000000

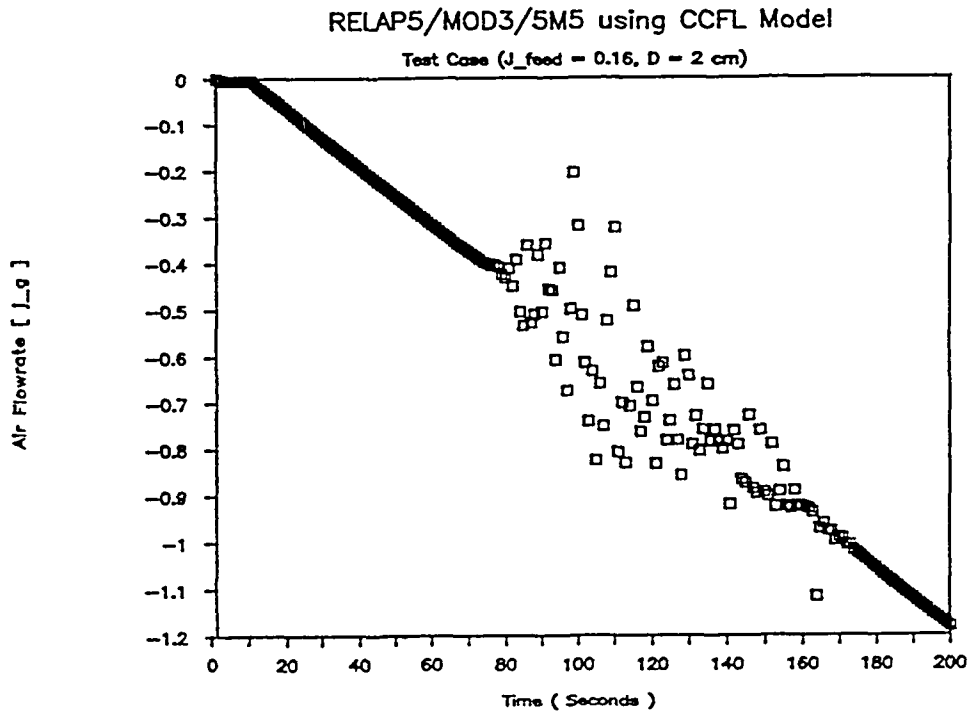

Fig. 4.9 Air Inlet Flowrate at the Junction 4000000

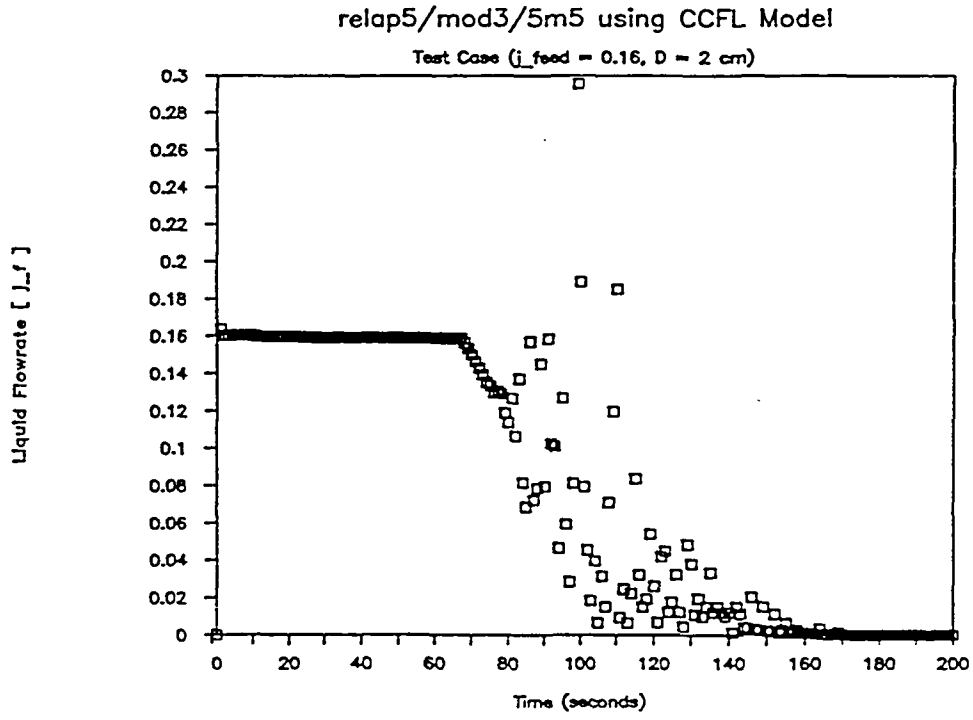

Fig. 4.10 Downward Liquid Flowrate at Junction 4000000

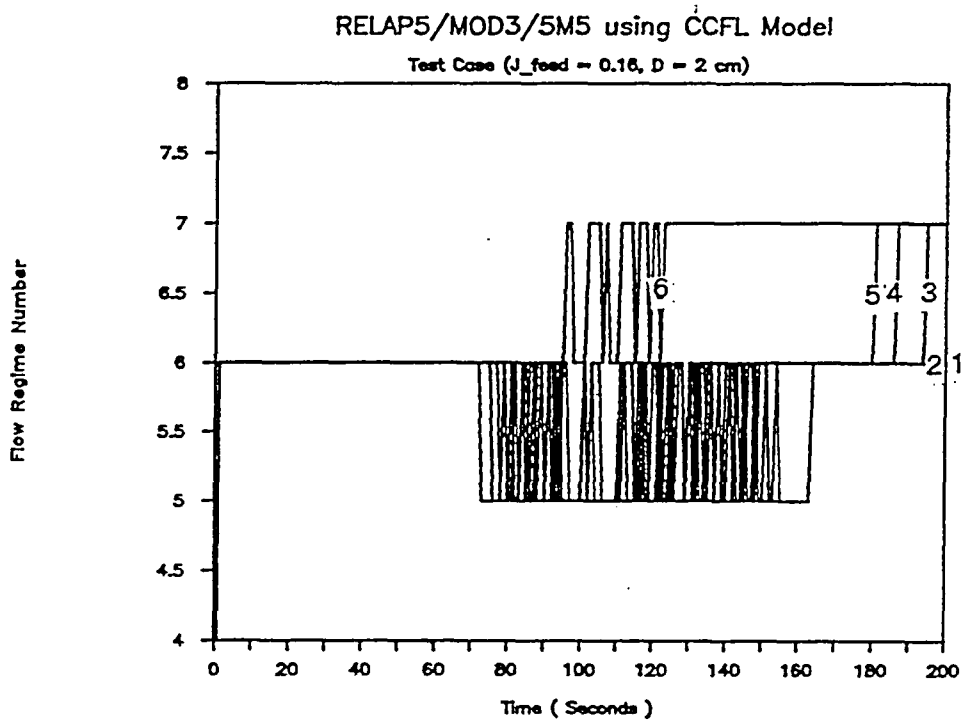

Fig. 4.11 Flow Regime Change at the Test Section Junction
(1 - jun.3010000 : 2 - jun.3020000 : 3 - jun.3030000
4 - jun.3040000 : 5 - jun.3050000 : 6 - jun.4000000)

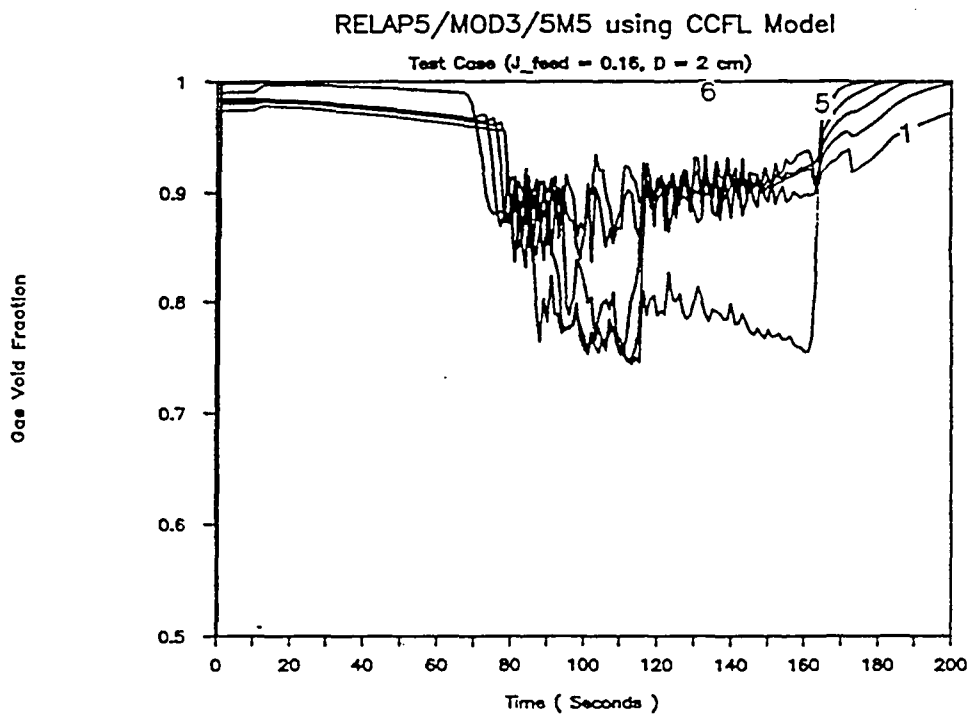

Fig. 4.12 Gas Void Fraction at the Test Section Junction
(1 - jun.3010000 : 2 - jun.3020000 : 3 - jun.3030000
4 - jun.3040000 : 5 - jun.3050000 : 6 - jun.4000000)

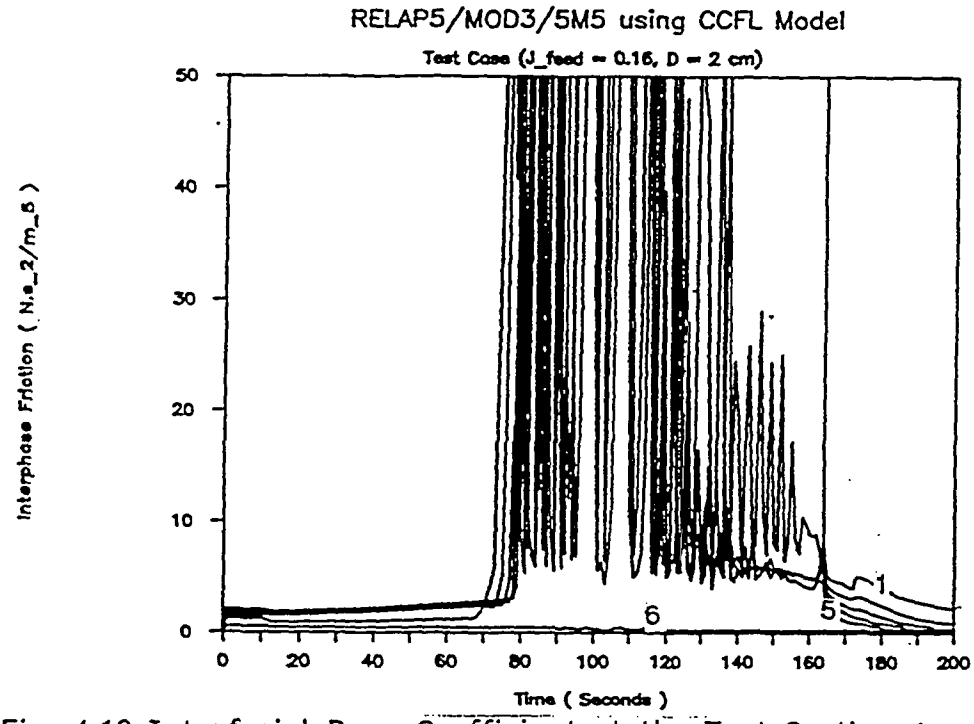

Fig. 4.13 Interfacial Drag Coefficient at the Test Section Junction
(1 - jun.3010000 : 2 - jun.3020000 : 3 - jun.3030000
4 - jun.3040000 : 5 - jun.3050000 : 6 - jun.4000000)

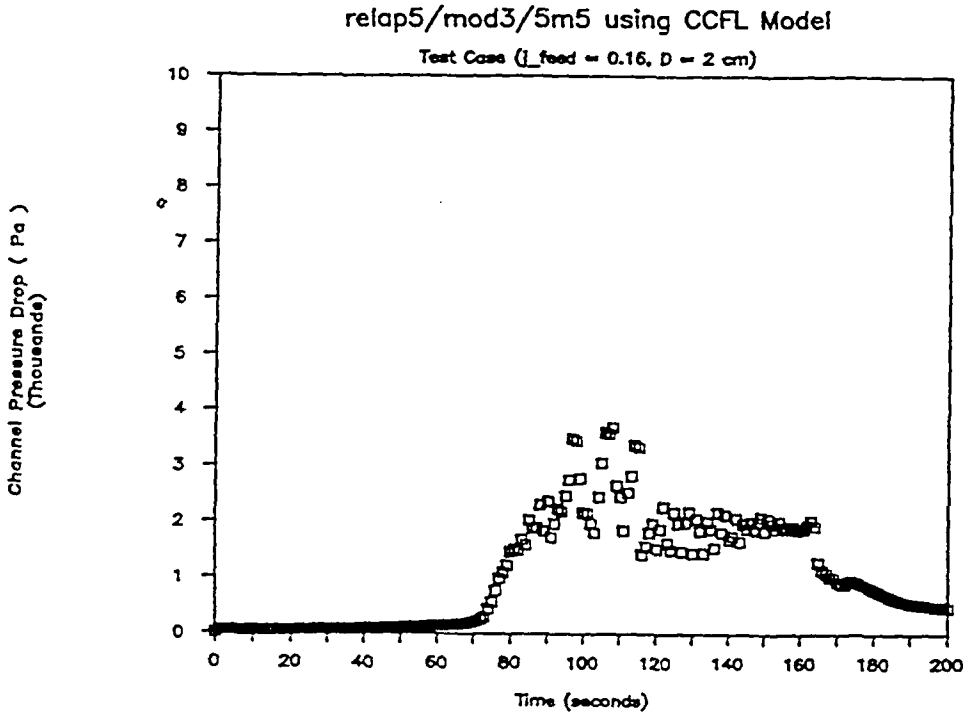

Fig. 4.14 Pressure Drop in the Test Section

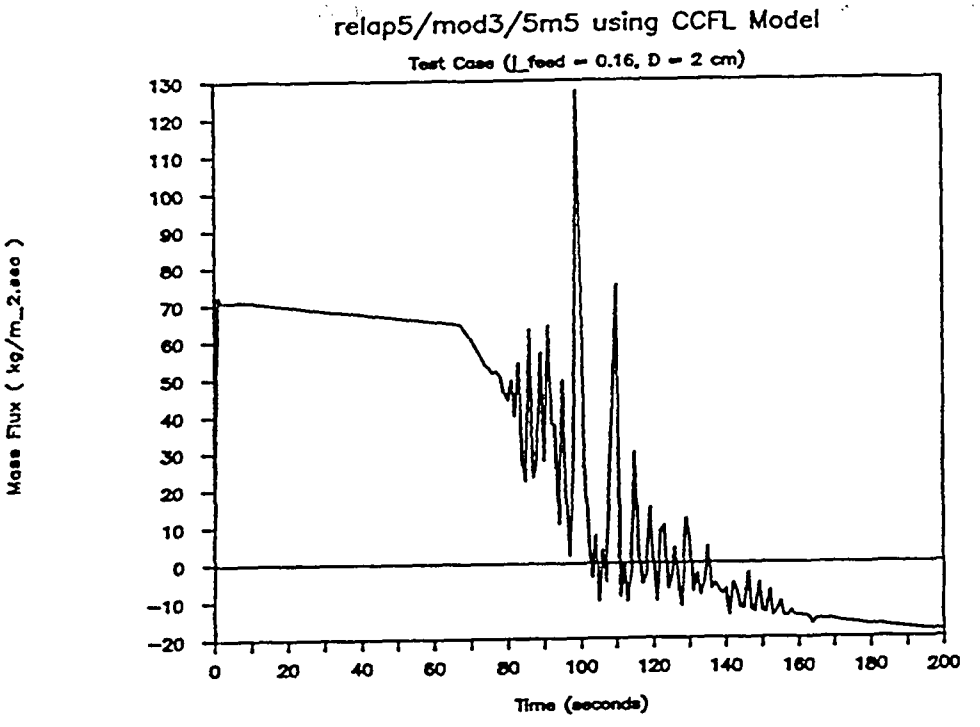

Fig. 4.15 Mass Flux through the Junction 4000000

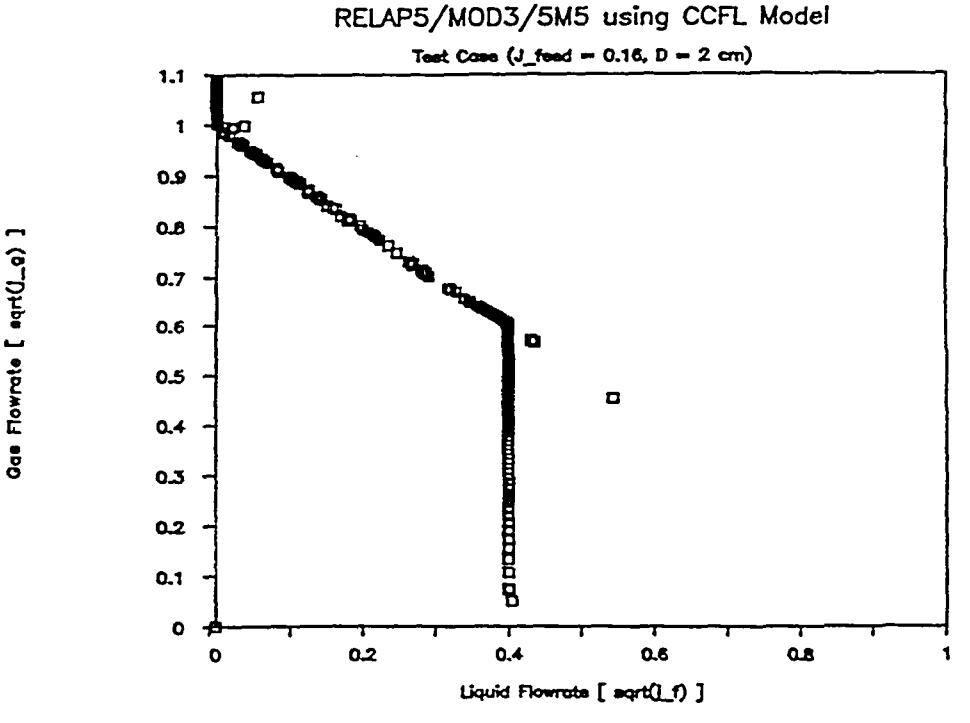

Fig. 4.16 Calculated Flooding Data at the Junction 4000000

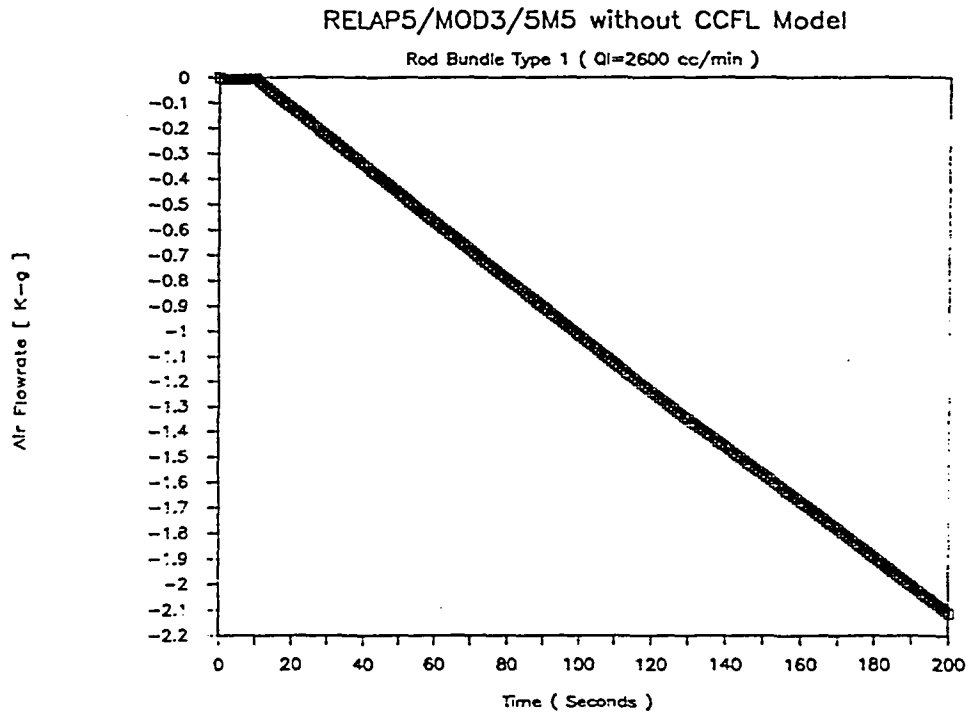

Fig. 4.17 Air Inlet Flowrate at the Junction 4000000

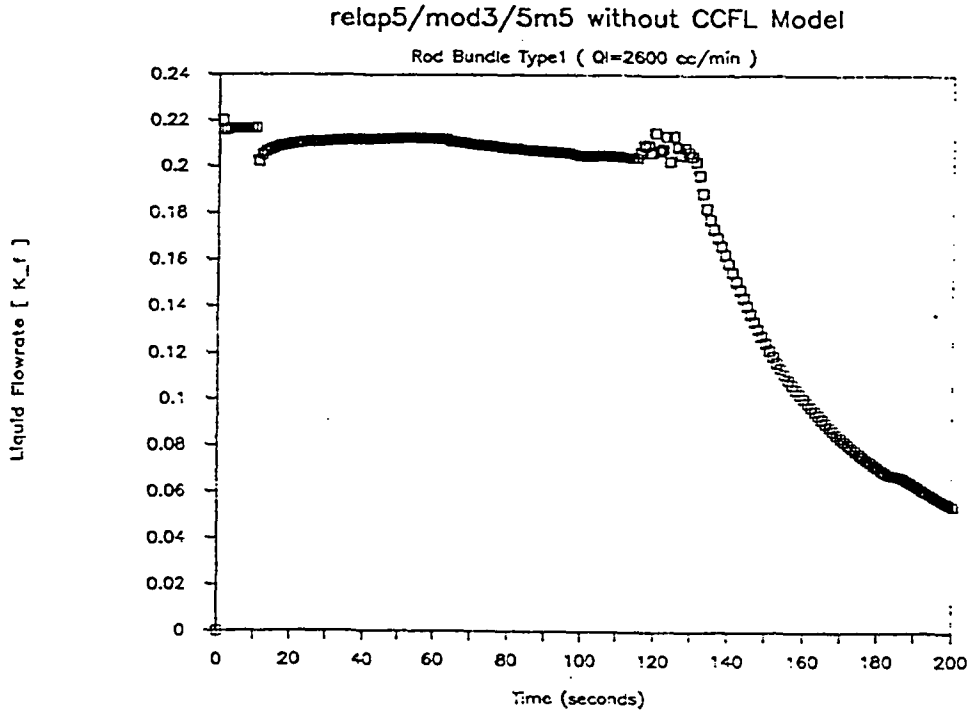

Fig. 4.18 Downward Liquid Flowrate at Junction 4000000

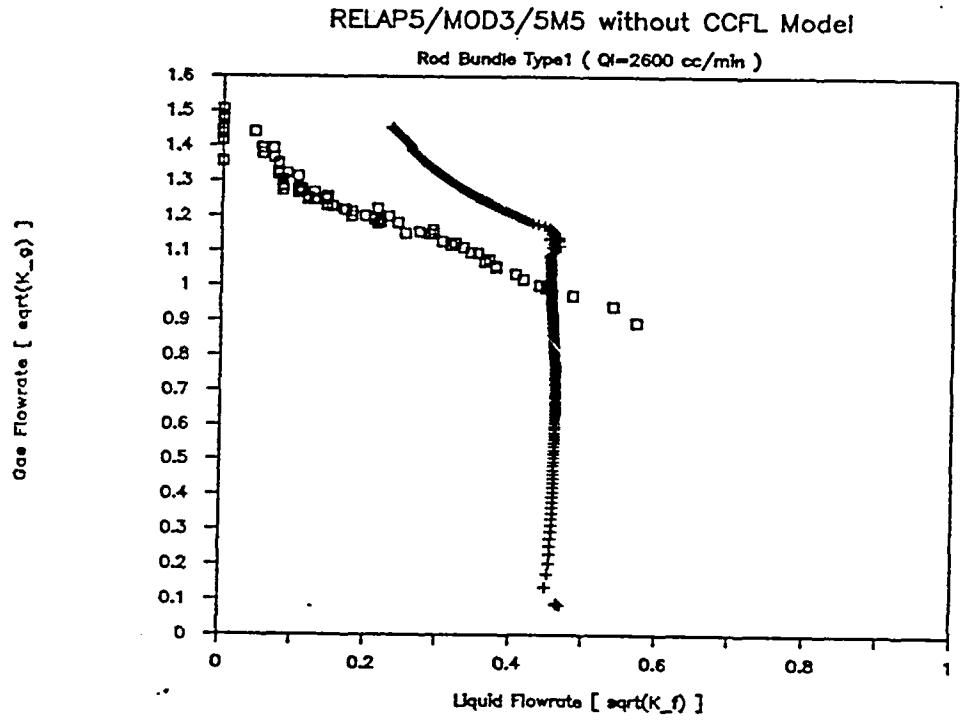

Fig. 4.19 Calculated Flooding Data at the Junction 4000000
(□ - Experiment ; + - Calculation)

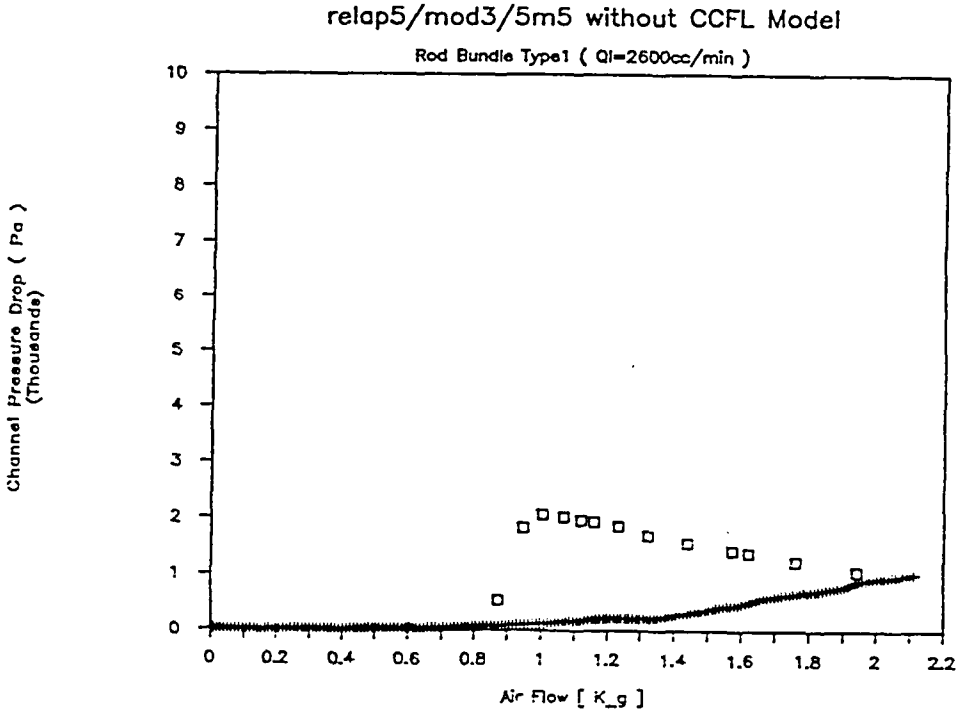

Fig. 4.20 Pressure Drop in the Test Section
(□ - Experiment ; + - Calculation)

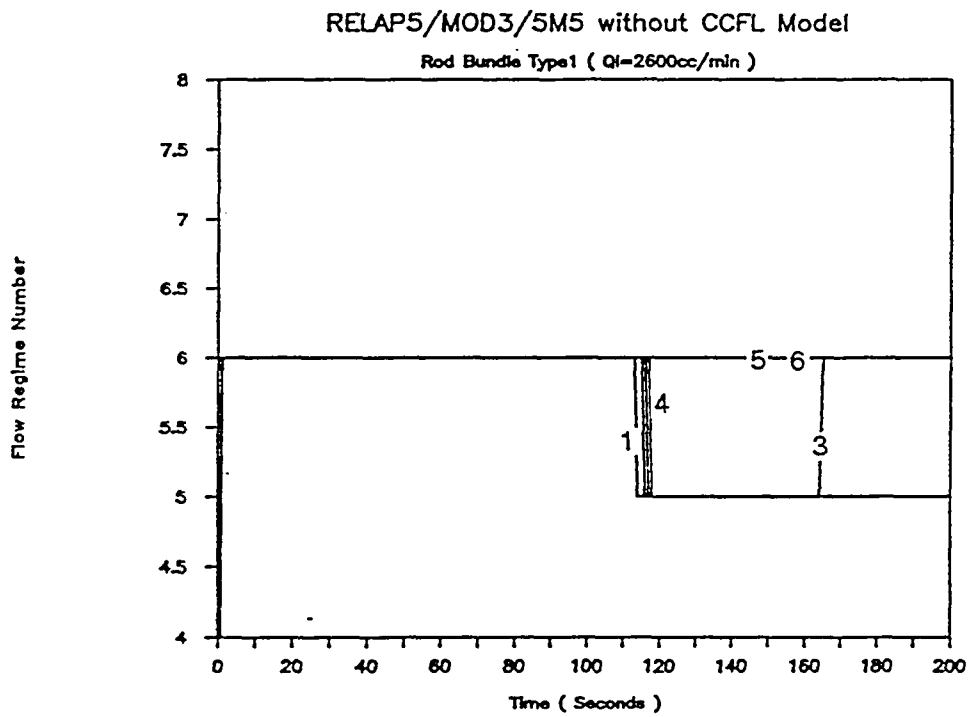

Fig. 4.21 Flow Regime Change at the Test Section Junction
(1 - jun.3010000 : 2 - jun.3020000 : 3 - jun.3030000
4 - jun.3040000 : 5 - jun.3050000 : 6 - jun.4000000)

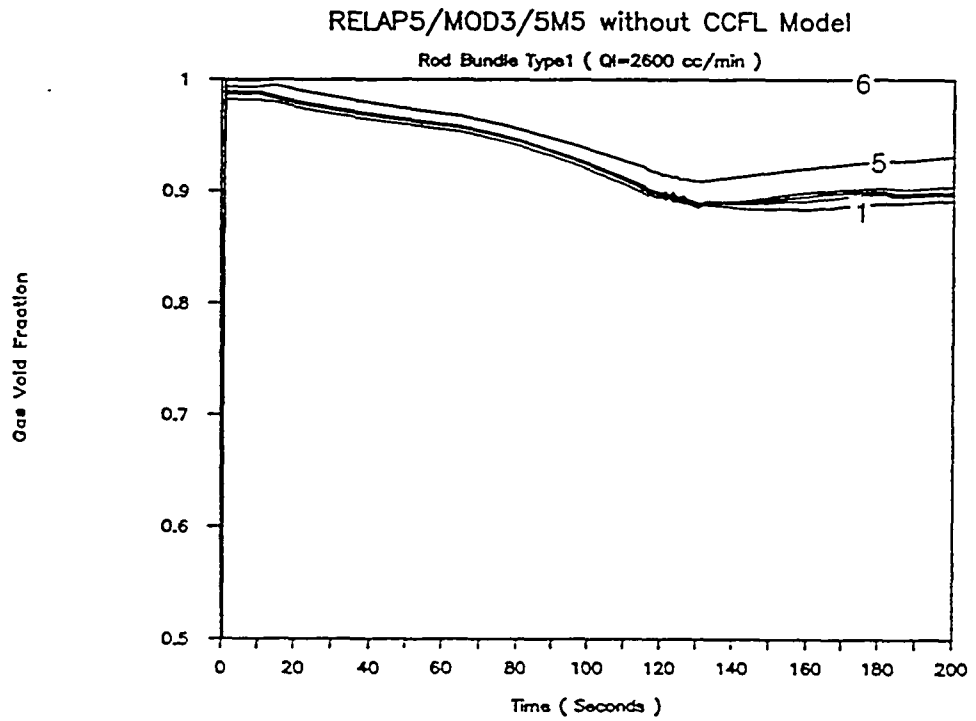

Fig. 4.22 Gas Void Fraction at the Test Section Junction
(1 - jun.3010000 : 2 - jun.3020000 : 3 - jun.3030000
4 - jun.3040000 : 5 - jun.3050000 : 6 - jun.4000000)

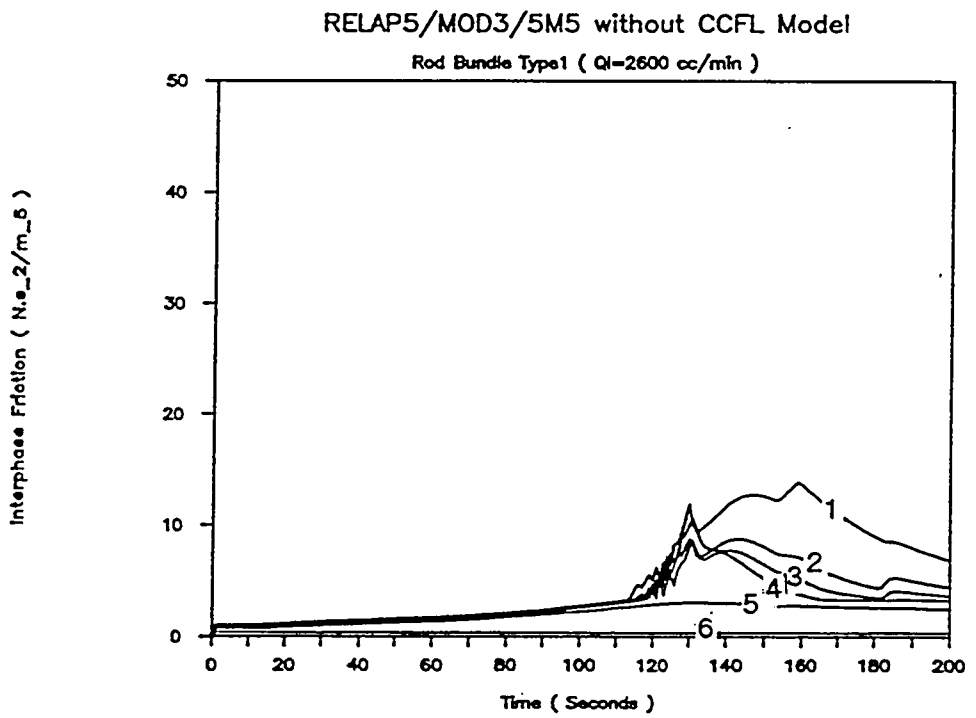

Fig. 4.23 Interfacial Drag Coefficient at the Test Section Junction
(1 - jun.3010000 : 2 - jun.3020000 : 3 - jun.3030000
4 - jun.3040000 : 5 - jun.3050000 : 6 - jun.4000000)

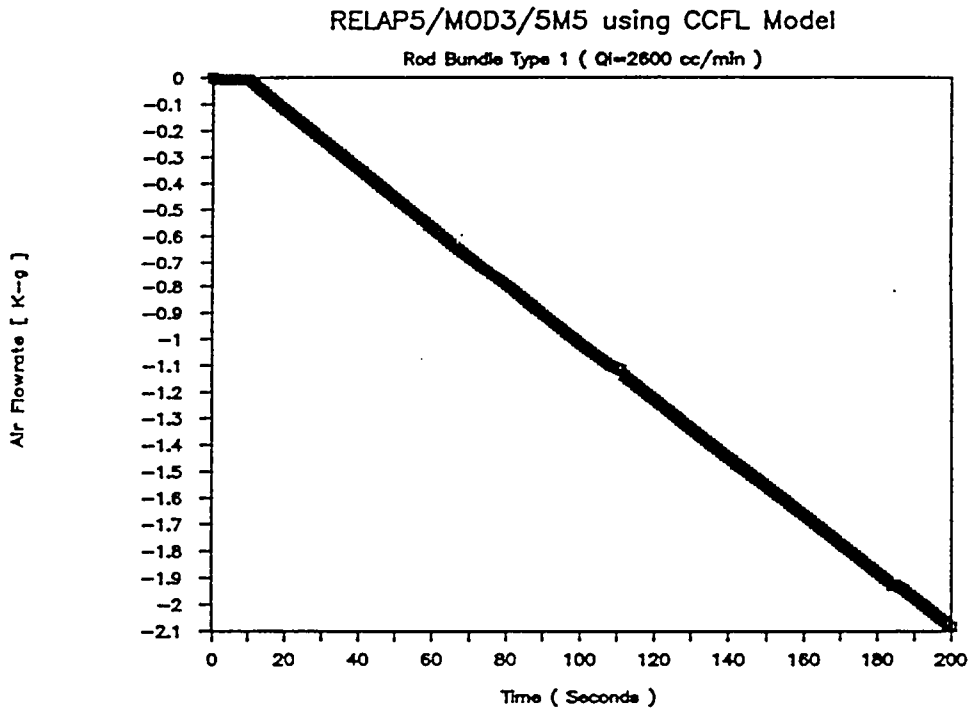

Fig. 4.24 Air Inlet Flowrate at the Junction 4000000

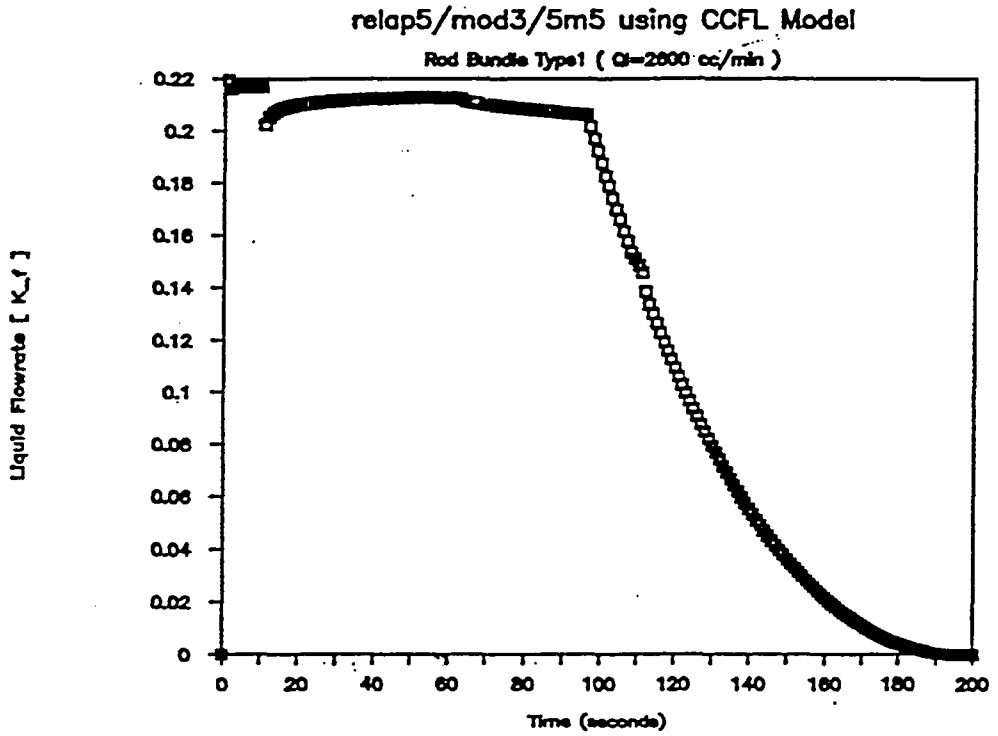

Fig. 4.25 Downward Liquid Flowrate at Junction 4000000

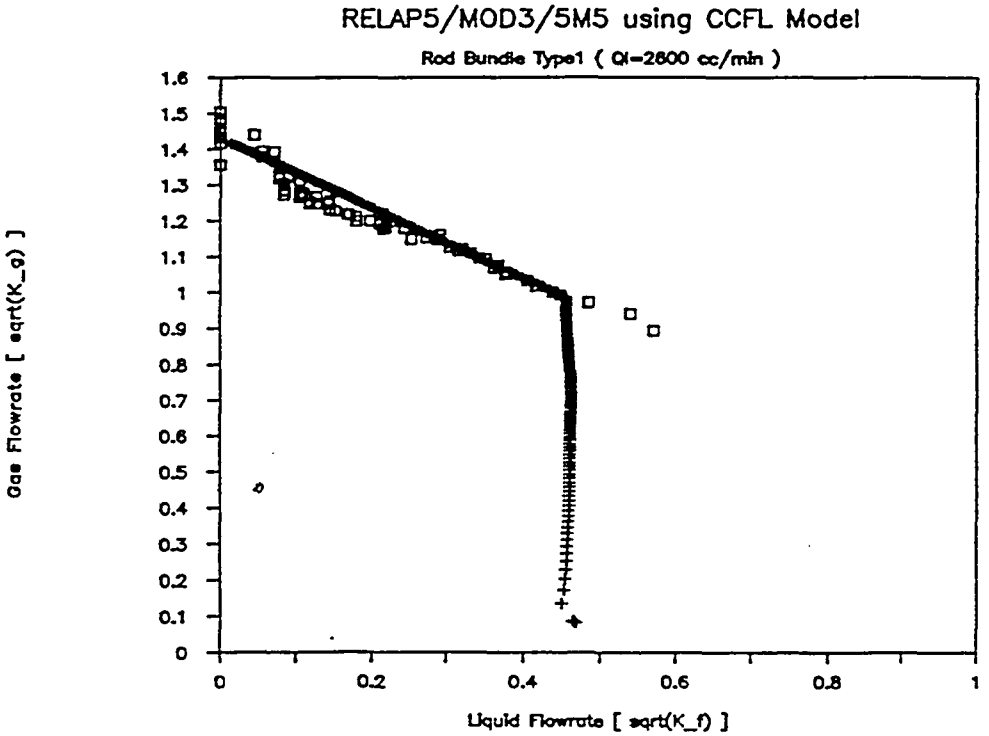

Fig. 4.26 Calculated Flooding Data at the Junction 4000000
(□ - Experiment ; + - Calculation)

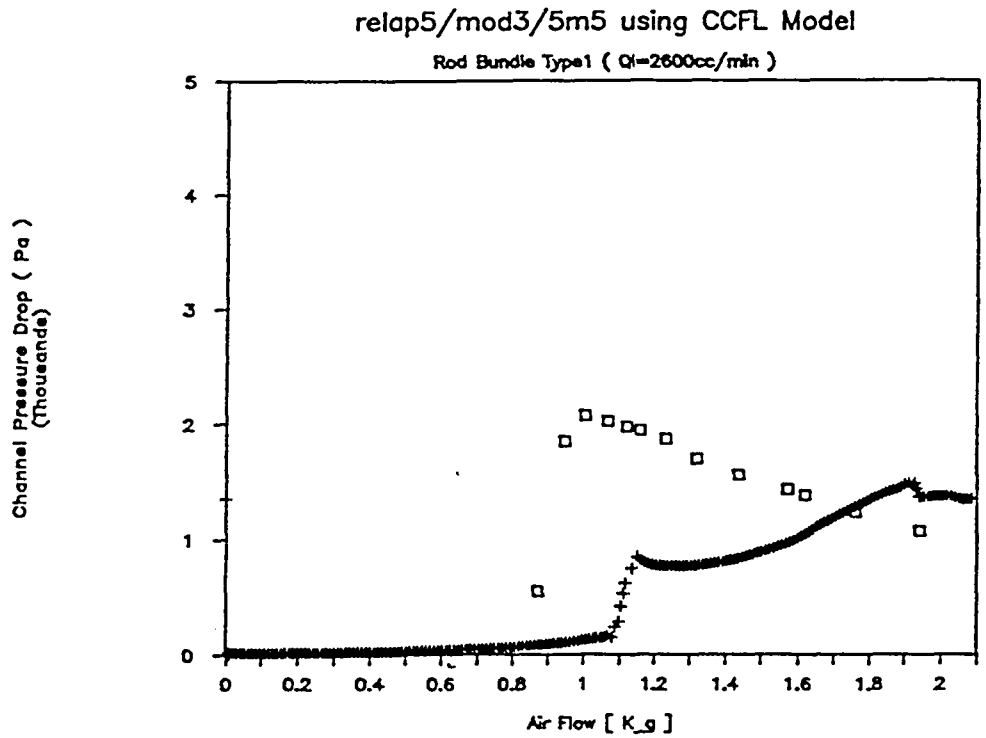

Fig. 4.27 Pressure Drop in the Test Section
(□ - Experiment ; + - Calculation)

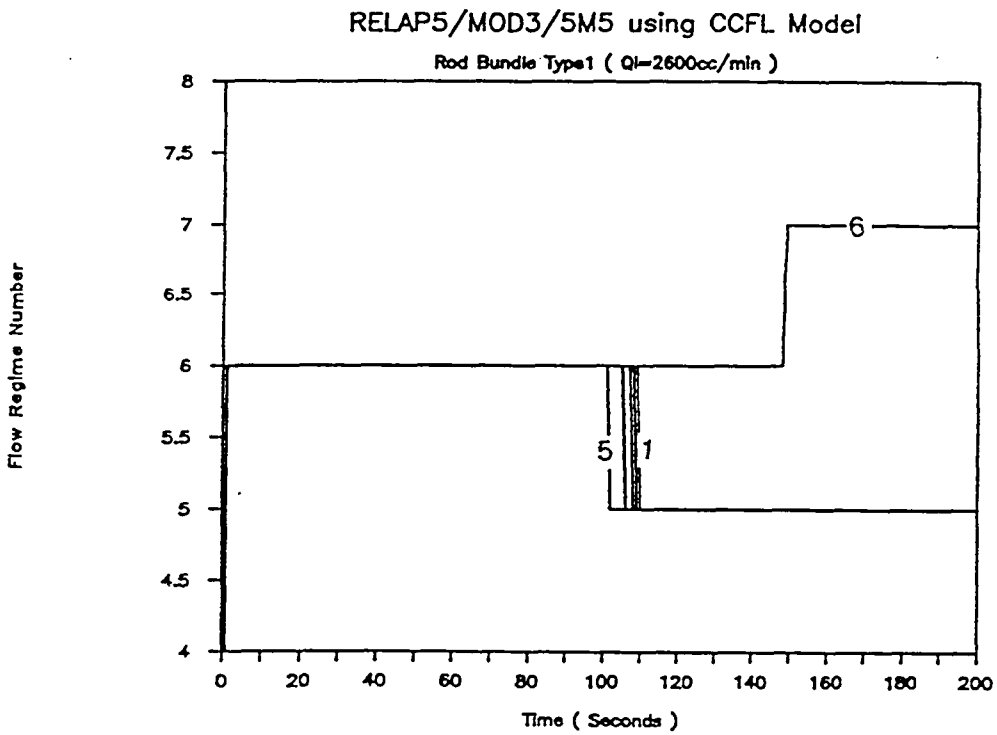

Fig. 4.28 Flow Regime Change at the Test Section Junction
(1 - jun.3010000 : 2 - jun.3020000 : 3 - jun.3030000
4 - jun.3040000 : 5 - jun.3050000 : 6 - jun.4000000)

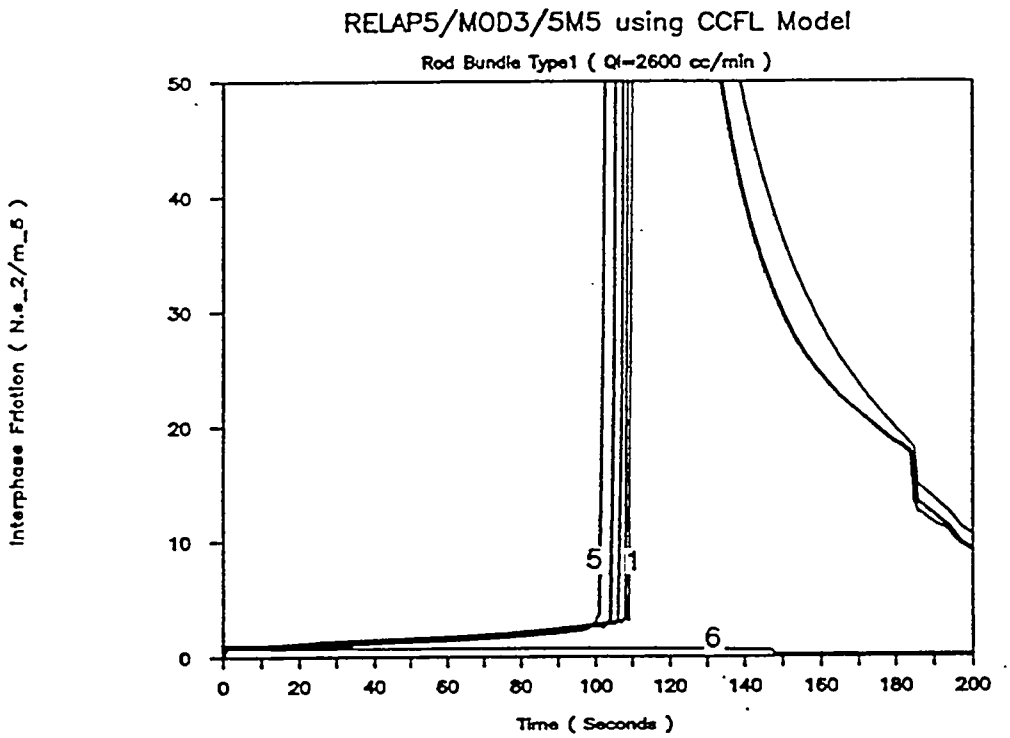

Fig. 4.29 Interfacial Drag Coefficient at the Test Section Junction
(1 - jun.3010000 : 2 - jun.3020000 : 3 - jun.3030000
4 - jun.3040000 : 5 - jun.3050000 : 6 - jun.4000000)

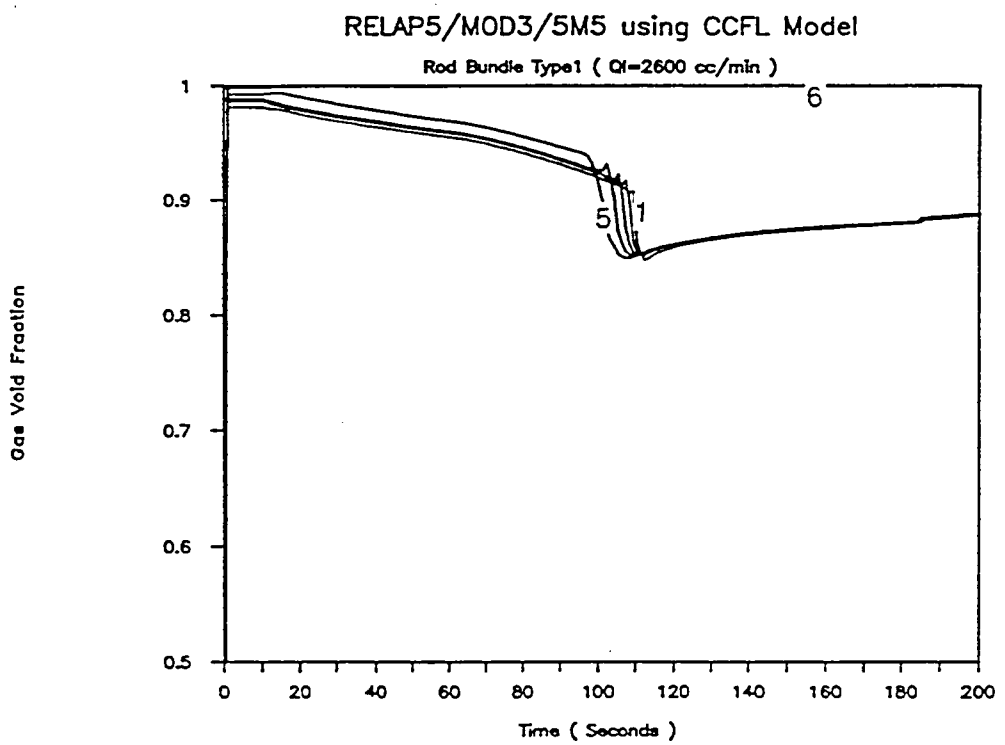

Fig. 4.30 Gas Void Fraction at the Test Section Junction
(1 - jun.3010000 : 2 - jun.3020000 : 3 - jun.3030000
4 - jun.3040000 : 5 - jun.3050000 : 6 - jun.4000000)

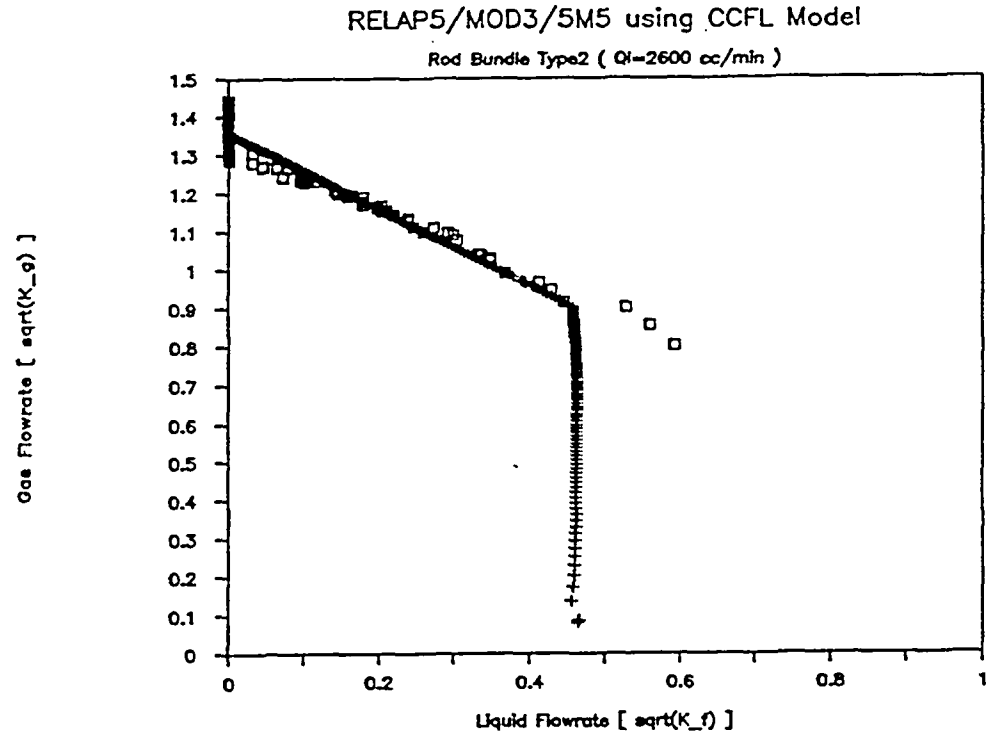

Fig. 4.31 Calculated Flooding Data at the Junction 3030000
(□ - Experiment ; + - Calculation)

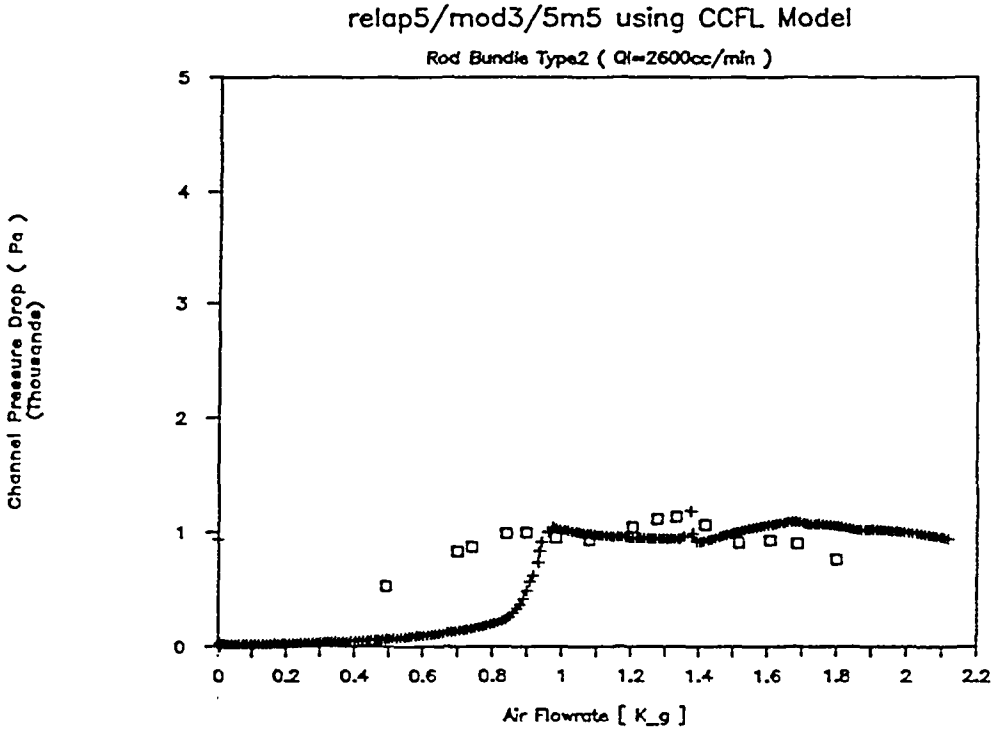

Fig. 4.32 Pressure Drop in the Test Section
(□ - Experiment ; + - Calculation)

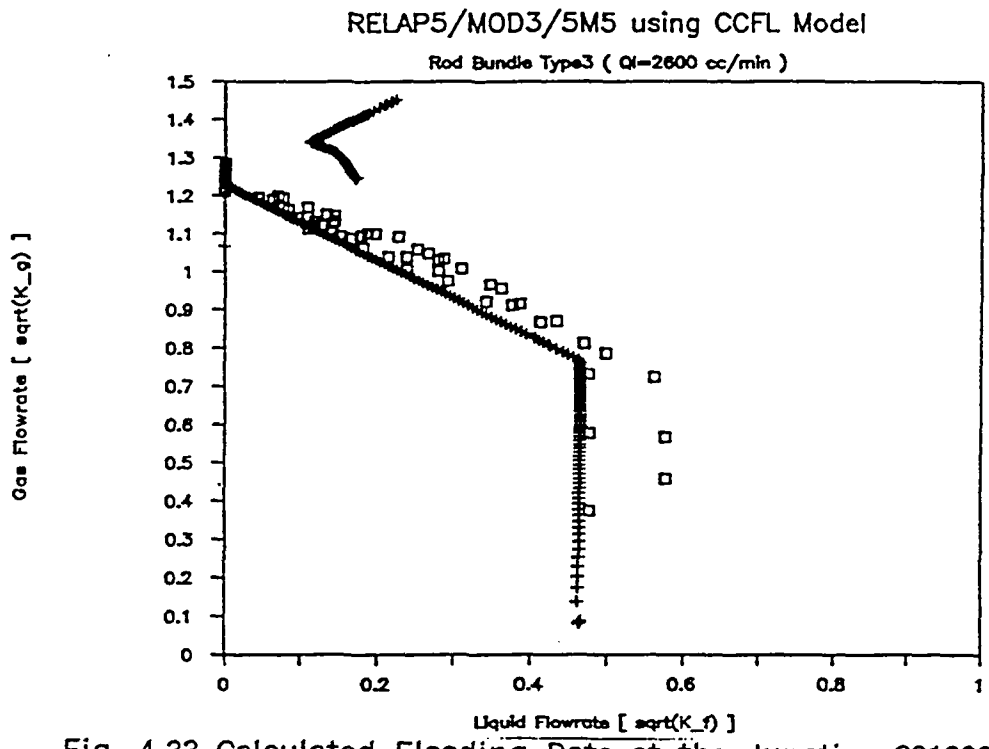

Fig. 4.33 Calculated Flooding Data at the Junction 3010000
(□ - Experiment ; + - Calculation)

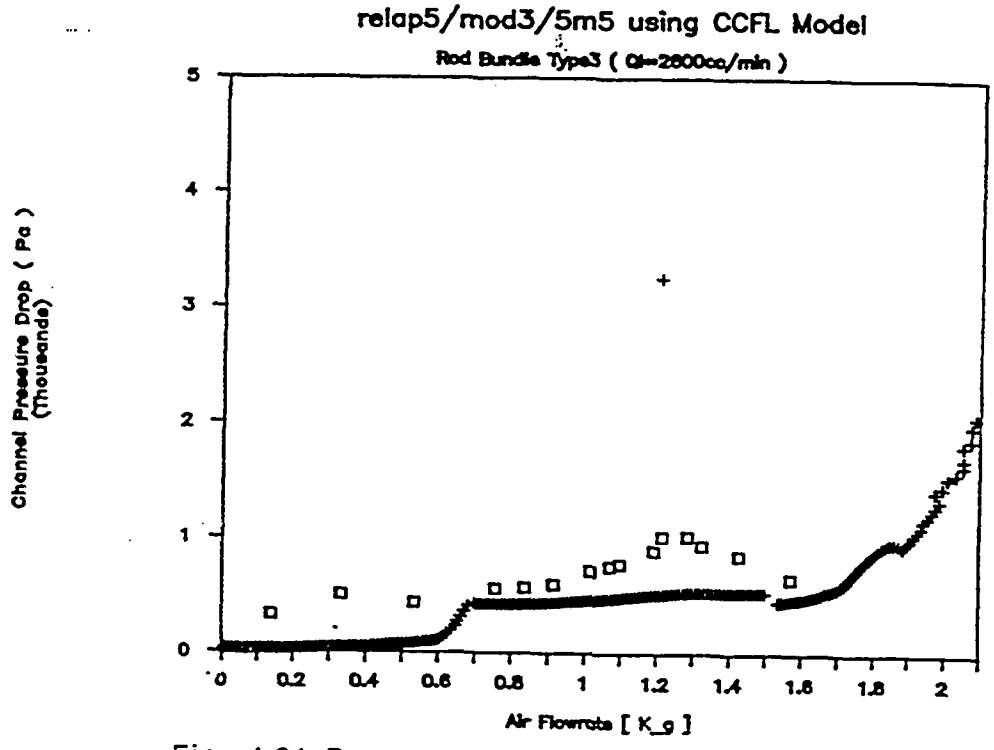

Fig. 4.34 Pressure Drop in the Test Section
(□ - Experiment ; + - Calculation)

5. Sensitivity Results and Discussion

5.1 Tube Diameter

The base calculations for the sample problem of a simple vertical tube the inside diameter of which is 2 cm has been performed. Although the inside diameter was selected for the reason of the similarity of the steam generator U-tubes, there are many other possibilities for the flooding in the tubes which have a different size of the diameter. The different hydraulic diameter causes the different interfacial drag and may result in different flooding characteristics. The calculations have been performed for a wide range of diameter size. A pair of calculations were done for each case of a tube diameter, with and without a CCFL junction option. The test cases and specified CCFL curves are summarized in Table 5.1

Table 5.1 Test cases for the simple vertical tubes.

Case	Tube Diameter	CCFL curves specified at junction 4000000 by user's input
1	0.5 cm	$j_g^{*\,1/2} + j_f^{*\,1/2} = 1.0$
2	1.0 cm	$j_g^{*\,1/2} + j_f^{*\,1/2} = 1.0$
3	2.0 cm	$j_g^{*\,1/2} + j_f^{*\,1/2} = 1.0$ (Base Case)
4	3.0 cm	$j_g^{*\,1/2} + j_f^{*\,1/2} = 1.0$
5	5.0 cm	$j_g^{*\,1/2} + j_f^{*\,1/2} = 1.0$
6	10.0 cm	$K_g^{*\,1/2} + K_f^{*\,1/2} = 3.2^{1/2}$ (Large Tube)

For the 0.5cm tube diameter (case 1), the flooding occurs much earlier than the flooding curve specified by user. Therefore there are no differences between the results obtained with a CCFL

option and those obtained without a CCFL option, as shown in Fig. 5.1, 5.2, 5.3 and 5.4. The calculated pressure drop increased monotonously with increasing air velocity, while most experiments showed a sudden jump of pressure drop. The dispersed values were due to oscillation before the reaching of the steady state for the free falling film flow.

For the 1 cm tube diameter (case 2), the flooding curve and the pressure drop in the test channel calculated without a CCFL option are presented in Fig. 5.5 and 5.6. With a specified CCFL option chosen for test junction, the downward liquid flow was restricted by the CCFL curve or the interfacial drag force in case the interfacial drag force resulted in a lower liquid down flow. In this case the flooding data would lie not on the CCFL curve but on the restriction line determined by interfacial drag, in the regions between $j_f^{*1/2}$= 0.05 and $j_f^{*1/2}$= 0.2. The calculated flooding curve and pressure drop are presented in Fig. 5.7 and 5.8. The pressure drop increase suddenly just after the flooding condition is reached due to the increase of liquid void fraction resulted from the restriction of downward liquid flow.

For the 2 cm tube diameter (case 3), the results were fully discussed as a base case in the previous section.

For the 3 cm tube diameter (case 4), a flooding occured at a much higher gas velocity when a CCFL junction option was not chosen and the pressure drop increased monotonously with increasing air velocity, as shown in Fig. 5.9 and 5.10. With a CCFL junction option, the flooding data lay well on the CCFL curve specified by user, and a sudden jump of pressure drop was predicted as shown in Fig. 5.11 and 5.12. The Fig. 5.12 shows a continuous oscillation of pressure drop during the flooding process. The above trend of pressure drop is a phenomenon which was observed in most experiments.

For the 5 cm tube diameter (case 5), the calculated flooding and pressure characteristics without a CCFL junction option have

almost similar trends of the case 4, except for the high oscillation due to flow instability (Fig.5.13, Fig. 5.14). This flow instability might be resulted from the reduced interfacial drag force and wall friction with increasing hydraulic diameter. When a CCFL option was applied at the junction, the flooding data lay on the specified flooding curve. However the high oscillations were calculated in the region between $j_f^{*1/2}$= 0.1 and $j_f^{*1/2}$= 0.3. The liquid flow oscillated from the countercurrent flow to cocurrent flow, while it was restricted by the CCFL curve, as shown in Fig. 5.15. The calculated pressure drop also oscillated continuously during the flooding process (Fig. 5.16). Since the oscillatory behavior are found in most experiments, the CCFL curve to be specified for the calculation was determined by the time averaging of the oscillatory values. Thus the calculated values oscillation should fall on the specified CCFL curve. The oscillations were resulted from the fact that the 5m5 code select the lower value of the two flows determined by a normal junction equation and the other by a CCFL junction equation.

For the 10 cm tube diameter (case 6) , the Wallis type of flooding curve is not valid any more due to the characteristics of a large diameter. Thus all calculated flooding data were presented by the form of Kutateladze form in Fig. 5.17 for the comparison of the experimental results. The calculation results show that high oscillations occurred and a complete flooding occurred at the K_g^*= 4.8 whereas the experimental results show that a complete flooding occurred at K_g^*= 3.2. The pressure drop, shown in Fig. 5.18, oscillated highly also. When the CCFL option was specified at the junction, the calculated flooding data lay well on the specified CCFL curve, although the downward flow oscillated between countercurrent flow and cocurrent flow as shown in Fig.5.19 and 20. The curious results were produced above the complete flooding, K_g^*=3.2. This might have been caused by a coding error or incorrect implementation of a CCFL model in

version 5m5. Therefore no further discussions are provided for the curious calculated results.

In summary of sensitivity studies using various tube diameters, the high interfacial drags of the code for the small diameter tubes can restrict the countercurrent flow before the CCFL condition is actually reached. As the tube diameter increases, the calculated downward liquid flow becomes unstable because the calculated flow regime oscillated between the annular mist flow and slug flow. The flooding occurs at a much higher air velocity than predicted by the experiments, and thus the application of the CCFL option at the specific junction is needed.

5.2 Nodalization

The flooding characteristics may be affected by the nodalization. The major concern for a nodalization effect was in the test section area in which the actual countercurrent flow existed. The figures of the fine nodalization are presented in Fig. 5.21 and 5.22. The results are shown in Fig. 5.23 to Fig. 33. The major calculated values of fine nodalization are not quite different from the results of the coarse nodalization as shown in the section 4, and thus it is concluded that flooding characteristics are not sensitive to the number of nodalization.

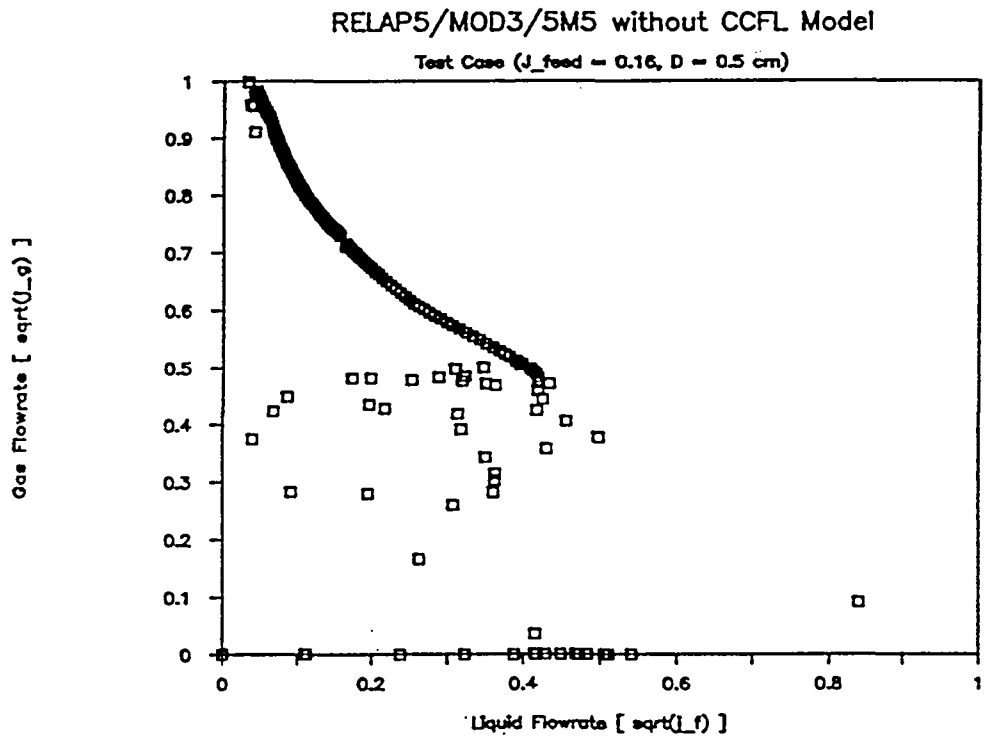

Fig. 5.1 Calculated Flooding Data without CCFL option (D = 0.5 cm)

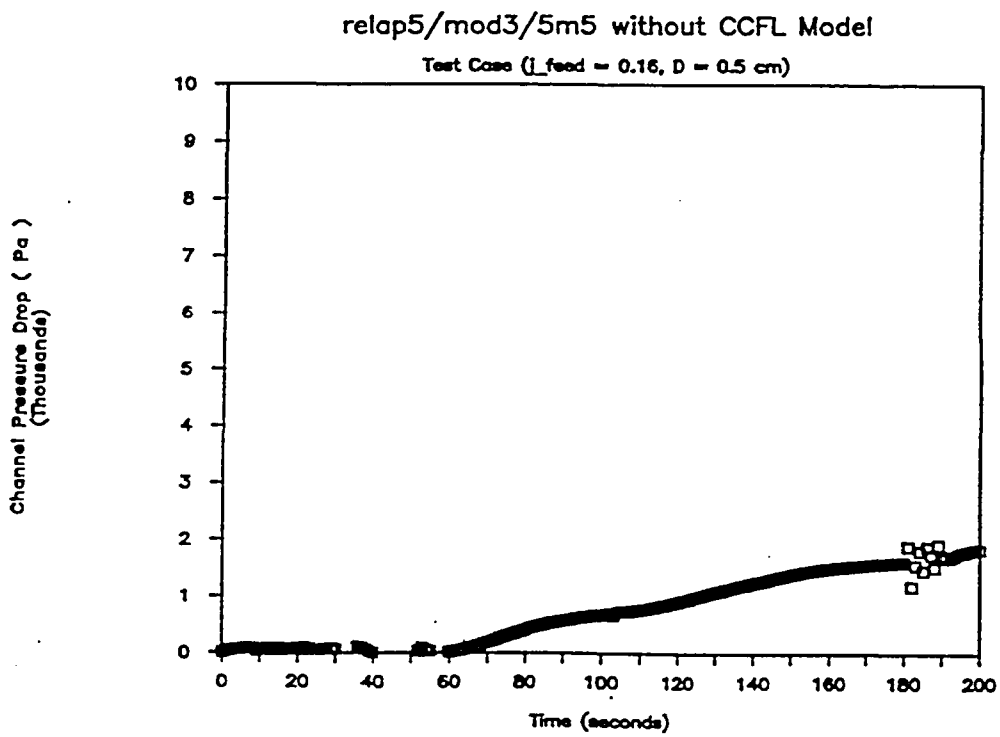

Fig. 5.2 Pressure Drop in the Test Section (D = 0.5 cm)

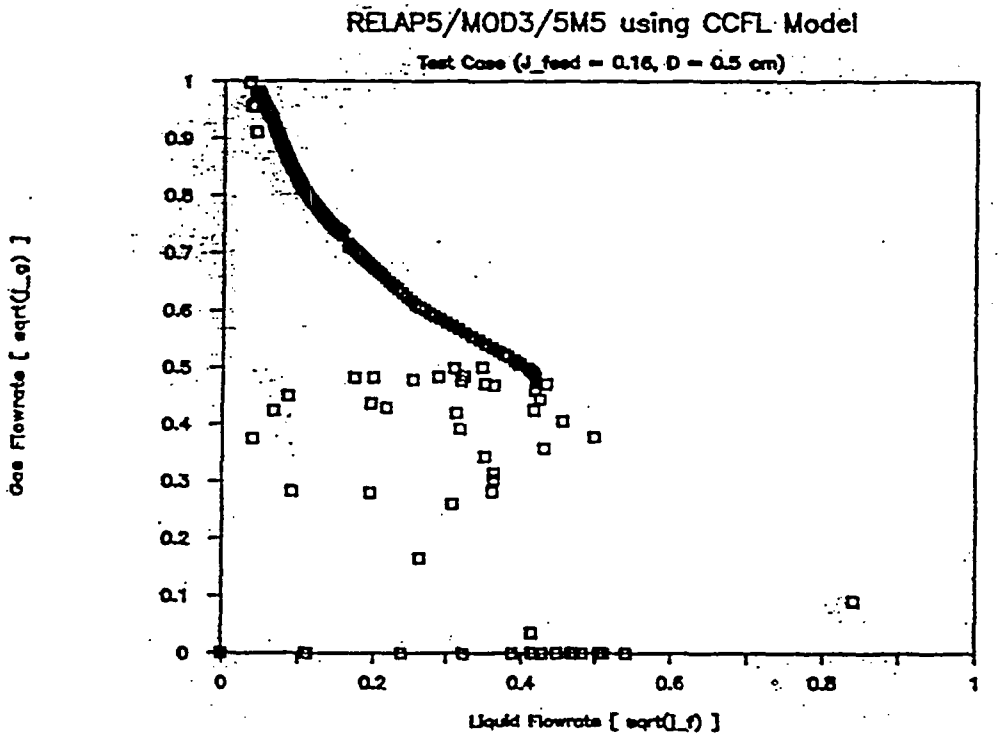

Fig. 5.3 Calculated Flooding Data with CCFL option (D = 0.5 cm)

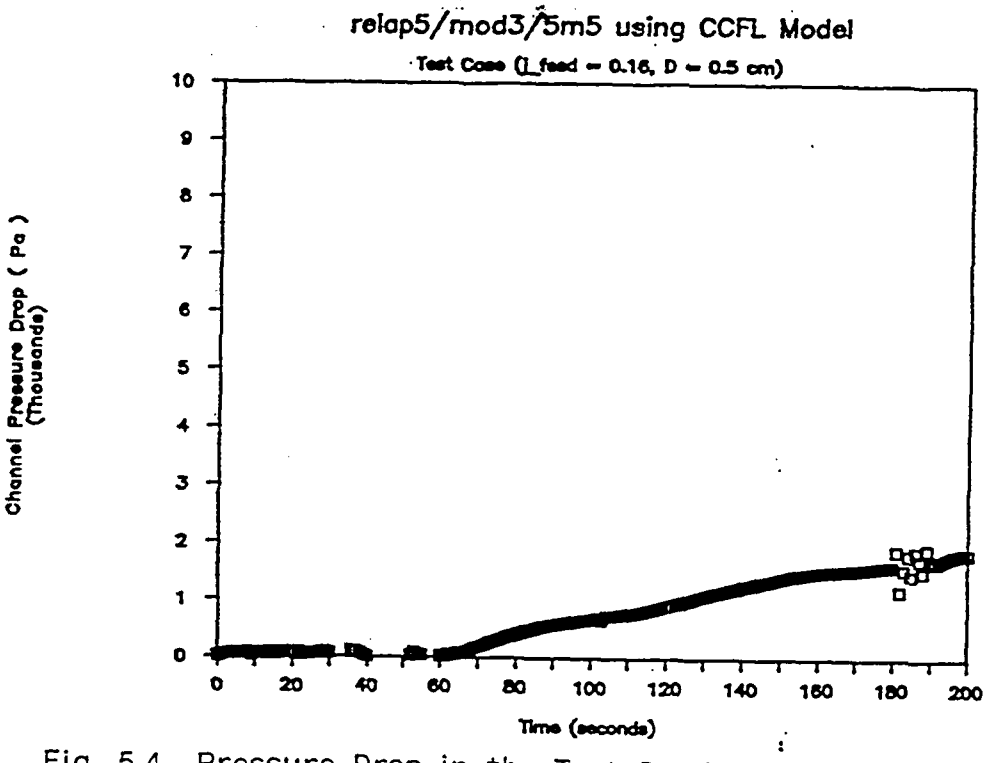

Fig. 5.4 Pressure Drop in the Test Section (D = 0.5 cm)

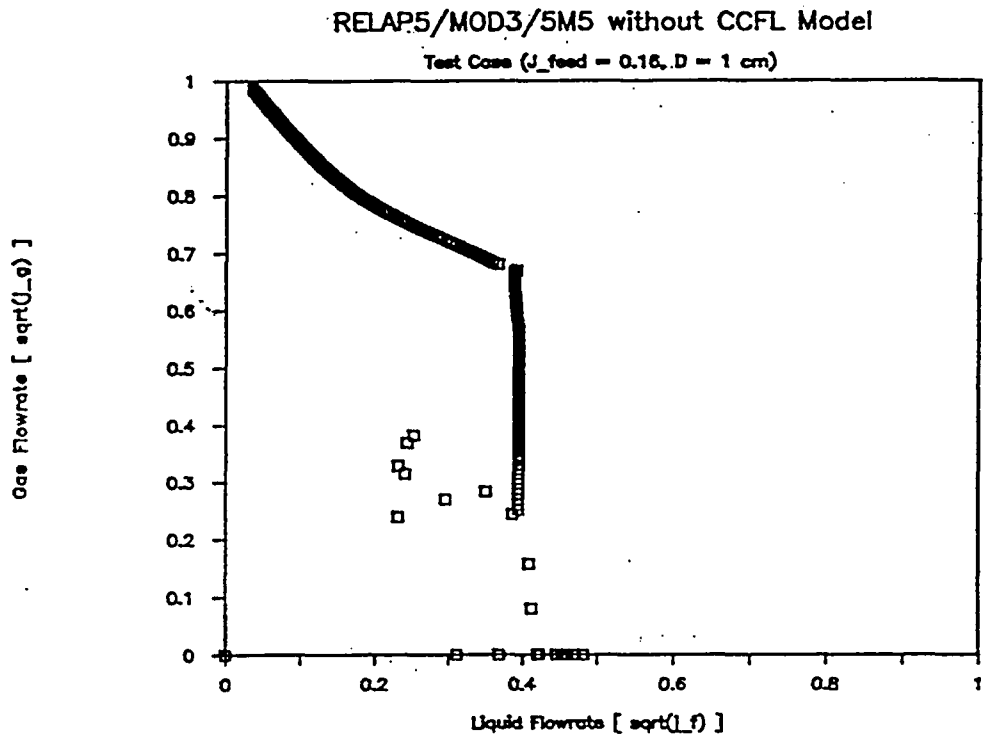

Fig. 5.5 Calculated Flooding Data without CCFL option (D = 1.0 cm)

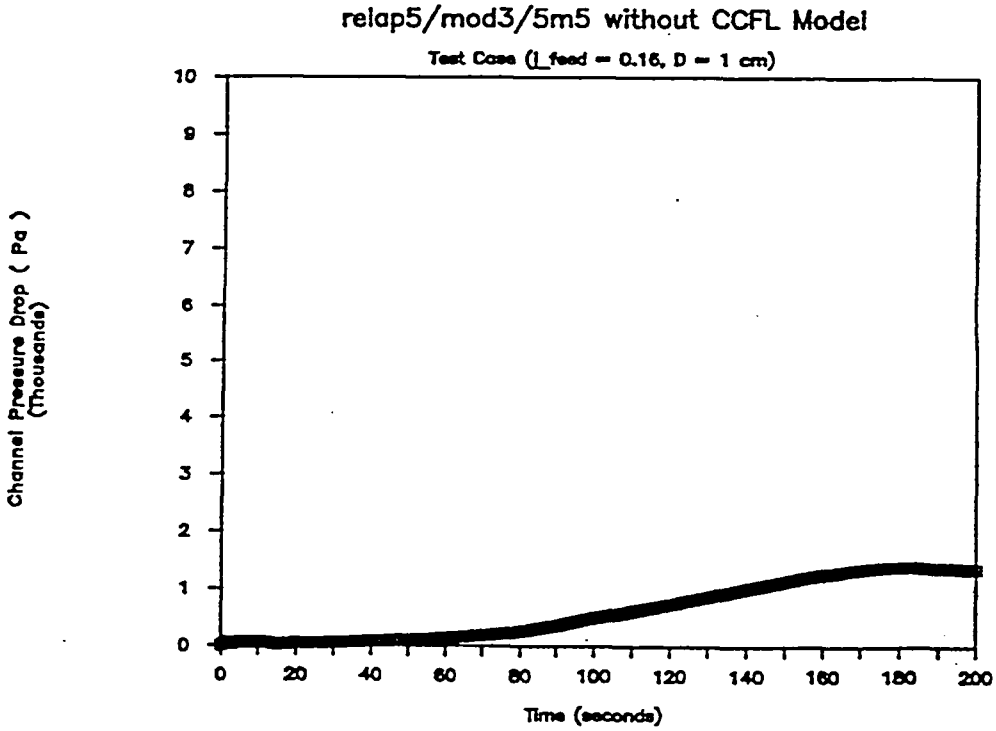

Fig. 5.6 Pressure Drop in the Test Section (D = 1.0 cm)

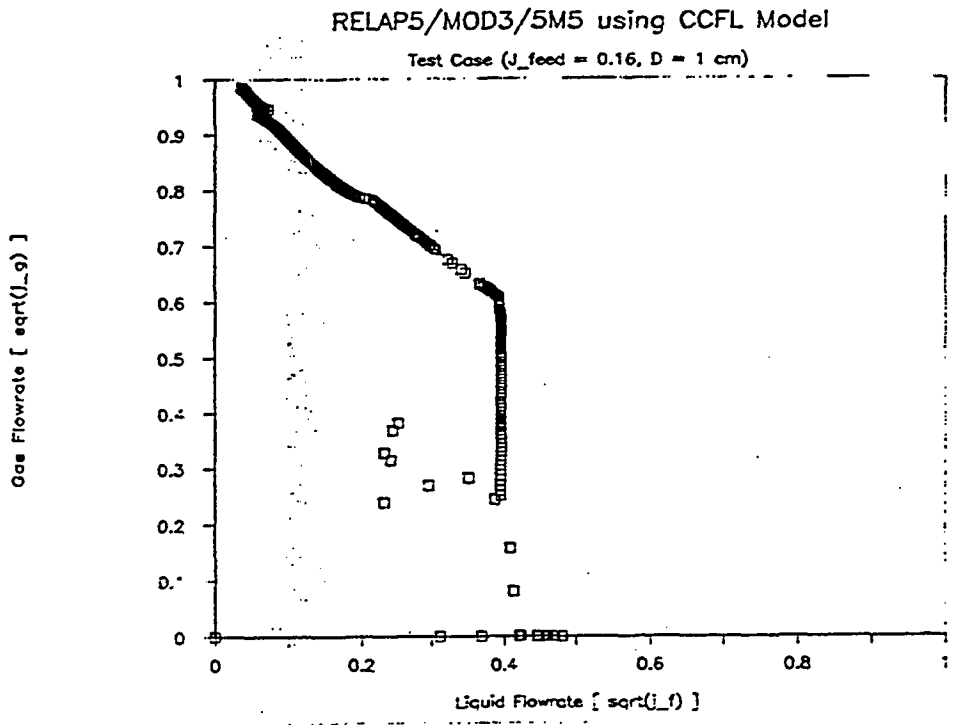

Fig. 5.7 Calculated Flooding Data with CCFL option (D = 1.0 cm)

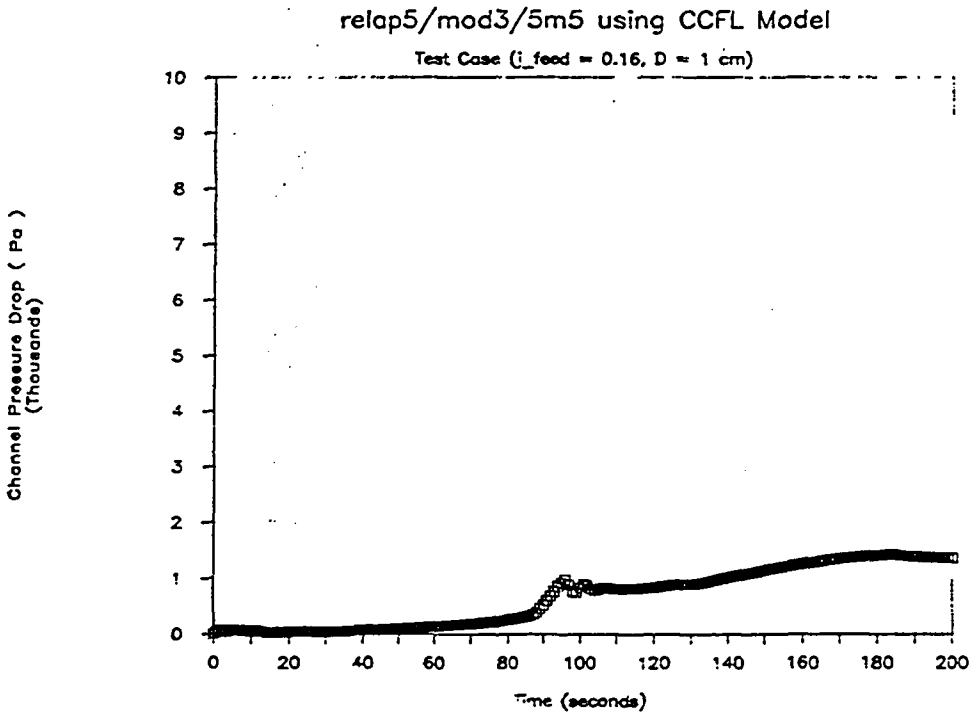

Fig. 5.8 Pressure Drop in the Test Section (D = 1.0 cm)

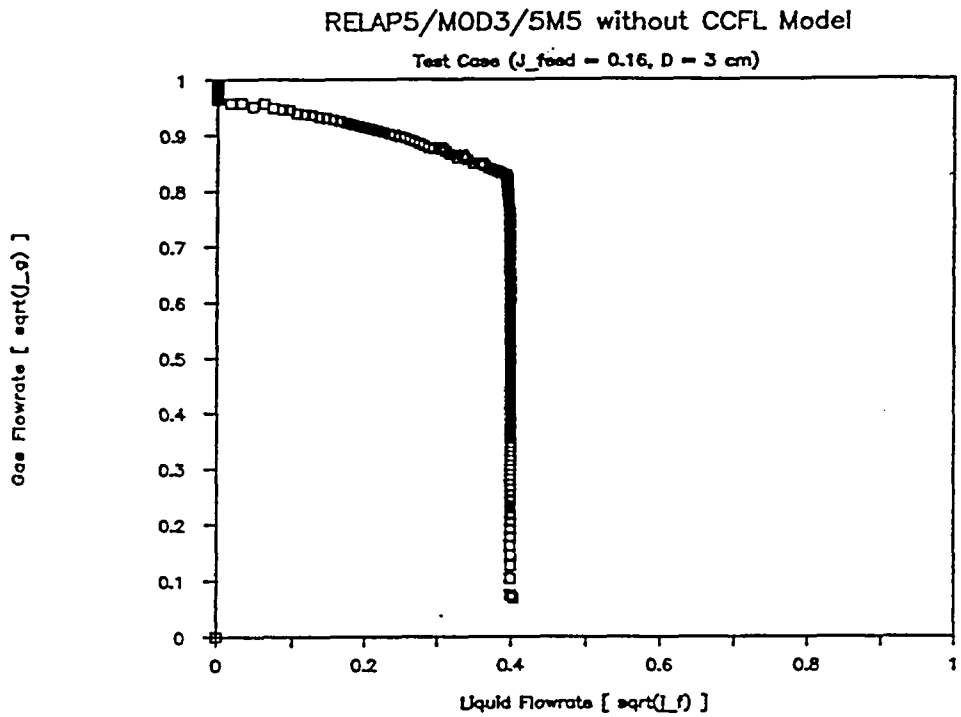

Fig. 5.9 Calculated Flooding Data without CCFL option (D = 3.0 cm)

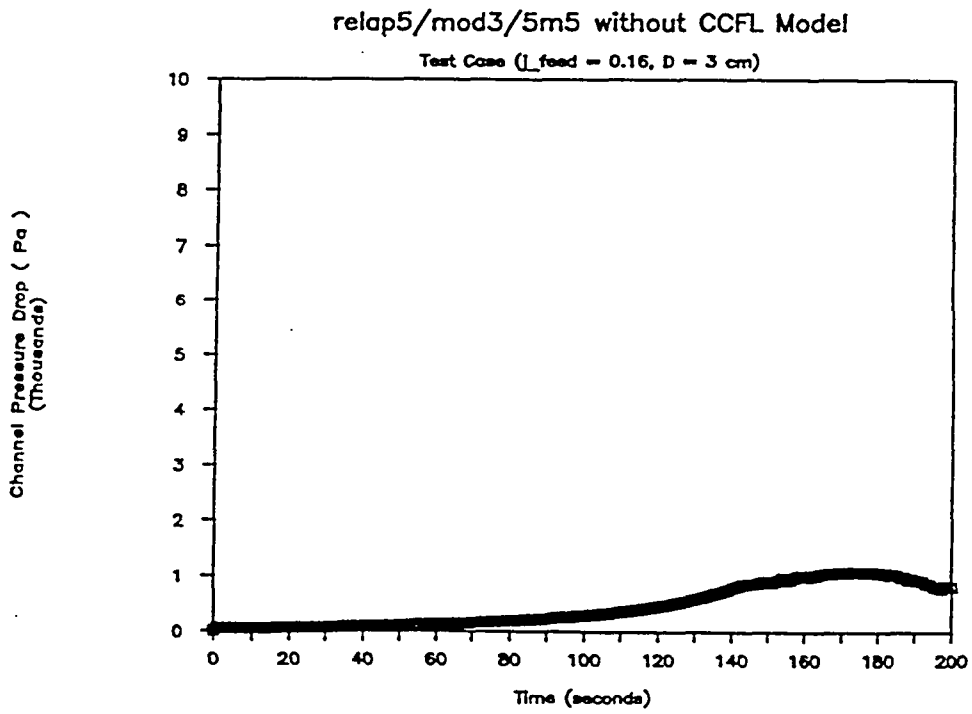

Fig. 5.10 Pressure Drop in the Test Section (D = 3.0 cm)

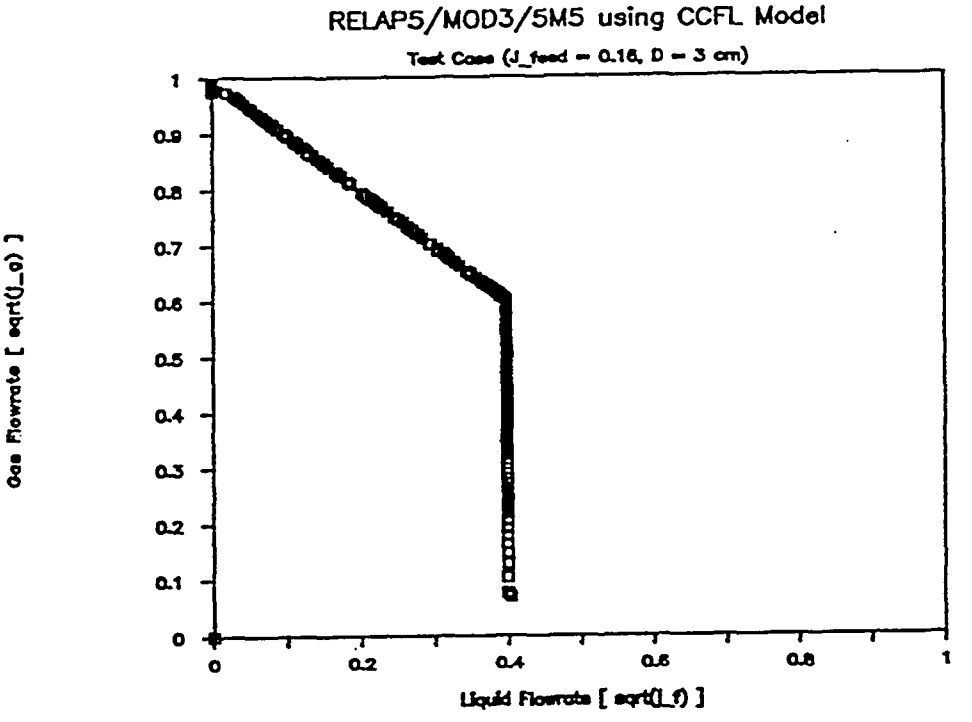

Fig. 5.11 Calculated Flooding Data with CCFL option (D = 3.0 cm)

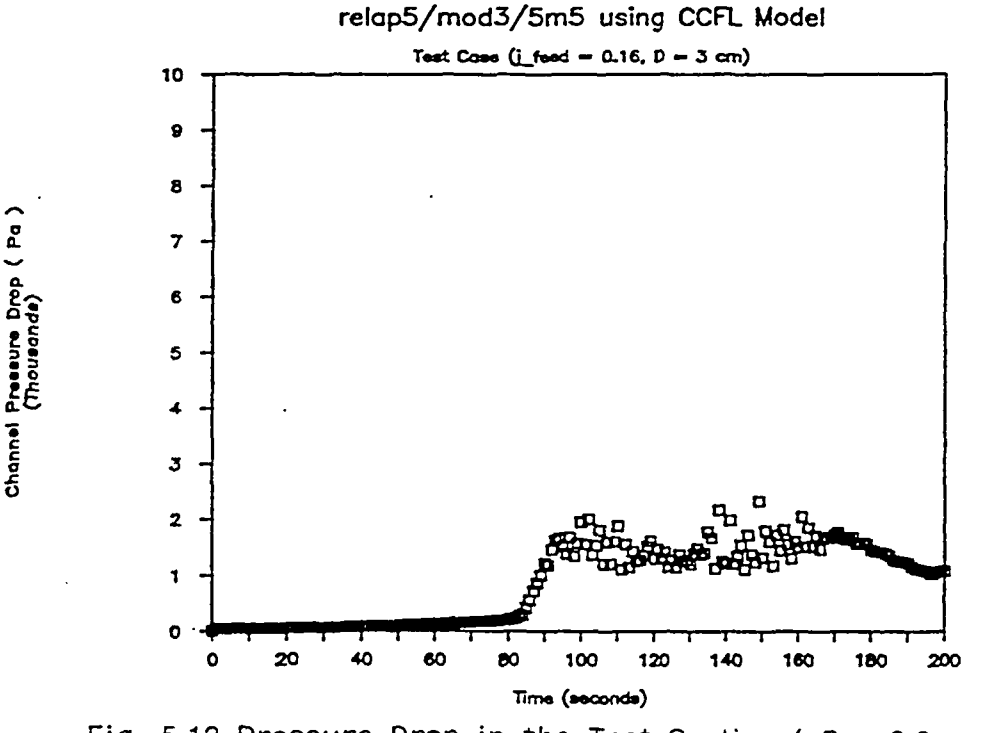

Fig. 5.12 Pressure Drop in the Test Section (D = 3.0 cm)

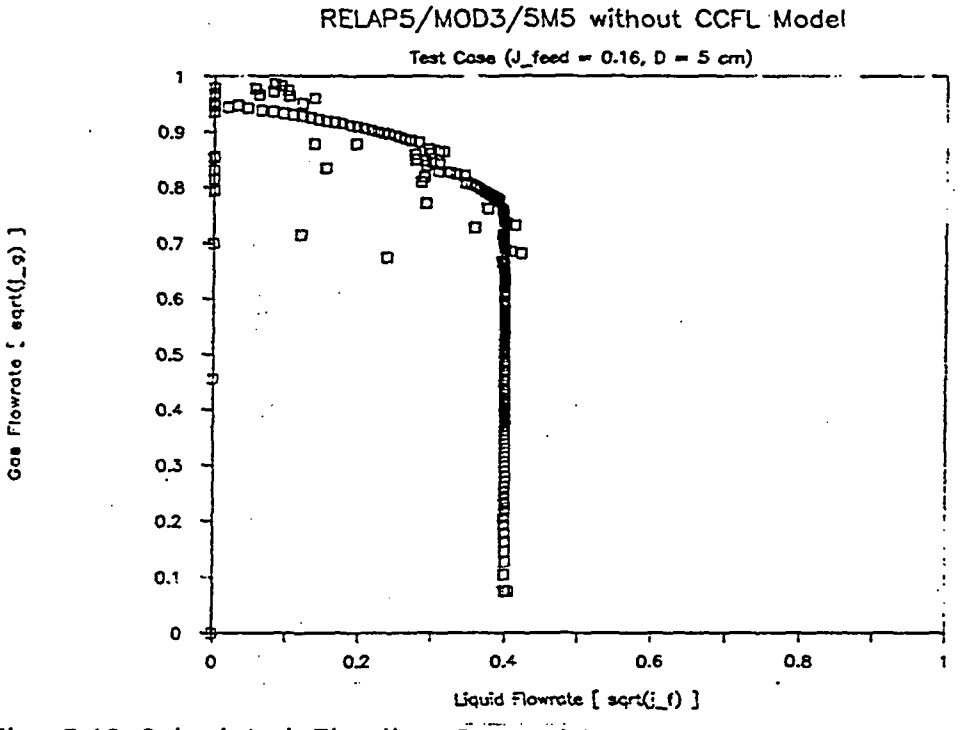

Fig. 5.13 Calculated Flooding Data without CCFL option (D = 5.0 cm)

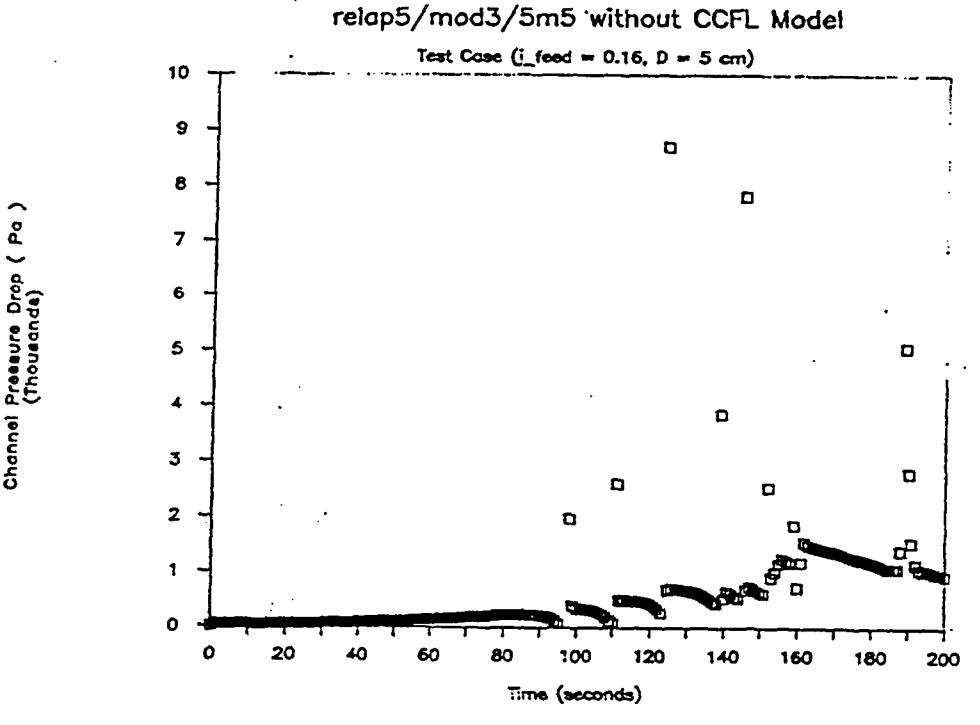

Fig. 5.14 Pressure Drop in the Test Section (D = 5.0 cm)

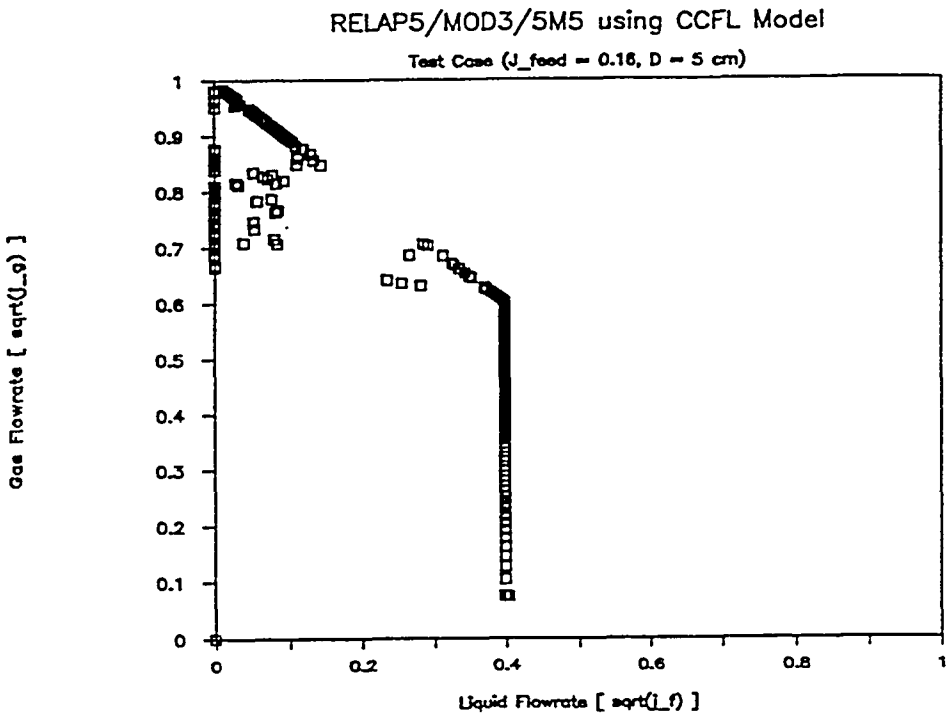

Fig. 5.15 Calculated Flooding Data with CCFL option (D = 5.0 cm)

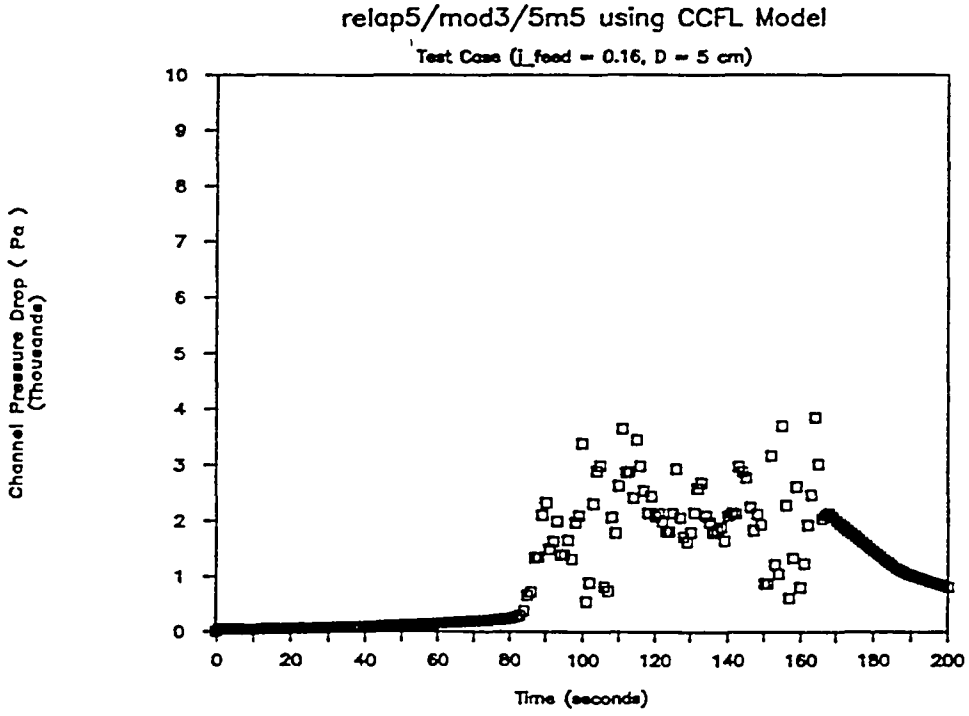

Fig. 5.16 Pressure Drop in the Test Section (D = 5.0 cm)

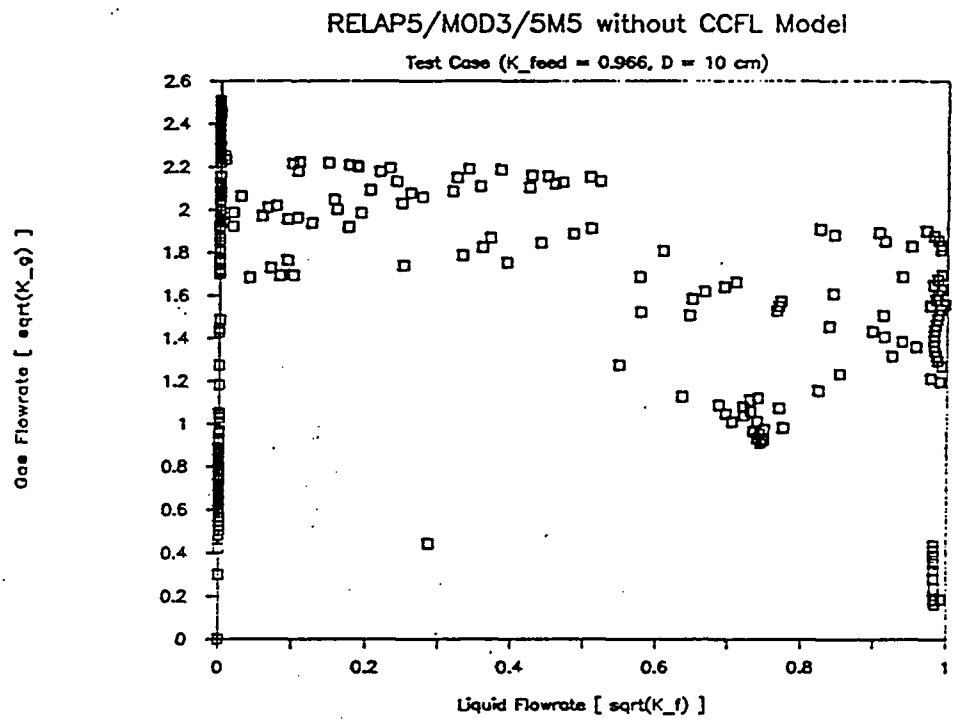

Fig. 5.17 Calculated Flooding Data without CCFL option (D = 10. cm)

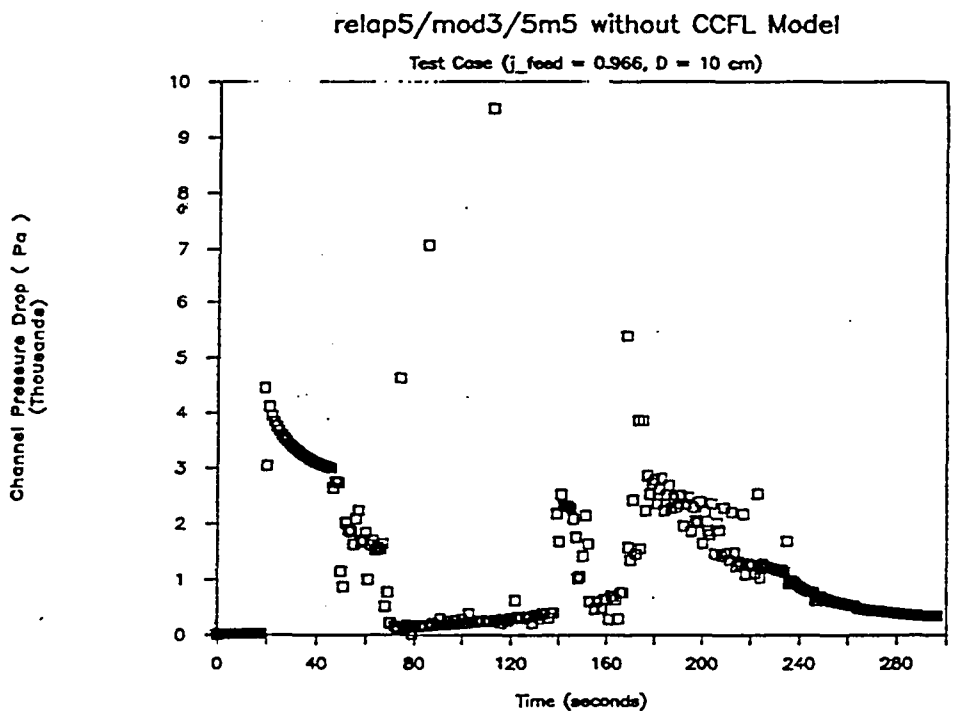

Fig. 5.18 Pressure Drop in the Test Section (D = 10. cm)

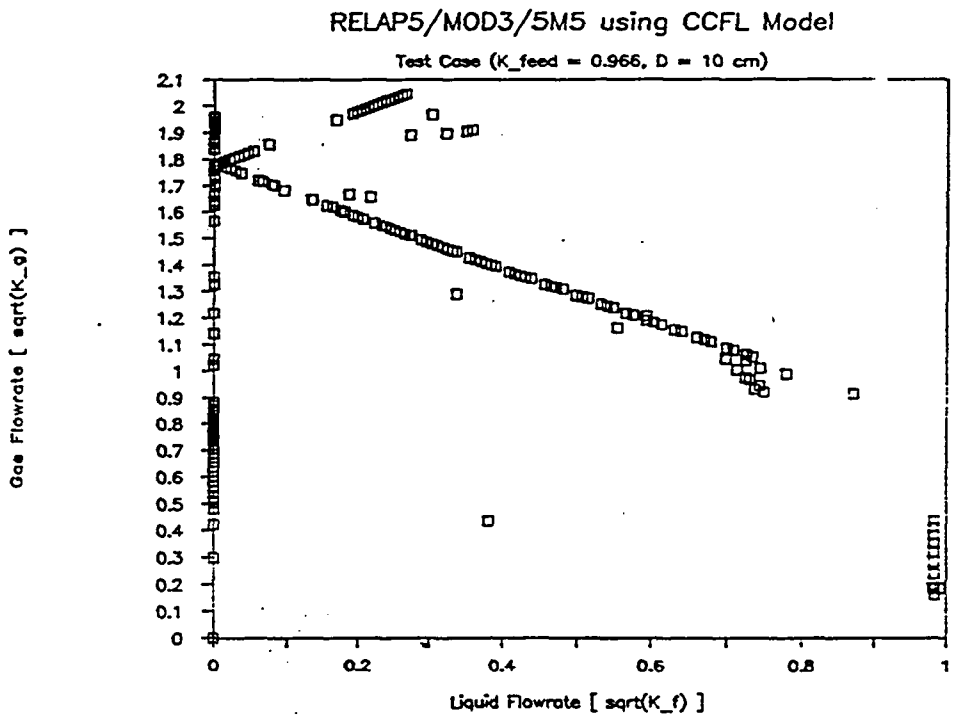

Fig. 5.19 Calculated Flooding Data with CCFL option (D = 10. cm)

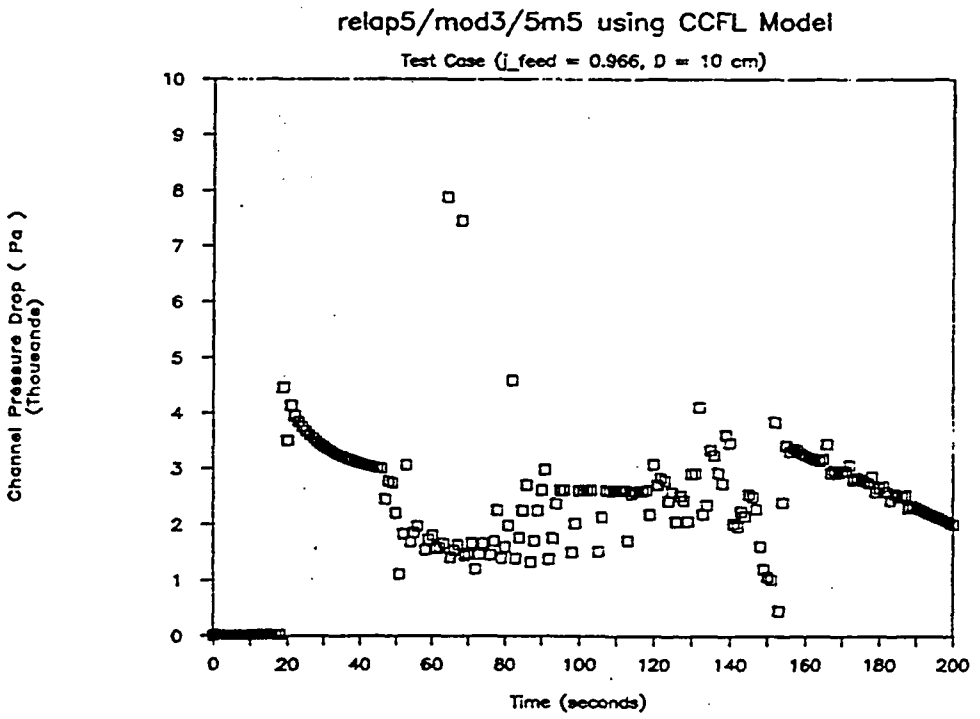

Fig. 5.20 Pressure Drop in the Test Section (D = 10. cm)

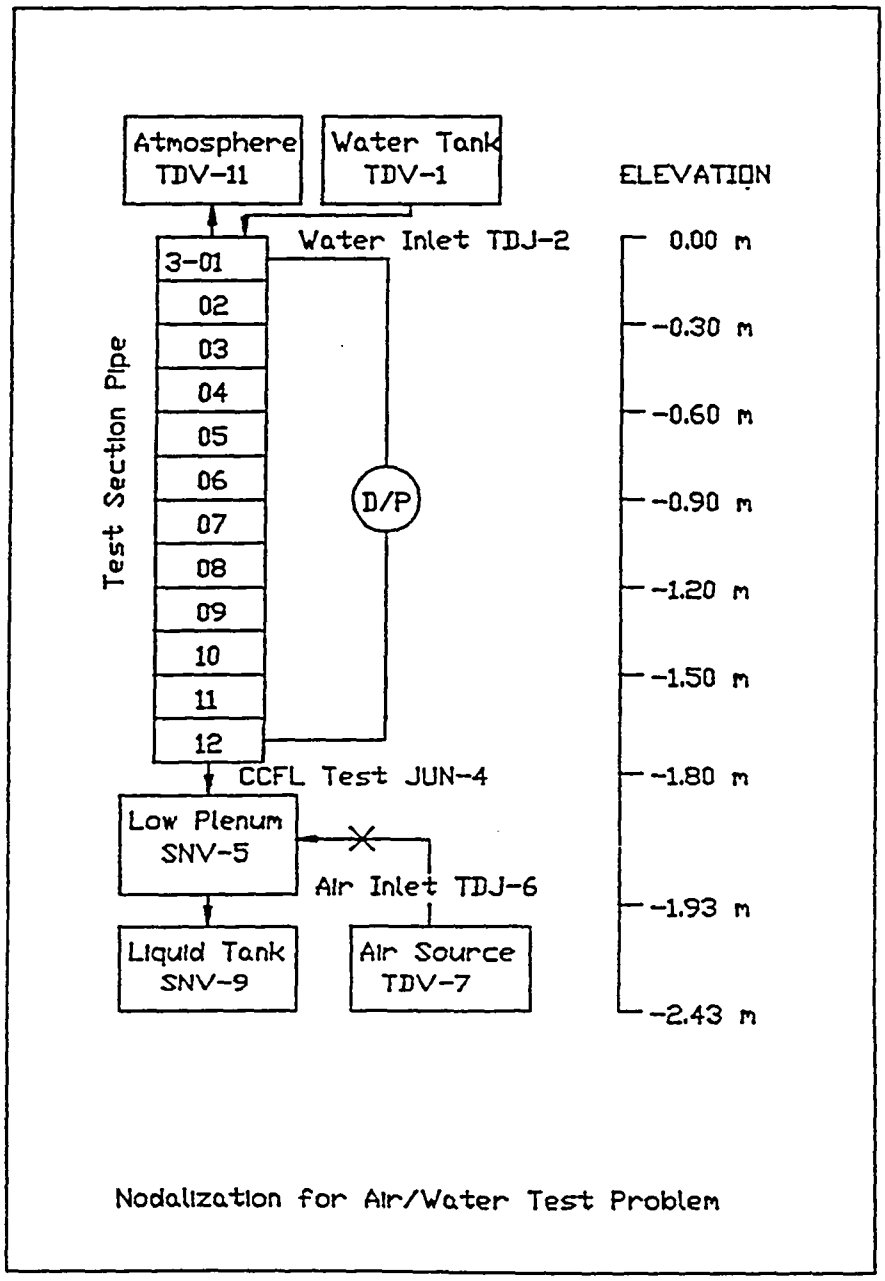

Fig. 5.21 RELAP5 Fine Nodalization for Air/Water Test Problem

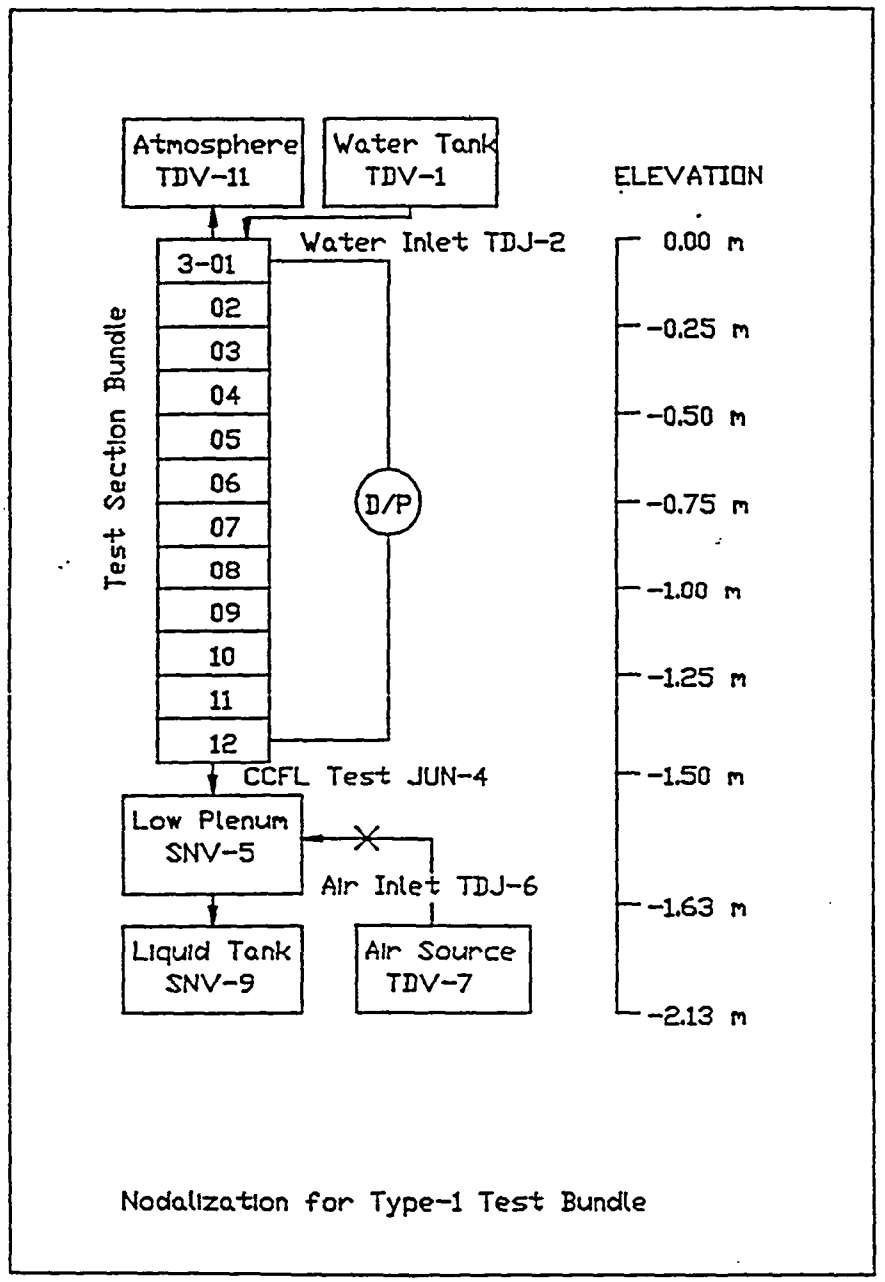

Fig. 5.22 RELAP5 Fine Nodalization for Type-1 Test Bundle

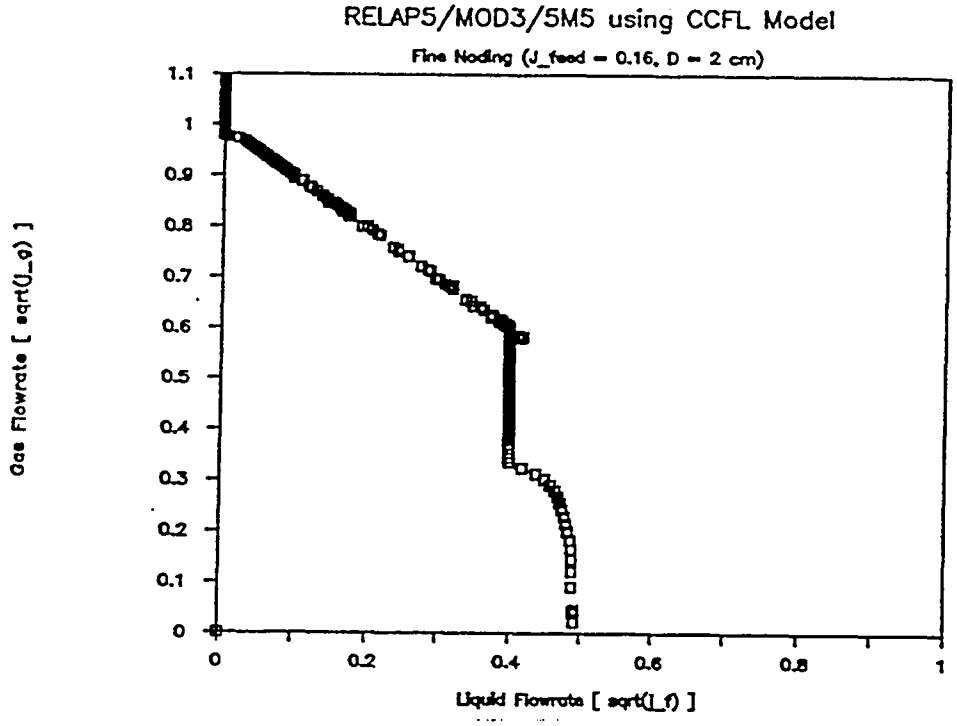

Fig. 5.23 Calculated Flooding Data with Fine Nodalization

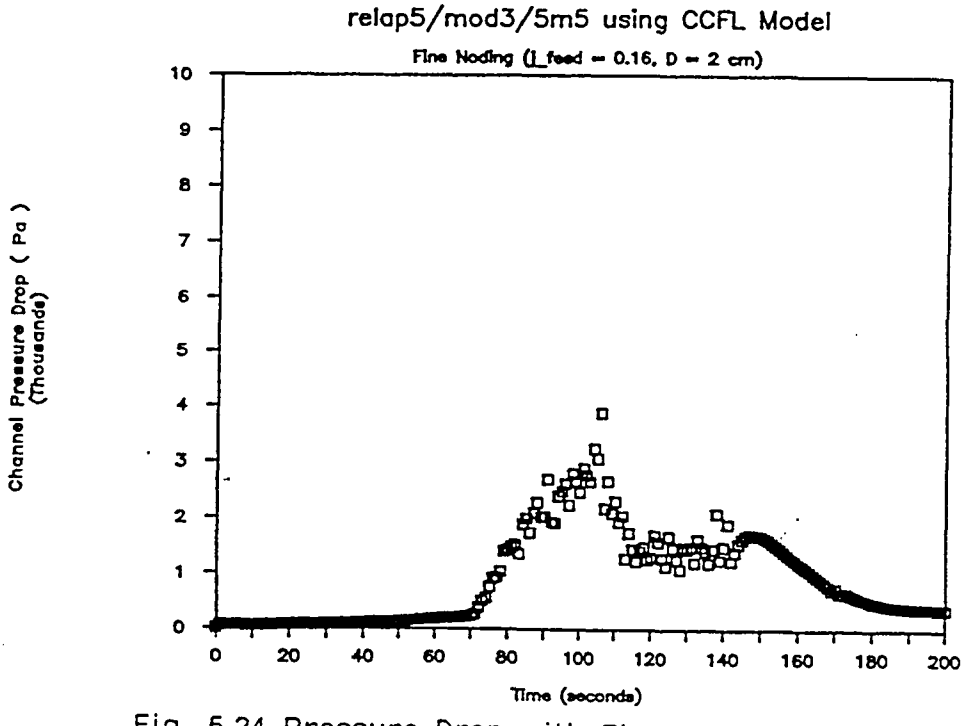

Fig. 5.24 Pressure Drop with Fine Nodalization

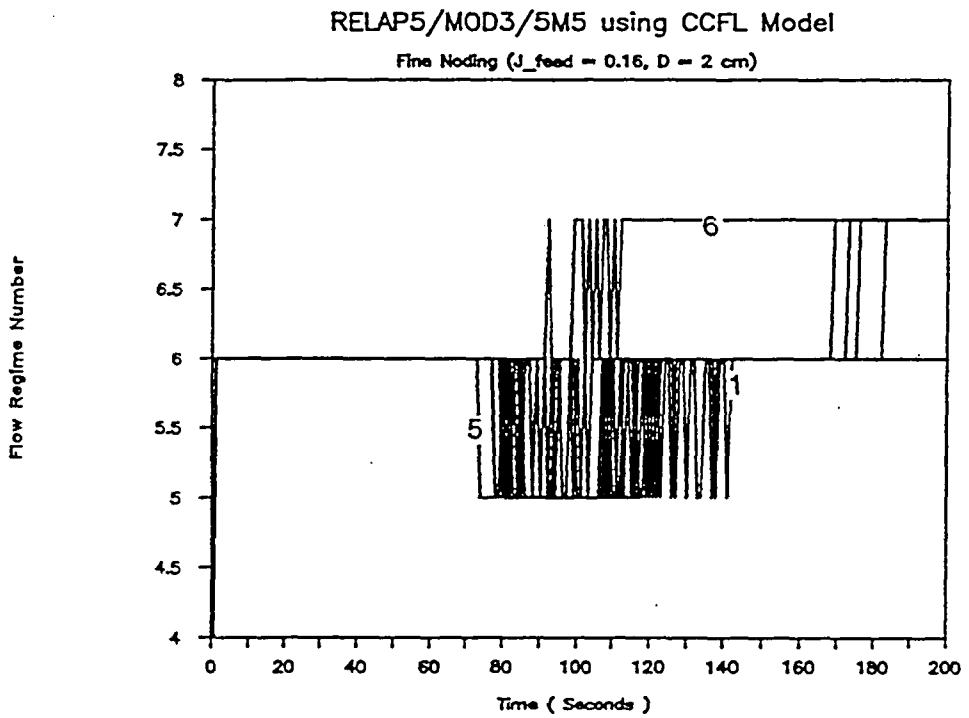

Fig. 5.25 Flow Regime Change at the Test Section Junction
(1 - jun.3010000 : 2 - jun.3020000 : 3 - jun.3030000
4 - jun.3040000 : 5 - jun.3050000 : 6 - jun.4000000)

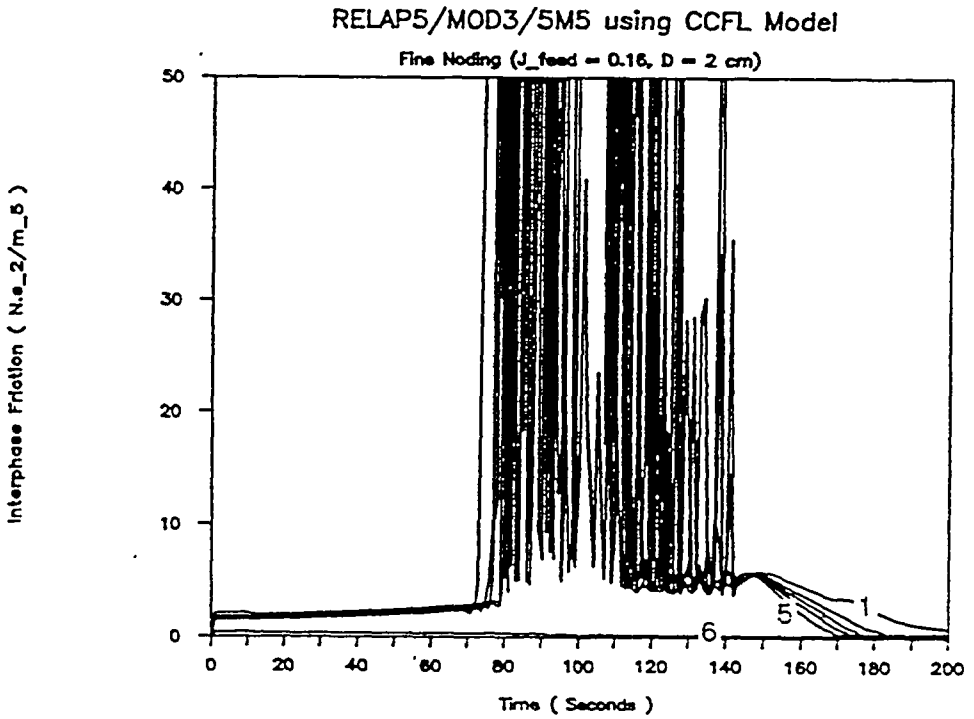

Fig. 5.26 Interfacial Drag Coefficient at the Test Section Junction
(1 - jun.3010000 : 2 - jun.3020000 : 3 - jun.3030000
4 - jun.3040000 : 5 - jun.3050000 : 6 - jun.4000000)

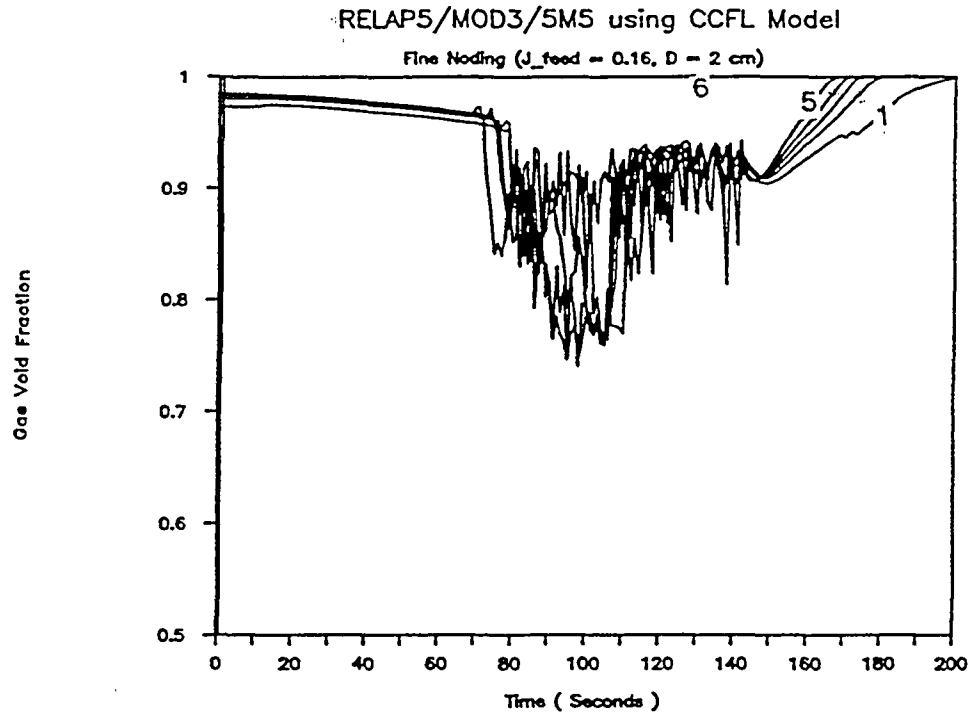

Fig. 5.27 Gas Void Fraction at the Test Section Junction
(1 - jun.3010000 : 2 - jun.3020000 : 3 - jun.3030000
4 - jun.3040000 : 5 - jun.3050000 : 6 - jun.4000000)

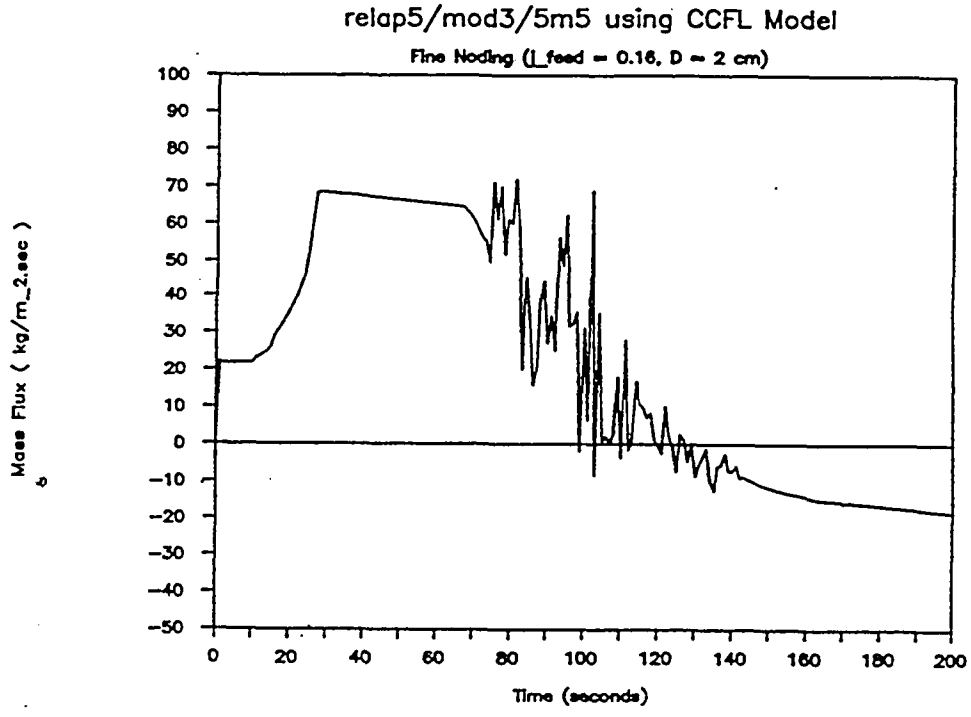

Fig. 5.28 Mass Flux through the Junction 4000000

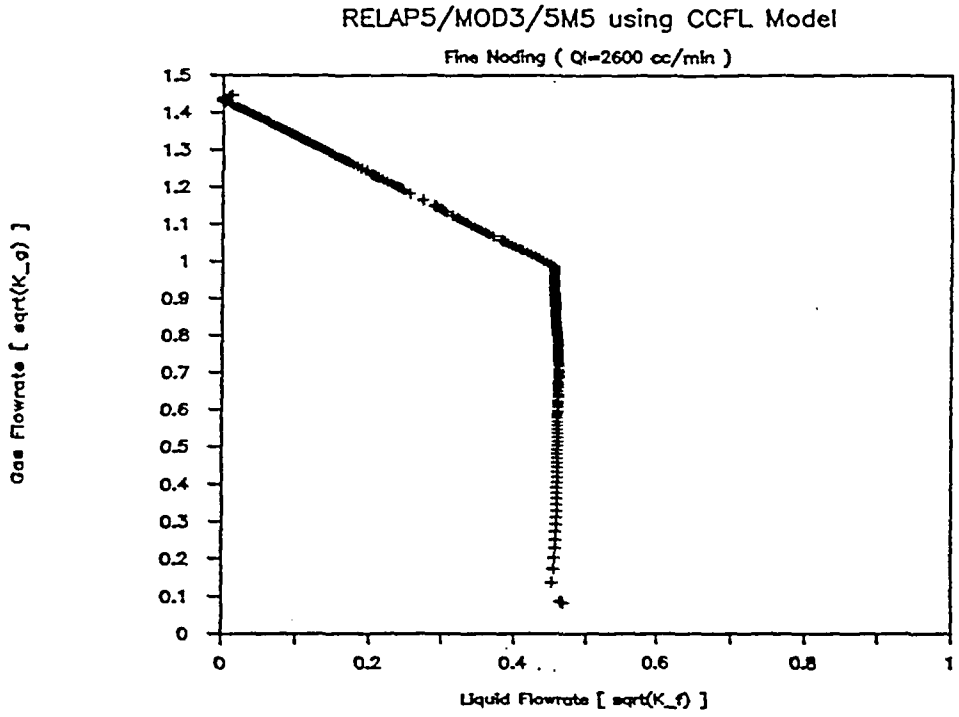

Fig. 5.29 Calculated Flooding Data with Fine Nodalization

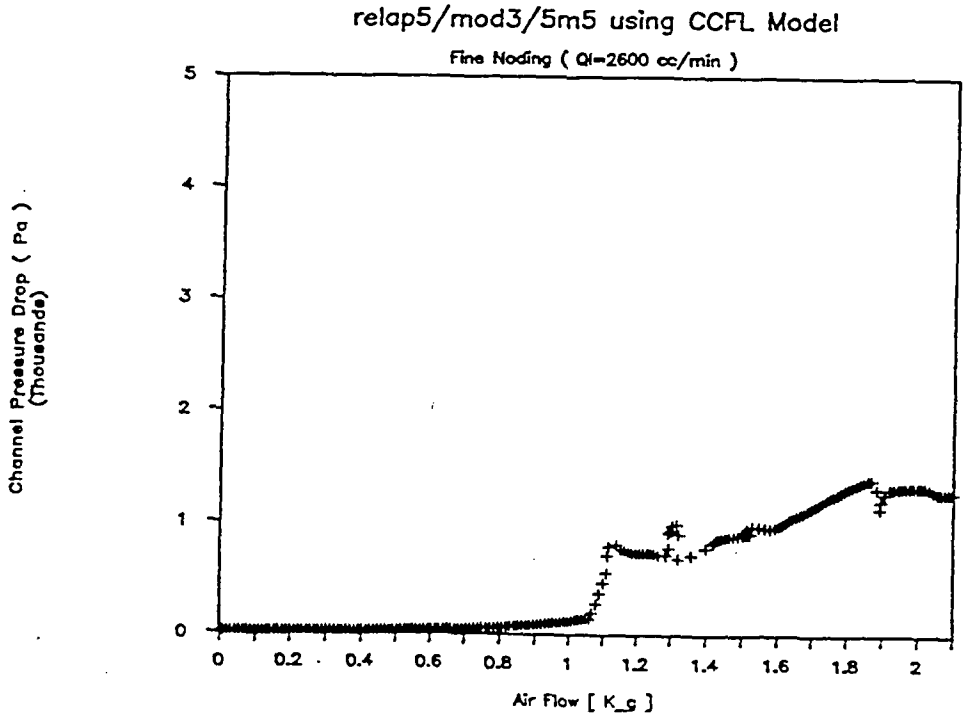

Fig. 5.30 Pressure Drop with Fine Nodalization

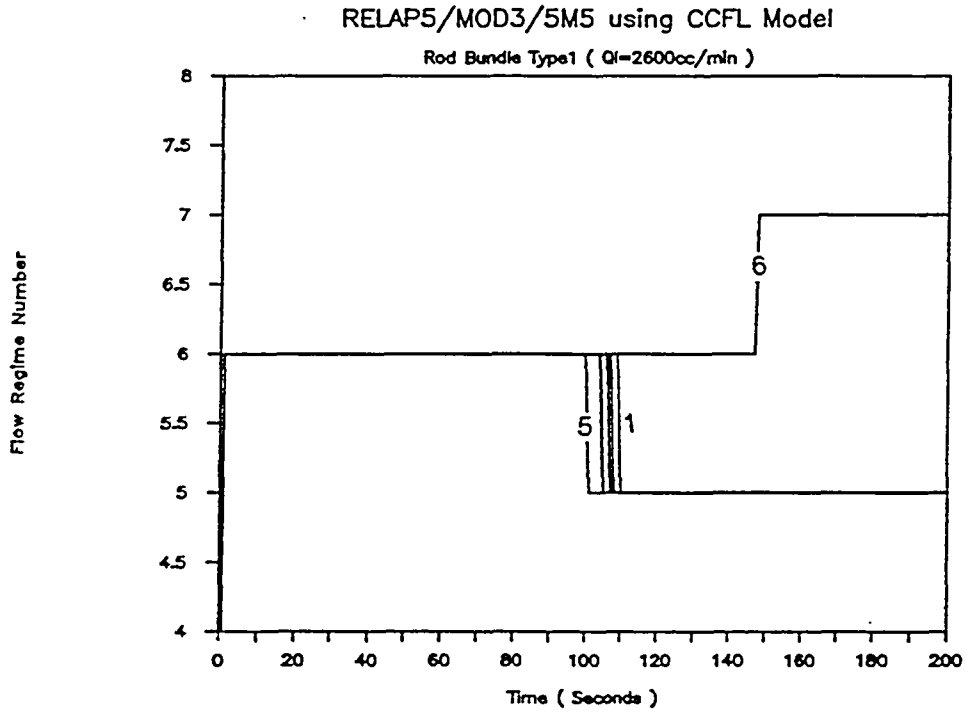

Fig. 5.31 Flow Regime Change at the Test Section Junction
(1 - jun.3010000 : 2 - jun.3020000 : 3 - jun.3030000
4 - jun.3040000 : 5 - jun.3050000 : 6 - jun.4000000)

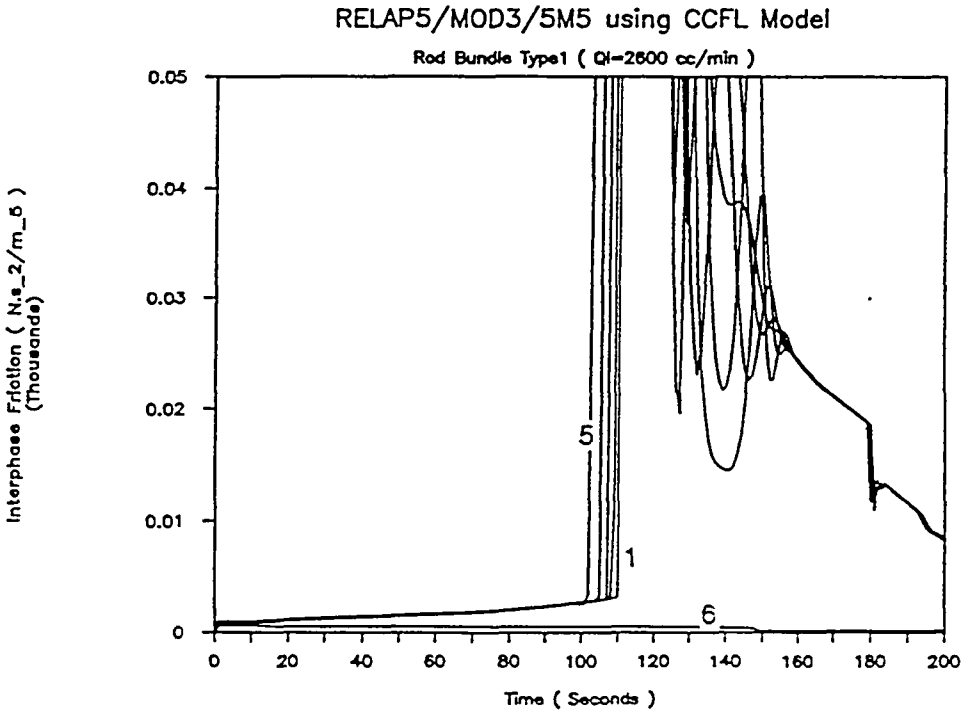

Fig. 5.32 Interfacial Drag Coefficient at the Test Section Junction
(1 - jun.3010000 : 2 - jun.3020000 : 3 - jun.3030000
4 - jun.3040000 : 5 - jun.3050000 : 6 - jun.4000000)

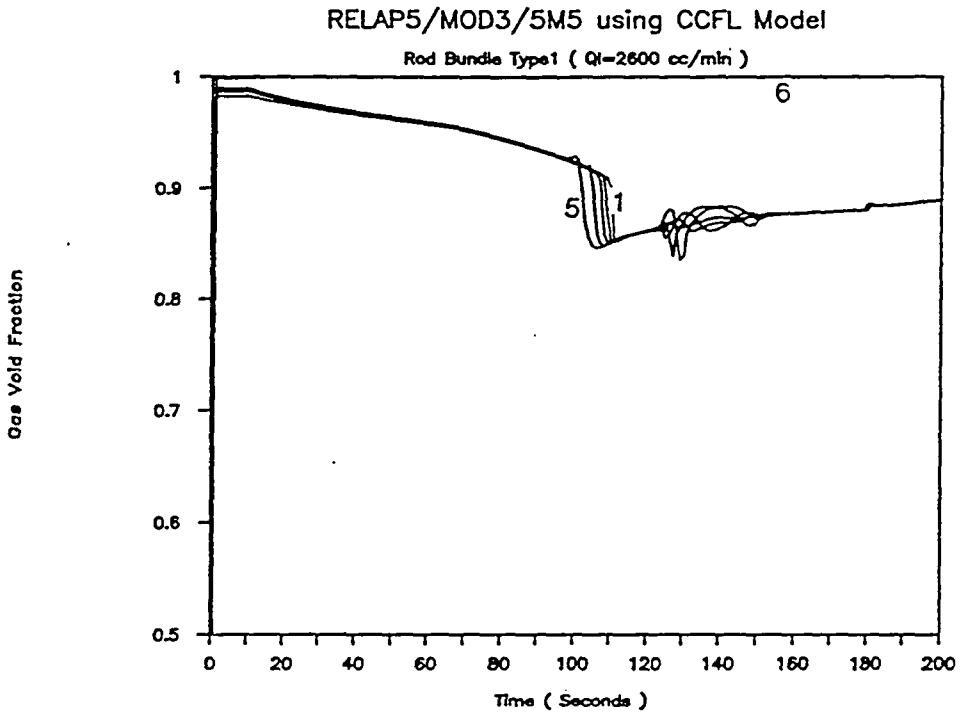

Fig. 5.33 Gas Void Fraction at the Test Section Junction
(1 - jun.3010000 : 2 - jun.3020000 : 3 - jun.3030000
4 - jun.3040000 : 5 - jun.3050000 : 6 - jun.4000000)

6. Run Statistics

The simulation for the CCFL model assessment is not a transient case basically, thus it is meaningless to compare the simulation time. However the range of air flow used to test the CCFL model was obtained by increasing air flow during a given period. Therefore the run time required by the simulation will be helpful for the other assessment or determination of the transient period.

The computer used for the simulation is a CRAY-2S which has 4 central process units, and the operating system is UNICOS. The time step size was fixed as 0.01 second to avoid the numerical instability of the liquid film flow, discussed in the section 4.1. The whole transient time was also fixed as 200 seconds. The computation efficiency is summarized in Table 6.1. A plot of CPU time was not needed because it increases linearly with the transient time.

Table 6.1 CPU time required in the simulation

Case	Transient Real Time (sec)	Computing Time (CPU)	Number of Total Volume (C)	Number of Time Step (DT)	Total Grind Time (CPU/C/DT)
1	200.0	151.52	11	20,000	6.89×10^{-4}
2	200.0	152.34	11	20,000	6.92×10^{-4}
3	200.0	156.41	11	20,000	7.11×10^{-4}
4	200.0	159.83	11	20,000	7.27×10^{-4}
5	200.0	263.14	17	20,000	7.74×10^{-4}

* case 1 : coarse noding without CCFL option in simple tube
* case 2 : coarse noding with CCFL option in simple tube
* case 3 : coarse noding without CCFL option in rod bundle
* case 4 : coarse noding with CCFL option in rod bundle
* case 5 : fine noding with CCFL option in simple tube

7. Conclusion

Assessment calculations for sample problems in a simple tube and a rod bundle were carried out using RELAP5/MOD3/5m5 code. For the purpose of comparison, a pair of calculations were performed with and without CCFL option. Sensitivity studies with respect to the diameter of tube was also performed. In the small diameter case, the flooding was calculated to occur before the CCFL occurred in the experiment, due to the increased interfacial drag force. In the large diameter case, the flooding occurs at a higher gas velocity than the experimental results, when the CCFL model option was not selected. With applying the CCFL option to the specific junction, the calculated values lay well on the curve specified by user, and the pressure oscillations and jump after onset of flooding agreed with most experimental observations. Curious calculation results obtained by specifying the Kutateladze CCFL curve for the large diameter tube may be resulted from a coding error of 5m5 version.

Other assessment calculations were carried out for a rod bundle test, which was performed by KINS(Korea Institute of Nuclear Safety). Calculated results were compared with experimental data for each type of test section ; type-1 which has no spacer grid, type-2 which has one spacer grid, and type-3 which has two spacer grids. A flooding curve which was determined by experiments was applied to the specific junction. Calculated values lay well on the curve specified by user, and the pressure drop increased suddenly just after onset of flooding due to restriction of downward liquid flow at the specific junction. However, the pressure jump before onset of flooding was not calculated because RELAP5 did not have models of "liquid mixing" which was observed in the experiment at the transition area before "onset of flooding".

The fine nodalization for the test section did not affect the

whole flooding phenomena, and it was concluded that the interfacial drag model and CCFL curve given by user mainly characterized the flooding process.

References

1. V.H. Ransom, et al.,"RELAP5/MOD2 Code Manual Volume 1: Code Structure, System Models, and Solution Methods",NUREG/CR-4312 (1985)

2. V.H. Ransom, et al.,"RELAP5/MOD1 Code Manual Volume 1: Code Structure, System Models, and Solution Methods",NUREG/CR-1826 (1982)

3. ICAP Relap5 Newsletter , NUREG/BR-0103,Vol.3, No.4, October (1987)

4. R.A. Riemke, "Report on CCFL and Interphase Drag Model for RELAP5/MOD3", EGG-TFM-8012, February (1988)

5. J.M. Putney, "Development of a New Bubbly-Slug Interfacial Friction Model for RELAP5 - Final Report", CEGB Draft Report, PWR/HTWG/P(89)722, June (1989)

6. G.B. Wallis and S. Makkenchery, "The Hanging Film Phenomena in Vertical Annular Two Phase Flows", Journal of Fluid Engg.,Sep., pp 297-298 (1974)

7. M.H.Chun and B.D.Chung, "Countercurrent Flow Limitation Experiments with Vertical Multi-tube Bundle with and without Spacer Grids", Int. Comm. Heat Mass Transfer, Vol.17, pp.237-246 (1990)

8. M.H.Chun et. al., "Experimental Investigation of Flooding in Air-Water Countercurrent Flow with a vertical adiabatic Multi-rod Bundle", FED-Vol.99, HTD-Vol.155, pp.237-242,Winter Annual Meeting, ASME, Nov. (1990)

9. S.G. Bankoff, R.S. Tankin, M.C. Yuen and C.L. Hsieh,"Countercurrent Flow of Air/Water and Steam/Water through a Horizontal Perforated Plate", Int. J. Heat & Mass Transfer, Vol.24, No.8, pp 1381-1395 (1981)

10. D. Bharathan, G.B. Wallis and H.J. Richter,"Air-water Countercurrent Annular Flow", EPRI NP-1165, Sep. (1979)

Appendix A. Experimental Data for Rod Bundle CCFL Test

Appendix A. Experimental Data for Rod Bundle CCFL Test

Numerical data for experiments of the three type of test section are tabulated as following. In the following tables the oscillation data are presented as averaged value ± 1 standard deviation. The nondimensional conversions are performed by using the physical and geometrical conditions of the present experiment. The conditions used for nondimensional conversions are listed as following.

T_l= Temperature of Liquid = 282 °K
T_g= Temperature of Gas = 280 °K
ρ_f= Density of Liquid = 1000 Kg/m^3
ρ_g= Density of Gas = 1.2713 Kg/m^3
μ_f= Dynamic Viscosity of Liquid = 1303 X 10^{-6}Kg/m.sec
μ_g= Dynamic Viscosity of Gas = 173.9 X 10^{-6}Kg/m.sec
σ = Surface Tension of Liquid = 73.656 X 10^{-3}N/m
g = Universal acceleration Constant = 9.81 m/sec^2
D_H= Equivalent Hydraulic Diameter = 4A/P = 1.03 X 10^{-2}m

The following lists of the nomenclatures are used in tables.

Q_l = Water Injection Rate
K_g^* = Kutateladze Number of Gas Flux = $\rho_g^{0.5}\alpha_g V_g/[g\sigma(\rho_f-\rho_g)]^{0.25}$
K_f^* = Kutateladze Number of Liquid = $\rho_f^{0.5}\alpha_f V_f/[g\sigma(\rho_f-\rho_g)]^{0.25}$
K_l^* = Kutateladze Number of Water Injection
j_g^* = Nondimensional Gas Flux = $\rho_g\alpha_g V_g/[gD_H(\rho_f-\rho_g)]^{0.5}$
j_f^* = Nondimensional Liquid Flux = $\rho_f\alpha_f V_f/[gD_H(\rho_f-\rho_g)]^{0.5}$
j_l^* = Nondimensional Liquid Injection
P^* = Nondimensional Pressure Gradient = $|dP/dz|/[g(\rho_f-\rho_g)]$

Re_Γ = Film Reynolds Number = $4\Gamma/\mu_f$ where Γ denotes film mass flowrate per unit width

V_c^* = Critical Nondimensional Gas Velocity

$$= \frac{\mu_f V_{g,c}}{\sigma} (\rho_g/\rho_f)^{0.5} (1/N_\mu)^{0.8},$$

where N_μ = Viscosity Number = $\mu_f/[\rho_f\sqrt{\sigma/g(\rho_f-\rho_g)}]^{1/2}$

$V_{g,c}$ = Gas Velocity which results flooding

Test Data for Single Phase Air Flow in Bare Rod Bundle
Q_l = 0 cc/min T_l = 282 °K T_g = 280 °K

	Air Flowrate (1000 cc/sec)	Channel Velocity (m/sec)	Pressure Drop (mm-H2O)	Liquid Flowrate Downward (cc/min)	Liquid Flowrate Upward (cc/min)
1	0.252± 0.257	0.224	1.3 ± 3.7	0.0	0.0
2	5.150± 0.061	4.573	16.4 ± 0.0	0.0	0.0
3	5.799± 0.053	5.149	20.8 ± 2.8	0.0	0.0
4	6.825± 0.023	6.061	25.2 ± 1.2	0.0	0.0
5	8.207± 0.066	7.288	34.0 ± 0.3	0.0	0.0
6	9.134± 0.053	8.111	38.4 ± 0.0	0.0	0.0
7	9.718± 0.046	8.629	43.8 ± 0.5	0.0	0.0
8	11.240± 0.053	9.981	77.7 ± 0.5	0.0	0.0
9	11.732± 0.063	10.418	79.2 ± 1.3	0.0	0.0

Nondimensional Form of Test Data

$K_l^* = 0.0$ $j_l^* = 0.0$ $Re_T = 0.0$ $V_c^* = 0.0$

	K_g^*	P^*	K_f^*	K_c^*	j_g^*	j_f^*	j_c^*
1	0.049± 0.050	0.001± 0.004	0.000	0.000	0.025± 0.026	0.000	0.000
2	0.995± 0.012	0.016± 0.000	0.000	0.000	0.513± 0.006	0.000	0.000
3	1.120± 0.010	0.021± 0.003	0.000	0.000	0.578± 0.005	0.000	0.000
4	1.318± 0.005	0.025± 0.001	0.000	0.000	0.680± 0.002	0.000	0.000
5	1.586± 0.013	0.034± 0.000	0.000	0.000	0.818± 0.007	0.000	0.000
6	1.765± 0.010	0.038± 0.000	0.000	0.000	0.911± 0.005	0.000	0.000
7	1.877± 0.009	0.044± 0.000	0.000	0.000	0.969± 0.005	0.000	0.000
8	2.171± 0.010	0.078± 0.001	0.000	0.000	1.120± 0.005	0.000	0.000
9	2.266± 0.012	0.079± 0.001	0.000	0.000	1.169± 0.006	0.000	0.000

Test Data for Two Phase Air Flow in Bare Rod Bundle
Q_l = 230 cc/min T_l = 282 °K T_g = 280 °K

	Air Flowrate (1000 cc/sec)	Channel Velocity (m/sec)	Pressure Drop (mm-H2O)	Liquid Flowrate Downward (cc/min)	Liquid Flowrate Upward (cc/min)
1	0.000± 0.000	0.000	26.7 ± 2.3	227.5	0.0
2	6.764± 0.035	6.007	28.4 ± 6.0	227.5	0.0
3	7.853± 0.016	6.974	33.9 ± 2.7	227.5	0.0
4	9.055± 0.069	8.041	82.7 ± 4.1	85.8	141.6
5	9.456± 0.044	8.397	94.7 ± 6.8	62.2	165.3
6	9.844± 0.054	8.741	110.3 ± 6.9	38.6	188.9
7	10.736± 0.026	9.533	80.5 ± 3.5	23.6	203.9
8	11.248± 0.073	9.988	82.3 ± 1.9	0.0	227.5
9	8.823± 0.012	7.834	91.9 ± 7.7	79.4	148.1
10	8.448± 0.066	7.502	99.1 ± 7.3	126.6	100.9
11	8.083± 0.039	7.178	111.9 ± 9.2	156.7	70.8

Nondimensional Form of Test Data

$K_l^* = 0.021$ $j_l^* = 0.011$ $Re_T = 43.7$ $V_c^* = 1.323$

	K_g^*	P^*	K_f^*	K_c^*	j_g^*	j_f^*	j_c^*
1	0.000± 0.000	0.027± 0.002	0.021	0.000	0.000± 0.000	0.011	0.000
2	1.307± 0.007	0.028± 0.006	0.021	0.000	0.674± 0.004	0.011	0.000
3	1.517± 0.003	0.034± 0.003	0.021	0.000	0.783± 0.002	0.011	0.000
4	1.749± 0.013	0.083± 0.004	0.008	0.013	0.903± 0.007	0.004	0.007
5	1.827± 0.009	0.095± 0.007	0.006	0.015	0.943± 0.004	0.003	0.008
6	1.902± 0.010	0.110± 0.007	0.003	0.017	0.981± 0.005	0.002	0.009
7	2.074± 0.005	0.081± 0.004	0.002	0.018	1.070± 0.003	0.001	0.009
8	2.173± 0.014	0.082± 0.002	0.000	0.021	1.121± 0.007	0.000	0.011
9	1.704± 0.002	0.092± 0.008	0.007	0.013	0.879± 0.001	0.004	0.007
10	1.632± 0.013	0.099± 0.007	0.011	0.009	0.842± 0.007	0.006	0.005
11	1.562± 0.008	0.112± 0.009	0.014	0.006	0.806± 0.004	0.007	0.003

Test Data for Two Phase Air Flow in Bare Rod Bundle
Q_l = 530 cc/min T_l = 282 °K T_g = 280 °K

	Air Flowrate (1000 cc/sec)	Channel Velocity (m/sec)	Pressure Drop (mm-H2O)	Liquid Flowrate Downward (cc/min)	Liquid Flowrate Upward (cc/min)
1	0.000± 0.000	0.000	25.6 ± 2.2	530.1	0.0
2	6.195± 0.023	5.501	55.5 ± 0.0	530.1	0.0
3	7.220± 0.072	6.411	123.3 ± 12.2	530.1	0.0
4	7.453± 0.045	6.618	130.0 ± 11.7	354.1	149.3
5	7.818± 0.045	6.942	127.7 ± 10.7	255.4	247.7
6	8.058± 0.051	7.155	122.7 ± 7.9	176.0	327.5
7	8.332± 0.020	7.399	119.2 ± 7.4	137.4	365.5
8	10.041± 0.034	8.916	87.3 ± 3.8	57.9	450.7
9	11.710± 0.072	10.399	85.9 ± 4.9	0.0	530.5

Nondimensional Form of Test Data

$K_l^* = 0.048$ $j_l^* = 0.025$ $Re_T = 100.7$ $V_c^* = 1.235$

	K_g^*	P^*	K_f^*	K_c^*	j_g^*	j_f^*	j_c^*
1	0.000± 0.000	0.026± 0.002	0.048	0.027	0.000± 0.000	0.025	0.000
2	1.197± 0.004	0.056± 0.000	0.048	0.027	0.618± 0.002	0.025	0.000
3	1.395± 0.014	0.123± 0.012	0.048	0.027	0.720± 0.007	0.025	0.000
4	1.440± 0.009	0.130± 0.012	0.032	0.040	0.743± 0.005	0.016	0.007
5	1.510± 0.009	0.128± 0.011	0.023	0.042	0.779± 0.004	0.012	0.012
6	1.557± 0.010	0.123± 0.008	0.016	0.044	0.803± 0.005	0.008	0.015
7	1.610± 0.004	0.119± 0.007	0.012	0.046	0.831± 0.002	0.006	0.017
8	1.940± 0.007	0.087± 0.004	0.005	0.041	1.001± 0.003	0.003	0.021
9	2.262± 0.014	0.086± 0.005	0.000	0.036	1.167± 0.007	0.000	0.025

Test Data for Two Phase Air Flow in Bare Rod Bundle
Q_l = 730 cc/min T_l = 282 °K T_g = 280 °K

	Air Flowrate (1000 cc/sec)	Channel Velocity (m/sec)	Pressure Drop (mm-H2O)	Liquid Flowrate Downward (cc/min)	Upward (cc/min)
1	0.535± 0.134	0.475	38.4 ± 0.6	727.6	-0.0
2	6.228± 0.024	5.530	57.3 ± 1.6	727.6	-0.0
3	6.829± 0.023	6.065	139.3 ± 11.5	706.1	21.5
4	7.287± 0.060	6.471	135.5 ± 12.6	530.1	197.5
5	7.677± 0.064	6.817	134.7 ± 11.6	321.9	405.6
6	8.045± 0.047	7.144	130.7 ± 11.2	216.8	510.8
7	8.299± 0.027	7.370	127.5 ± 8.3	176.0	551.6
8	8.472± 0.068	7.523	124.7 ± 6.8	133.1	594.5
9	8.946± 0.046	7.944	116.4 ± 4.0	118.0	609.5
10	9.683± 0.038	8.599	101.3 ± 2.4	57.9	669.6
11	10.375± 0.030	9.213	85.4 ± 4.0	0.0	727.6
12	10.807± 0.042	9.597	80.5 ± 2.2	0.0	727.6
13	11.421± 0.043	10.142	84.7 ± 2.7	0.0	727.6
14	8.396± 0.047	7.456	123.2 ± 6.3	137.4	590.2
15	7.859± 0.020	6.979	133.5 ± 10.2	236.1	491.5
16	7.176± 0.080	6.372	139.0 ± 11.4	510.8	216.8
17	7.336± 0.020	6.515	136.4 ± 11.4	491.5	236.1
18	7.466± 0.048	6.630	134.1 ± 11.4	431.4	296.2
19	7.704± 0.074	6.841	133.7 ± 10.5	313.3	414.2

Nondimensional Form of Test Data

$K_l^* = 0.066$ $j_l^* = 0.034$ $Re_T = 138.7$ $V_c^* = 1.147$

	K_g^*	P^*	K_f^*	K_c^*	j_g^*	j_f^*	j_c^*
1	0.103± 0.026	0.038± 0.001	0.066	-0.000	0.053± 0.013	0.034	-0.000
2	1.203± 0.005	0.057± 0.002	0.066	-0.000	0.621± 0.002	0.034	-0.000
3	1.319± 0.005	0.139± 0.012	0.064	0.002	0.681± 0.002	0.033	0.001
4	1.408± 0.012	0.136± 0.013	0.048	0.018	0.726± 0.006	0.025	0.009
5	1.483± 0.012	0.135± 0.012	0.029	0.037	0.765± 0.006	0.015	0.019
6	1.554± 0.009	0.131± 0.011	0.020	0.046	0.802± 0.005	0.010	0.024
7	1.603± 0.005	0.128± 0.008	0.016	0.050	0.827± 0.003	0.008	0.026
8	1.637± 0.013	0.125± 0.007	0.012	0.054	0.844± 0.007	0.006	0.028
9	1.728± 0.009	0.117± 0.004	0.011	0.055	0.892± 0.005	0.005	0.028
10	1.871± 0.007	0.101± 0.002	0.005	0.060	0.965± 0.004	0.003	0.031
11	2.004± 0.006	0.086± 0.004	0.000	0.066	1.034± 0.003	0.000	0.034
12	2.088± 0.008	0.081± 0.002	0.000	0.066	1.077± 0.004	0.000	0.034
13	2.206± 0.008	0.085± 0.003	0.000	0.066	1.138± 0.004	0.000	0.034
14	1.622± 0.009	0.123± 0.006	0.012	0.053	0.837± 0.005	0.006	0.027
15	1.518± 0.004	0.134± 0.010	0.021	0.044	0.783± 0.002	0.011	0.023
16	1.386± 0.016	0.139± 0.011	0.046	0.020	0.715± 0.008	0.024	0.010
17	1.417± 0.004	0.137± 0.011	0.044	0.021	0.731± 0.002	0.023	0.011
18	1.442± 0.009	0.134± 0.011	0.039	0.027	0.744± 0.005	0.020	0.014
19	1.488± 0.014	0.134± 0.011	0.028	0.037	0.768± 0.007	0.015	0.019

Test Data for Two Phase Air Flow in Bare Rod Bundle
Q_l = 1570 cc/min T_l = 282 °K T_g = 280 °K

	Air Flowrate (1000 cc/sec)	Channel Velocity (m/sec)	Pressure Drop (mm-H2O)	Liquid Flowrate Downward (cc/min)	Liquid Flowrate Upward (cc/min)
1	0.052± 0.150	0.046	13.3 ± 0.7	1571.0	-0.0
2	4.711± 0.055	4.183	45.6 ± 7.5	1571.0	-0.0
3	5.715± 0.058	5.075	135.7 ± 15.7	1571.0	0.0
4	6.214± 0.027	5.518	161.1 ± 17.6	1296.3	274.7
5	6.454± 0.063	5.631	161.6 ± 18.4	1098.9	472.2
6	6.563± 0.043	5.827	158.3 ± 14.6	1021.6	549.4
7	6.808± 0.023	6.046	158.3 ± 13.5	903.5	667.5
8	6.892± 0.045	6.120	154.9 ± 14.8	824.1	746.9
9	7.206± 0.076	6.399	153.8 ± 14.1	652.4	918.6
10	7.613± 0.029	6.760	148.9 ± 12.0	354.1	1216.9
11	8.066± 0.045	7.163	140.3 ± 11.8	156.7	1414.3
12	8.290± 0.032	7.361	137.6 ± 11.2	118.0	1453.0
13	8.535± 0.042	7.579	132.8 ± 9.5	79.4	1491.6
14	9.014± 0.049	8.005	123.1 ± 4.6	62.2	1508.8
15	10.065± 0.044	8.937	99.5 ± 5.0	38.6	1532.4
16	10.657± 0.058	9.463	85.1 ± 3.1	0.0	1571.0

Nondimensional Form of Test Data

$K_l^* = 0.142$ $j_l^* = 0.073$ $Re_T = 298.3$ $V_c^* = 1.015$

	K_g^*	P^*	K_f^*	K_c^*	j_g^*	j_f^*	j_c^*
1	0.010± 0.029	0.013± 0.001	0.142	-0.000	0.005± 0.015	0.073	-0.000
2	0.910± 0.011	0.046± 0.007	0.142	-0.000	0.470± 0.005	0.073	-0.000
3	1.104± 0.011	0.136± 0.016	0.142	-0.000	0.570± 0.006	0.073	-0.000
4	1.200± 0.005	0.161± 0.018	0.117	0.025	0.619± 0.003	0.060	0.013
5	1.247± 0.012	0.162± 0.018	0.099	0.043	0.643± 0.006	0.051	0.022
6	1.268± 0.008	0.158± 0.015	0.092	0.050	0.654± 0.004	0.048	0.026
7	1.315± 0.004	0.158± 0.014	0.082	0.060	0.679± 0.002	0.042	0.031
8	1.331± 0.009	0.155± 0.015	0.074	0.067	0.687± 0.004	0.038	0.035
9	1.392± 0.015	0.154± 0.014	0.059	0.083	0.718± 0.008	0.030	0.043
10	1.471± 0.006	0.149± 0.012	0.032	0.110	0.759± 0.003	0.016	0.057
11	1.558± 0.009	0.140± 0.012	0.014	0.128	0.804± 0.005	0.007	0.066
12	1.601± 0.006	0.138± 0.011	0.011	0.131	0.826± 0.003	0.005	0.068
13	1.649± 0.008	0.133± 0.010	0.007	0.135	0.851± 0.004	0.004	0.069
14	1.741± 0.009	0.123± 0.005	0.006	0.136	0.899± 0.005	0.003	0.070
15	1.944± 0.009	0.100± 0.005	0.003	0.138	1.003± 0.004	0.002	0.071
16	2.059± 0.011	0.085± 0.003	0.000	0.142	1.062± 0.006	0.000	0.073

Test Data for Two Phase Air Flow in Bare Rod Bundle
Q_l = 2600 cc/min T_l = 282 °K T_g = 280 °K

	Air Flowrate (1000 cc/sec)	Channel Velocity (m/sec)	Pressure Drop (mm-H2O)	Liquid Flowrate Downward (cc/min)	Upward (cc/min)
1	4.509± 0.120	4.004	55.8 ± 1.5	2590.5	-0.0
2	4.898± 0.065	4.349	187.7 ± 30.1	2590.5	-0.0
3	5.194± 0.059	4.612	210.4 ± 34.6	2120.4	470.0
4	5.517± 0.063	4.900	205.5 ± 31.9	1807.1	783.4
5	5.790± 0.081	5.142	200.4 ± 32.1	1571.0	1019.4
6	5.995± 0.103	5.324	197.9 ± 29.9	1491.6	1098.9
7	6.377± 0.080	5.663	189.8 ± 25.5	1216.9	1373.6
8	6.832± 0.027	6.066	172.9 ± 18.0	942.2	1648.3
9	7.441± 0.045	6.608	159.3 ± 14.3	588.1	2002.4
10	8.136± 0.061	7.225	146.2 ± 12.5	156.7	2433.8
11	8.387± 0.042	7.448	140.5 ± 12.1	79.4	2511.1
12	9.114± 0.061	8.093	125.5 ± 7.5	62.2	2528.2
13	10.056± 0.040	8.929	108.8 ± 7.1	0.0	2590.5

Nondimensional Form of Test Data

$K_l^* = 0.234$ $j_l^* = 0.121$ $Re_T = 494.0$ $V_c^* = 0.794$

	K_g^*	P^*	K_f^*	K_c^*	j_g^*	j_f^*	j_c^*
1	0.871± 0.023	0.056± 0.001	0.234	-0.000	0.449± 0.012	0.121	-0.000
2	0.946± 0.013	0.188± 0.030	0.234	-0.000	0.488± 0.006	0.121	-0.000
3	1.003± 0.011	0.211± 0.035	0.191	0.042	0.518± 0.006	0.099	0.022
4	1.066± 0.012	0.206± 0.032	0.163	0.071	0.550± 0.006	0.084	0.036
5	1.119± 0.016	0.201± 0.032	0.142	0.092	0.577± 0.008	0.073	0.047
6	1.158± 0.020	0.198± 0.030	0.135	0.099	0.598± 0.010	0.069	0.051
7	1.232± 0.015	0.190± 0.026	0.110	0.124	0.636± 0.008	0.057	0.064
8	1.320± 0.005	0.173± 0.018	0.085	0.149	0.681± 0.003	0.044	0.077
9	1.438± 0.009	0.159± 0.014	0.053	0.181	0.742± 0.005	0.027	0.093
10	1.572± 0.012	0.146± 0.012	0.014	0.220	0.811± 0.006	0.007	0.113
11	1.620± 0.008	0.141± 0.012	0.007	0.227	0.836± 0.004	0.004	0.117
12	1.761± 0.012	0.126± 0.008	0.006	0.228	0.908± 0.006	0.003	0.118
13	1.943± 0.008	0.109± 0.007	0.000	0.234	1.002± 0.004	0.000	0.121

Test Data for Two Phase Air Flow in Bare Rod Bundle

Q_l = 3600 cc/min T_l = 282 °K T_g = 280 °K

	Air Flowrate (1000 cc/sec)	Channel Velocity (m/sec)	Pressure Drop (mm-H2O)	Liquid Flowrate Downward (cc/min)	Liquid Flowrate Upward (cc/min)
1	4.137± 0.118	3.673	39.6 ± 8.1	3612.1	-0.0
2	4.580± 0.155	4.067	194.3 ± 37.2	3219.3	392.8
3	5.110± 0.092	4.538	213.5 ± 32.7	2199.9	1412.2
4	5.355± 0.124	4.756	218.1 ± 29.2	1901.5	1710.5
5	5.900± 0.076	5.239	208.1 ± 25.1	1455.1	2156.9
6	6.184± 0.036	5.491	201.2 ± 24.2	1373.6	2238.5
7	6.510± 0.054	5.781	188.9 ± 21.5	1139.6	2472.4
8	6.972± 0.062	6.191	176.2 ± 15.3	942.2	2669.9
9	7.722± 0.083	6.857	156.5 ± 9.8	510.8	3101.3
10	8.172± 0.072	7.257	151.4 ± 10.3	236.1	3376.0
11	8.584± 0.040	7.623	143.5 ± 10.5	79.4	3532.6
12	9.521± 0.072	8.455	118.6 ± 6.7	0.0	3612.1

Nondimensional Form of Test Data

K_l^* = 0.326 j_l^* = 0.128 Re_T = 684.0 V_c^* = 0.706

	K_g^*	P^*	K_f^*	K_c^*	j_g^*	j_f^*	j_c^*
1	0.799± 0.023	0.040± 0.008	0.326	-0.000	0.412± 0.012	0.168	-0.000
2	0.885± 0.030	0.195± 0.037	0.291	0.035	0.457± 0.015	0.150	0.018
3	0.987± 0.018	0.214± 0.033	0.199	0.128	0.509± 0.009	0.102	0.066
4	1.035± 0.024	0.218± 0.029	0.172	0.154	0.534± 0.012	0.089	0.080
5	1.140± 0.015	0.208± 0.025	0.131	0.195	0.588± 0.008	0.068	0.100
6	1.195± 0.007	0.201± 0.024	0.124	0.202	0.616± 0.004	0.064	0.104
7	1.258± 0.011	0.189± 0.022	0.103	0.223	0.649± 0.005	0.053	0.115
8	1.347± 0.012	0.176± 0.015	0.085	0.241	0.695± 0.006	0.044	0.124
9	1.492± 0.016	0.157± 0.010	0.046	0.280	0.770± 0.008	0.024	0.144
10	1.579± 0.014	0.152± 0.010	0.021	0.305	0.815± 0.007	0.011	0.157
11	1.658± 0.008	0.144± 0.010	0.007	0.319	0.856± 0.004	0.004	0.165
12	1.839± 0.014	0.119± 0.007	0.000	0.326	0.949± 0.007	0.000	0.168

Test Data for Single Phase Air Flow in Single Grid Rod Bundle

Q_l = 0 cc/min T_l = 282 °K T_g = 280 °K

	Air Flowrate (1000 cc/sec)	Channel Velocity (m/sec)	Pressure Drop (mm-H2O)	Liquid Flowrate Downward (cc/min)	Liquid Flowrate Upward (cc/min)
1	3.243± 0.102	2.880	15.4 ± 1.3	0.0	0.0
2	4.597± 0.109	4.082	20.8 ± 3.2	0.0	0.0
3	5.524± 0.024	4.905	24.7 ± 2.7	0.0	0.0
4	6.316± 0.058	5.608	29.2 ± 3.2	0.0	0.0
5	7.295± 0.034	6.478	34.2 ± 1.2	0.0	0.0
6	7.842± 0.020	6.963	37.2 ± 1.9	0.0	0.0
7	8.569± 0.023	7.609	42.3 ± 3.3	0.0	0.0
8	8.841± 0.028	7.851	52.6 ± 5.3	0.0	0.0
9	10.134± 0.055	8.999	74.5 ± 3.9	0.0	0.0
10	10.757± 0.035	9.552	88.8 ± 5.4	0.0	0.0

Nondimensional Form of Test Data

$K_l^* = 0.0$ $j_l^* = 0.0$ $Re_T = 0.0$ $V_c^* = 0.0$

	K_g^*	P^*	K_f^*	K_c^*	j_g^*	j_f^*	j_c^*
1	0.626± 0.020	0.015± 0.001	0.000	0.000	0.323± 0.010	0.000	0.000
2	0.888± 0.021	0.021± 0.003	0.000	0.000	0.458± 0.011	0.000	0.000
3	1.067± 0.005	0.025± 0.003	0.000	0.000	0.551± 0.002	0.000	0.000
4	1.220± 0.011	0.029± 0.003	0.000	0.000	0.630± 0.006	0.000	0.000
5	1.409± 0.007	0.034± 0.001	0.000	0.000	0.727± 0.003	0.000	0.000
6	1.515± 0.004	0.037± 0.002	0.000	0.000	0.782± 0.002	0.000	0.000
7	1.655± 0.004	0.042± 0.003	0.000	0.000	0.854± 0.002	0.000	0.000
8	1.708± 0.005	0.053± 0.005	0.000	0.000	0.881± 0.003	0.000	0.000
9	1.958± 0.011	0.075± 0.004	0.000	0.000	1.010± 0.005	0.000	0.000
10	2.078± 0.007	0.089± 0.005	0.000	0.000	1.072± 0.003	0.000	0.000

Test Data for Two Phase Air Flow in Single Grid Rod Bundle
Q_l = 180 cc/min T_l = 282 °K T_g = 280 °K

	Air Flowrate (1000 cc/sec)	Channel Velocity (m/sec)	Pressure Drop (mm-H2O)	Liquid Flowrate Downward (cc/min)	Liquid Flowrate Upward (cc/min)
1	3.434± 0.033	3.050	42.7 ± 3.0	180.6	0.0
2	5.655± 0.045	5.022	56.8 ± 0.8	180.6	0.0
3	7.843± 0.020	6.965	124.4 ± 3.6	157.1	23.6
4	7.980± 0.051	7.086	128.5 ± 5.4	117.8	62.8
5	7.978± 0.059	7.084	130.2 ± 6.6	94.2	86.4
6	8.027± 0.050	7.128	127.9 ± 4.9	110.0	70.7
7	8.277± 0.036	7.350	129.4 ± 6.6	62.8	117.8
8	8.819± 0.015	7.831	120.9 ± 5.1	15.7	164.9
9	8.977± 0.041	7.972	107.2 ± 5.6	4.7	175.9
10	9.374± 0.042	8.325	76.1 ± 3.0	0.0	180.6
11	10.064± 0.042	8.937	54.7 ± 3.0	0.0	180.6

Nondimensional Form of Test Data

$K_l^* = 0.016$ $j_l^* = 0.008$ $Re_T = 34.2$ $V_c^* = 1.323$

	K_g^*	P^*	K_f^*	K_c^*	j_g^*	j_f^*	j_c^*
1	0.663± 0.006	0.043± 0.003	0.016	0.000	0.342± 0.003	0.008	0.000
2	1.092± 0.009	0.057± 0.001	0.016	0.000	0.564± 0.005	0.008	0.000
3	1.515± 0.004	0.125± 0.004	0.014	0.002	0.782± 0.002	0.007	0.001
4	1.542± 0.010	0.129± 0.005	0.011	0.006	0.795± 0.005	0.005	0.003
5	1.541± 0.011	0.130± 0.007	0.009	0.008	0.795± 0.006	0.004	0.004
6	1.551± 0.010	0.128± 0.005	0.010	0.006	0.800± 0.005	0.005	0.003
7	1.599± 0.007	0.130± 0.007	0.006	0.011	0.825± 0.004	0.003	0.005
8	1.704± 0.003	0.121± 0.005	0.001	0.015	0.879± 0.001	0.001	0.008
9	1.734± 0.008	0.107± 0.006	0.000	0.016	0.895± 0.004	0.000	0.008
10	1.811± 0.008	0.076± 0.003	0.000	0.016	0.934± 0.004	0.000	0.008
11	1.944± 0.008	0.055± 0.003	0.000	0.016	1.003± 0.004	0.000	0.008

Test Data for Two Phase Air Flow in Single Grid Rod Bundle
Q_l = 530 cc/min T_l = 282 °K T_g = 280 °K

	Air Flowrate (1000 cc/sec)	Channel Velocity (m/sec)	Pressure Drop (mm-H2O)	Liquid Flowrate Downward (cc/min)	Upward (cc/min)
1	2.554± 0.078	2.268	53.3 ± 4.6	530.1	0.0
2	5.132± 0.067	4.557	71.4 ± 4.4	530.1	0.0
3	6.977± 0.051	6.195	109.7 ± 8.2	432.0	98.2
4	7.318± 0.027	6.498	104.0± 11.1	353.4	149.2
5	7.445± 0.047	6.611	104.8 ± 8.2	255.2	255.2
6	7.865± 0.022	6.984	104.6 ± 8.0	98.2	412.3
7	7.954± 0.047	7.063	88.5 ± 7.4	58.9	471.2
8	8.282± 0.030	7.354	83.0 ± 6.3	39.3	490.9
9	8.361± 0.016	7.424	90.1± 12.8	19.6	510.5
10	8.819± 0.007	7.831	88.1 ± 8.6	3.9	530.0
11	9.228± 0.023	8.195	76.1 ± 3.4	0.0	530.1

Nondimensional Form of Test Data

$K_l^* = 0.048$ $j_l^* = 0.025$ $Re_T = 100.7$ $V_c^* = 1.191$

	K_g^*	P^*	K_f^*	K_c^*	j_g^*	j_f^*	j_c^*
1	0.493± 0.015	0.053± 0.005	0.048	0.000	0.255± 0.008	0.025	0.000
2	0.991± 0.013	0.072± 0.004	0.048	0.000	0.512± 0.007	0.025	0.000
3	1.348± 0.010	0.110± 0.008	0.039	0.009	0.695± 0.005	0.020	0.005
4	1.414± 0.005	0.104± 0.011	0.032	0.013	0.729± 0.003	0.016	0.007
5	1.438± 0.009	0.105± 0.008	0.023	0.023	0.742± 0.005	0.012	0.012
6	1.519± 0.004	0.105± 0.008	0.009	0.037	0.784± 0.002	0.005	0.019
7	1.537± 0.009	0.089± 0.007	0.005	0.043	0.793± 0.005	0.003	0.022
8	1.600± 0.006	0.083± 0.006	0.004	0.044	0.826± 0.003	0.002	0.023
9	1.615± 0.003	0.090± 0.013	0.002	0.046	0.833± 0.002	0.001	0.024
10	1.704± 0.001	0.088± 0.009	0.000	0.048	0.879± 0.001	0.000	0.025
11	1.783± 0.005	0.076± 0.003	0.000	0.048	0.920± 0.002	0.000	0.025

Test Data for Two Phase Air Flow in Single Grid Rod Bundle
Q_l = 750 cc/min T_l = 282 °K T_g = 280 °K

	Air Flowrate (1000 cc/sec)	Channel Velocity (m/sec)	Pressure Drop (mm-H2O)	Liquid Flowrate Downward (cc/min)	Upward (cc/min)
1	2.849± 0.008	2.530	46.1 ± 7.6	746.1	0.0
2	5.495± 0.058	4.879	53.7± 14.8	746.1	0.0
3	6.249± 0.011	5.549	74.1 ± 5.1	742.2	3.9
4	6.895± 0.045	6.122	107.0 ± 9.8	490.9	255.2
5	7.052± 0.047	6.262	108.3 ± 8.4	451.6	294.5
6	7.404± 0.036	6.574	107.1 ± 9.0	294.5	451.6
7	7.792± 0.066	6.919	107.6 ± 7.2	106.0	628.3
8	8.013± 0.052	7.116	105.2 ± 6.7	58.9	687.2
9	8.312± 0.022	7.381	97.1 ± 8.2	19.6	726.5
10	8.630± 0.069	7.664	80.8 ± 2.2	3.9	742.2
11	9.154± 0.048	8.129	71.8 ± 5.9	0.0	746.1

Nondimensional Form of Test Data

$K_l^* = 0.067$ $j_l^* = 0.035$ $Re_T = 142.5$ $V_c^* = 1.059$

	K_g^*	P^*	K_f^*	K_c^*	j_g^*	j_f^*	j_c^*
1	0.550± 0.002	0.046± 0.008	0.067	0.000	0.284± 0.001	0.035	0.000
2	1.061± 0.011	0.054± 0.015	0.067	0.000	0.548± 0.006	0.035	0.000
3	1.207± 0.002	0.074± 0.005	0.067	0.000	0.623± 0.001	0.035	0.000
4	1.332± 0.009	0.107± 0.010	0.044	0.023	0.687± 0.005	0.023	0.012
5	1.362± 0.009	0.108± 0.008	0.041	0.027	0.703± 0.005	0.021	0.014
6	1.430± 0.007	0.107± 0.009	0.027	0.041	0.738± 0.004	0.014	0.021
7	1.505± 0.013	0.108± 0.007	0.010	0.057	0.777± 0.007	0.005	0.029
8	1.548± 0.010	0.105± 0.007	0.005	0.062	0.799± 0.005	0.003	0.032
9	1.606± 0.004	0.097± 0.008	0.002	0.066	0.829± 0.002	0.001	0.034
10	1.667± 0.013	0.081± 0.002	0.000	0.067	0.860± 0.007	0.000	0.035
11	1.768± 0.009	0.072± 0.006	0.000	0.067	0.913± 0.005	0.000	0.035

Test Data for Two Phase Air Flow in Single Grid Rod Bundle

Q_l = 1650 cc/min T_l = 282 °K T_g = 280 °K

	Air Flowrate (1000 cc/sec)	Channel Velocity (m/sec)	Pressure Drop (mm-H2O)	Liquid Flowrate Downward (cc/min)	Upward (cc/min)
1	4.365± 0.054	3.876	72.5 ± 6.3	1649.3	0.0
2	4.714± 0.050	4.186	79.8 ± 6.1	1649.3	7.9
3	5.412± 0.114	4.806	92.0± 11.8	1335.2	314.2
4	5.599± 0.023	4.972	94.0± 11.6	1217.4	432.0
5	6.167± 0.036	5.476	91.7± 10.3	981.7	667.6
6	6.371± 0.078	5.658	105.2± 10.9	824.7	824.7
7	6.666± 0.095	5.920	110.9 ± 9.8	628.3	1021.0
8	7.070± 0.043	6.278	112.0 ± 8.4	353.4	1295.9
9	7.424± 0.048	6.592	108.7 ± 7.7	235.6	1413.7
10	7.922± 0.044	7.035	104.9 ± 7.4	117.8	1531.5
11	8.293± 0.029	7.364	105.4 ± 7.5	39.3	1610.1
12	8.587± 0.025	7.625	79.1 ± 2.5	0.0	1649.3

Nondimensional Form of Test Data

K_l^* = 0.149 j_l^* = 0.077 Re_T = 313.5 V_c^* = 0.750

	K_g^*	P^*	K_f^*	K_c^*	j_g^*	j_f^*	j_c^*
1	0.843± 0.010	0.073± 0.006	0.149	0.000	0.435± 0.005	0.077	0.000
2	0.911± 0.010	0.080± 0.006	0.149	0.001	0.470± 0.005	0.077	0.000
3	1.046± 0.022	0.092± 0.012	0.121	0.028	0.539± 0.011	0.062	0.015
4	1.082± 0.004	0.094± 0.012	0.110	0.039	0.558± 0.002	0.057	0.020
5	1.191± 0.007	0.092± 0.010	0.089	0.060	0.615± 0.004	0.046	0.031
6	1.231± 0.015	0.105± 0.011	0.074	0.074	0.635± 0.008	0.038	0.038
7	1.288± 0.018	0.111± 0.010	0.057	0.092	0.665± 0.010	0.029	0.048
8	1.366± 0.008	0.112± 0.008	0.032	0.117	0.705± 0.004	0.016	0.060
9	1.434± 0.009	0.109± 0.008	0.021	0.128	0.740± 0.005	0.011	0.066
10	1.530± 0.009	0.105± 0.007	0.011	0.138	0.790± 0.004	0.005	0.071
11	1.602± 0.006	0.105± 0.008	0.004	0.145	0.827± 0.003	0.002	0.075
12	1.659± 0.005	0.079± 0.003	0.000	0.149	0.856± 0.002	0.000	0.077

Test Data for Two Phase Air Flow in Single Grid Rod Bundle

Q_l = 2800 cc/min T_l = 282 °K T_g = 280 °K

	Air Flowrate (1000 cc/sec)	Channel Velocity (m/sec)	Pressure Drop (mm-H2O)	Liquid Flowrate Downward (cc/min)	Liquid Flowrate Upward (cc/min)
1	2.545± 0.135	2.260	54.2 ± 6.3	2827.4	0.0
2	3.614± 0.173	3.209	84.7± 11.5	2811.7	15.7
3	3.826± 0.113	3.397	88.7± 11.8	2772.5	55.0
4	4.340± 0.070	3.854	101.2± 13.3	2200.0	628.3
5	4.640± 0.087	4.120	101.8± 12.4	2042.0	785.4
6	5.086± 0.077	4.516	97.2± 11.3	1492.3	1335.2
7	5.574± 0.028	4.950	95.3± 10.8	1256.6	1570.8
8	6.230± 0.023	5.532	106.8± 11.1	942.5	1885.0
9	6.604± 0.077	5.865	113.9 ± 8.6	628.3	2199.1
10	6.892± 0.045	6.120	115.4 ± 7.6	455.5	2371.9
11	7.335± 0.022	6.514	108.7 ± 8.1	274.9	2552.5
12	7.846± 0.045	6.967	92.6 ± 9.2	117.8	2709.6
13	8.316± 0.025	7.385	94.6 ± 9.7	39.3	2788.1
14	8.725± 0.085	7.748	91.9 ± 6.7	0.0	2827.4
15	9.311± 0.048	8.268	77.6 ± 2.8	0.0	2827.4

Nondimensional Form of Test Data

K_l^* = 0.255 j_l^* = 0.132 Re_T = 532.0 V_c^* = 0.662

	K_g^*	P^*	K_f^*	K_c^*	j_g^*	j_f^*	j_c^*
1	0.492± 0.026	0.054± 0.006	0.255	0.000	0.254± 0.013	0.132	0.000
2	0.698± 0.033	0.085± 0.012	0.254	0.001	0.360± 0.017	0.131	0.001
3	0.739± 0.022	0.089± 0.012	0.250	0.005	0.381± 0.011	0.129	0.003
4	0.838± 0.014	0.101± 0.013	0.199	0.057	0.433± 0.007	0.103	0.029
5	0.896± 0.017	0.102± 0.012	0.184	0.071	0.463± 0.009	0.095	0.037
6	0.982± 0.015	0.097± 0.011	0.135	0.121	0.507± 0.008	0.070	0.062
7	1.077± 0.005	0.095± 0.011	0.113	0.142	0.556± 0.003	0.059	0.073
8	1.204± 0.004	0.107± 0.011	0.085	0.170	0.621± 0.002	0.044	0.088
9	1.276± 0.015	0.114± 0.009	0.057	0.199	0.658± 0.008	0.029	0.102
10	1.331± 0.009	0.116± 0.008	0.041	0.214	0.687± 0.004	0.021	0.111
11	1.417± 0.004	0.109± 0.008	0.025	0.230	0.731± 0.002	0.013	0.119
12	1.516± 0.009	0.093± 0.009	0.011	0.245	0.782± 0.004	0.005	0.126
13	1.607± 0.005	0.095± 0.010	0.004	0.252	0.829± 0.002	0.002	0.130
14	1.686± 0.016	0.092± 0.007	0.000	0.255	0.870± 0.008	0.000	0.132
15	1.799± 0.009	0.078± 0.003	0.000	0.255	0.928± 0.005	0.000	0.132

Test Data for Two Phase Air Flow in Single Grid Rod Bundle

Q_l = 3900 cc/min T_l = 282 °K T_g = 280 °K

	Air Flowrate (1000 cc/sec)	Channel Velocity (m/sec)	Pressure Drop (mm-H2O)	Liquid Flowrate Downward (cc/min)	Liquid Flowrate Upward (cc/min)
1	3.326± 0.137	2.953	97.0± 15.6	3887.7	39.3
2	3.778± 0.153	3.355	109.3± 14.2	3479.3	447.7
3	4.199± 0.078	3.729	106.8± 13.0	3102.3	1138.8
4	4.836± 0.032	4.295	103.9± 11.7	1885.0	2042.0
5	5.490± 0.067	4.875	101.0± 10.8	1335.2	2591.8
6	6.013± 0.093	5.339	102.6± 12.4	1021.0	2906.0
7	6.403± 0.073	5.686	117.0 ± 9.6	667.6	3259.4
8	6.758± 0.063	6.001	115.4 ± 9.2	526.2	3400.8
9	7.177± 0.079	6.373	112.6 ± 8.1	353.4	3573.6
10	7.542± 0.050	6.697	106.5 ± 8.3	223.8	3703.2
11	7.913± 0.035	7.027	92.9 ± 8.1	110.0	3817.0
12	8.497± 0.061	7.545	77.5 ± 3.5	7.9	3919.1
13	9.105± 0.059	8.086	85.6 ± 5.4	0.0	3927.0

Nondimensional Form of Test Data

K_l^* = 0.351 j_l^* = 0.181 Re_T = 741.0 V_c^* = 0.556

	K_g^*	P^*	K_f^*	K_c^*	j_g^*	j_f^*	j_c^*
1	0.642± 0.027	0.097± 0.016	0.351	0.004	0.332± 0.014	0.181	0.002
2	0.730± 0.030	0.109± 0.014	0.314	0.040	0.377± 0.015	0.162	0.021
3	0.811± 0.015	0.107± 0.013	0.280	0.103	0.419± 0.008	0.145	0.053
4	0.934± 0.006	0.104± 0.012	0.170	0.184	0.482± 0.003	0.088	0.095
5	1.061± 0.013	0.101± 0.011	0.121	0.234	0.547± 0.007	0.062	0.121
6	1.162± 0.018	0.103± 0.012	0.092	0.262	0.599± 0.009	0.048	0.135
7	1.237± 0.014	0.117± 0.010	0.060	0.294	0.638± 0.007	0.031	0.152
8	1.305± 0.012	0.116± 0.009	0.048	0.307	0.674± 0.006	0.025	0.158
9	1.387± 0.015	0.113± 0.008	0.032	0.323	0.715± 0.008	0.016	0.167
10	1.457± 0.010	0.107± 0.008	0.020	0.334	0.752± 0.005	0.010	0.173
11	1.529± 0.007	0.093± 0.008	0.010	0.345	0.789± 0.003	0.005	0.178
12	1.641± 0.012	0.078± 0.003	0.001	0.354	0.847± 0.006	0.000	0.183
13	1.759± 0.011	0.086± 0.005	0.000	0.355	0.908± 0.006	0.000	0.183

Test Data for Single Phase Air Flow in Double Grid Rod Bundle

Q_l = 0 cc/min T_l = 282 °K T_g = 280 °K

	Air Flowrate (1000 cc/sec)	Channel Velocity (m/sec)	Pressure Drop (mm-H2O)	Liquid Flowrate Downward (cc/min)	Upward (cc/min)
1	2.706± 0.024	2.403	13.8 ± 0.4	0.0	0.0
2	3.993± 0.027	3.546	22.5 ± 1.7	0.0	0.0
3	5.119± 0.065	4.546	29.7 ± 1.7	0.0	0.0
4	6.248± 0.014	5.548	35.8 ± 2.2	0.0	0.0
5	7.205± 0.078	6.398	46.1 ± 5.5	0.0	0.0
6	7.645± 0.044	6.788	55.7 ± 2.7	0.0	0.0
7	8.323± 0.017	7.391	61.7 ± 5.4	0.0	0.0
8	8.579± 0.023	7.619	72.4 ± 4.6	0.0	0.0
9	9.093± 0.063	8.075	78.0 ± 1.4	0.0	0.0
10	9.496± 0.068	8.433	87.3 ± 2.5	0.0	0.0
11	9.722± 0.052	8.633	90.2 ± 4.9	0.0	0.0
12	10.125± 0.066	8.991	104.9 ± 4.6	0.0	0.0

Nondimensional Form of Test Data

$K_l^* = 0.0$ $j_l^* = 0.0$ $Re_T = 0.0$ $V_c^* = 0.0$

	K_g^*	P^*	K_f^*	K_c^*	j_g^*	j_f^*	j_c^*
1	0.523± 0.005	0.014± 0.000	0.000	0.000	0.270± 0.002	0.000	0.000
2	0.771± 0.005	0.023± 0.002	0.000	0.000	0.398± 0.003	0.000	0.000
3	0.989± 0.012	0.030± 0.002	0.000	0.000	0.510± 0.006	0.000	0.000
4	1.207± 0.003	0.036± 0.002	0.000	0.000	0.623± 0.001	0.000	0.000
5	1.392± 0.015	0.046± 0.005	0.000	0.000	0.718± 0.008	0.000	0.000
6	1.477± 0.008	0.056± 0.003	0.000	0.000	0.762± 0.004	0.000	0.000
7	1.608± 0.003	0.062± 0.005	0.000	0.000	0.830± 0.002	0.000	0.000
8	1.657± 0.005	0.072± 0.005	0.000	0.000	0.855± 0.002	0.000	0.000
9	1.757± 0.012	0.078± 0.001	0.000	0.000	0.906± 0.006	0.000	0.000
10	1.834± 0.013	0.087± 0.002	0.000	0.000	0.947± 0.007	0.000	0.000
11	1.878± 0.010	0.090± 0.005	0.000	0.000	0.969± 0.005	0.000	0.000
12	1.956± 0.013	0.105± 0.005	0.000	0.000	1.009± 0.007	0.000	0.000

Test Data for Two Phase Air Flow in Double Grid Rod Bundle

Q_l = 170 cc/min T_l = 282 °K T_g = 280 °K

	Air Flowrate (1000 cc/sec)	Channel Velocity (m/sec)	Pressure Drop (mm-H2O)	Liquid Flowrate Downward (cc/min)	Liquid Flowrate Upward (cc/min)
1	2.847± 0.011	2.529	0.2 ± 2.1	172.8	0.0
2	4.666± 0.052	4.144	20.2 ± 3.0	172.8	0.0
3	5.574± 0.028	4.949	32.3 ± 0.7	172.8	0.0
4	6.421± 0.070	5.702	40.0 ± 3.2	128.8	44.0
5	6.756± 0.053	6.000	55.5 ± 1.0	94.2	78.6
6	7.074± 0.037	6.282	58.7 ± 2.1	62.8	110.0
7	7.366± 0.023	6.541	81.5 ± 6.6	23.6	149.2
8	7.624± 0.020	6.771	87.4 ± 1.1	3.1	169.7
9	8.110± 0.043	7.202	87.1 ± 1.6	0.0	172.8
10	8.491± 0.064	7.540	66.2 ± 3.2	0.0	172.8

Nondimensional Form of Test Data

$K_l^* = 0.016$ $j_l^* = 0.008$ $Re_T = 32.3$ $V_c^* = 1.059$

	K_g^*	P^*	K_f^*	K_c^*	j_g^*	j_f^*	j_c^*
1	0.550± 0.002	0.000± 0.002	0.016	0.000	0.284± 0.001	0.008	0.000
2	0.901± 0.010	0.020± 0.003	0.016	0.000	0.465± 0.005	0.008	0.000
3	1.077± 0.005	0.032± 0.001	0.016	0.000	0.556± 0.003	0.008	0.000
4	1.240± 0.014	0.040± 0.003	0.012	0.004	0.640± 0.007	0.006	0.002
5	1.305± 0.010	0.056± 0.001	0.009	0.007	0.673± 0.005	0.004	0.004
6	1.367± 0.007	0.059± 0.002	0.006	0.010	0.705± 0.004	0.003	0.005
7	1.423± 0.005	0.082± 0.007	0.002	0.013	0.734± 0.002	0.001	0.007
8	1.473± 0.004	0.088± 0.001	0.000	0.015	0.760± 0.002	0.000	0.008
9	1.567± 0.008	0.087± 0.002	0.000	0.016	0.808± 0.004	0.000	0.008
10	1.640± 0.012	0.066± 0.003	0.000	0.016	0.846± 0.006	0.000	0.008

Test Data for Two Phase Air Flow in Double Grid Rod Bundle

Q_l = 510 cc/min T_l = 282 °K T_g = 280 °K.

	Air Flowrate (1000 cc/sec)	Channel Velocity (m/sec)	Pressure Drop (mm-H2O)	Liquid Flowrate Downward (cc/min)	Upward (cc/min)
1	1.922± 0.065	1.707	34.2 ± 0.8	510.5	0.0
2	3.906± 0.030	3.468	38.6 ± 1.3	510.5	0.0
3	5.134± 0.063	4.559	55.8 ± 0.6	502.7	7.9
4	5.848± 0.056	5.193	36.8 ± 1.4	361.3	149.2
5	6.191± 0.018	5.498	43.6 ± 6.0	255.3	255.3
6	6.515± 0.032	5.786	47.7 ± 7.0	176.7	333.8
7	6.792± 0.018	6.031	53.9 ± 4.7	137.4	373.1
8	7.102± 0.044	6.307	87.0 ± 1.8	58.9	451.6
9	7.314± 0.029	6.495	82.5 ± 1.3	39.3	471.2
10	7.594± 0.039	6.744	89.8 ± 5.3	0.0	510.5
11	8.042± 0.048	7.141	87.6 ± 0.8	0.0	510.5
12	8.554± 0.035	7.596	63.3 ± 3.7	0.0	510.5

Nondimensional Form of Test Data

K_l^* = 0.046 j_l^* = 0.024 Re_T = 96.9 V_c^* = 0.882

	K_g^*	P^*	K_f^*	K_c^*	j_g^*	j_f^*	j_c^*
1	0.371± 0.013	0.034± 0.001	0.046	0.000	0.192± 0.006	0.024	0.000
2	0.754± 0.006	0.039± 0.001	0.046	0.000	0.389± 0.003	0.024	0.000
3	0.992± 0.012	0.056± 0.001	0.045	0.001	0.512± 0.006	0.023	0.000
4	1.130± 0.011	0.037± 0.001	0.033	0.013	0.583± 0.006	0.017	0.007
5	1.196± 0.003	0.044± 0.006	0.023	0.023	0.617± 0.002	0.012	0.012
6	1.259± 0.006	0.048± 0.007	0.016	0.030	0.649± 0.003	0.008	0.016
7	1.312± 0.004	0.054± 0.005	0.012	0.034	0.677± 0.002	0.006	0.017
8	1.372± 0.009	0.087± 0.002	0.005	0.041	0.708± 0.004	0.003	0.021
9	1.413± 0.006	0.083± 0.001	0.004	0.043	0.729± 0.003	0.002	0.022
10	1.467± 0.007	0.090± 0.005	0.000	0.046	0.757± 0.004	0.000	0.024
11	1.554± 0.009	0.088± 0.001	0.000	0.046	0.802± 0.005	0.000	0.024
12	1.653± 0.007	0.063± 0.004	0.000	0.046	0.853± 0.003	0.000	0.024

Test Data for Two Phase Air Flow in Double Grid Rod Bundle

Q_l = 750 cc/min T_l = 282 °K T_g = 280 °K

	Air Flowrate (1000 cc/sec)	Channel Velocity (m/sec)	Pressure Drop (mm-H2O)	Liquid Flowrate Downward (cc/min)	Liquid Flowrate Upward (cc/min)
1	2.329± 0.232	2.068	36.5 ± 1.4	746.1	0.0
2	4.261± 0.074	3.784	22.9 ± 1.5	746.1	0.0
3	4.956± 0.062	4.401	33.2 ± 0.7	687.2	58.9
4	5.614± 0.027	4.985	38.9 ± 2.2	451.6	294.5
5	6.116± 0.044	5.431	44.7 ± 7.3	314.2	432.0
6	6.312± 0.063	5.605	53.8 ± 5.1	216.0	530.1
7	6.633± 0.086	5.890	57.8 ± 3.1	157.1	589.0
8	7.071± 0.038	6.279	65.9 ± 5.3	58.9	687.2
9	7.407± 0.030	6.578	58.6 ± 1.7	19.6	726.5
10	7.862± 0.020	6.981	57.8 ± 1.3	0.0	746.1
11	8.386± 0.042	7.447	68.0± 10.4	0.0	746.1
12	5.228± 0.019	4.643	59.0 ± 2.6	628.3	117.8
13	5.589± 0.022	4.963	58.8 ± 3.1	510.5	235.6

Nondimensional Form of Test Data

$K_l^* = 0.067$ $j_l^* = 0.035$ $Re_T = 142.5$ $V_c^* = 0.838$

	K_g^*	P^*	K_f^*	K_c^*	j_g^*	j_f^*	j_c^*
1	0.450± 0.045	0.037± 0.001	0.067	0.000	0.232± 0.023	0.035	0.000
2	0.823± 0.014	0.023± 0.001	0.067	0.000	0.425± 0.007	0.035	0.000
3	0.957± 0.012	0.033± 0.001	0.062	0.005	0.494± 0.006	0.032	0.003
4	1.084± 0.005	0.039± 0.002	0.041	0.027	0.560± 0.003	0.021	0.014
5	1.181± 0.009	0.045± 0.007	0.028	0.039	0.610± 0.004	0.015	0.020
6	1.219± 0.012	0.054± 0.005	0.020	0.048	0.629± 0.006	0.010	0.025
7	1.281± 0.017	0.058± 0.003	0.014	0.053	0.661± 0.009	0.007	0.027
8	1.366± 0.007	0.066± 0.005	0.005	0.062	0.705± 0.004	0.003	0.032
9	1.431± 0.006	0.059± 0.002	0.002	0.066	0.738± 0.003	0.001	0.034
10	1.519± 0.004	0.058± 0.001	0.000	0.067	0.784± 0.002	0.000	0.035
11	1.620± 0.008	0.068± 0.010	0.000	0.067	0.836± 0.004	0.000	0.035
12	1.010± 0.004	0.059± 0.003	0.057	0.011	0.521± 0.002	0.029	0.005
13	1.080± 0.004	0.059± 0.003	0.046	0.021	0.557± 0.002	0.024	0.011

Test Data for Two Phase Air Flow in Double Grid Rod Bundle

Q_l = 1500 cc/min T_l = 282 °K T_g = 280 °K

	Air Flowrate (1000 cc/sec)	Channel Velocity (m/sec)	Pressure Drop (mm-H2O)	Liquid Flowrate Downward (cc/min)	Liquid Flowrate Upward (cc/min)
1	3.246± 0.100	2.882	45.6 ± 6.7	1492.3	0.0
2	3.989± 0.023	3.542	55.8 ± 1.0	1413.7	78.5
3	4.391± 0.031	3.899	57.1 ± 1.3	1295.9	196.3
4	4.916± 0.045	4.365	64.7 ± 4.4	942.5	549.8
5	5.198± 0.032	4.616	66.5 ± 4.0	863.9	628.3
6	5.573± 0.027	4.949	71.1 ± 5.2	628.3	863.9
7	6.201± 0.020	5.506	84.5 ± 5.3	353.4	1138.8
8	6.583± 0.061	5.846	96.1 ± 7.1	219.9	1272.3
9	7.010± 0.053	6.225	79.9 ± 1.7	78.5	1413.7
10	7.313± 0.030	6.494	64.5 ± 3.3	47.1	1445.1
11	7.723± 0.081	6.858	63.0 ± 8.8	0.0	1492.3
12	8.319± 0.028	7.387	80.7 ± 3.9	0.0	1492.3

Nondimensional Form of Test Data

$K_l^* = 0.135$ $j_l^* = 0.070$ $Re_T = 285.0$ $V_c^* = 0.662$

	K_g^*	P^*	K_f^*	K_c^*	j_g^*	j_f^*	j_c^*
1	0.627± 0.019	0.046± 0.007	0.135	0.000	0.324± 0.010	0.070	0.000
2	0.771± 0.004	0.056± 0.001	0.128	0.007	0.398± 0.002	0.066	0.004
3	0.848± 0.006	0.057± 0.001	0.117	0.018	0.438± 0.003	0.060	0.009
4	0.950± 0.009	0.065± 0.004	0.085	0.050	0.490± 0.004	0.044	0.026
5	1.004± 0.006	0.067± 0.004	0.078	0.057	0.518± 0.003	0.040	0.029
6	1.077± 0.005	0.071± 0.005	0.057	0.078	0.555± 0.003	0.029	0.040
7	1.198± 0.004	0.085± 0.005	0.032	0.103	0.618± 0.002	0.016	0.053
8	1.272± 0.012	0.096± 0.007	0.020	0.115	0.656± 0.006	0.010	0.059
9	1.354± 0.010	0.080± 0.002	0.007	0.128	0.699± 0.005	0.004	0.066
10	1.413± 0.006	0.065± 0.003	0.004	0.130	0.729± 0.003	0.002	0.067
11	1.492± 0.016	0.063± 0.009	0.000	0.135	0.770± 0.008	0.000	0.070
12	1.607± 0.005	0.081± 0.004	0.000	0.135	0.829± 0.003	0.000	0.070

Test Data for Two Phase Air Flow in Double Grid Rod Bundle
Q_l = 2500 cc/min T_l = 282 °K T_g = 280 °K

	Air Flowrate (1000 cc/sec)	Channel Velocity (m/sec)	Pressure Drop (mm-H2O)	Liquid Flowrate Downward (cc/min)	Liquid Flowrate Upward (cc/min)
1	0.723± 0.152	0.642	33.2 ± 0.6	2513.3	0.0
2	1.722± 0.188	1.530	51.4 ± 6.1	2513.3	0.0
3	2.763± 0.049	2.454	44.2 ± 6.4	2497.6	15.7
4	3.919± 0.033	3.480	56.4 ± 1.4	2081.3	432.0
5	4.330± 0.070	3.845	58.0 ± 2.3	1649.3	863.9
6	4.731± 0.051	4.201	60.6 ± 3.6	1453.0	1060.3
7	5.258± 0.050	4.669	73.4 ± 5.1	1060.3	1453.0
8	5.546± 0.022	4.925	77.2 ± 3.6	903.2	1610.1
9	5.689± 0.053	5.052	78.7 ± 3.6	785.4	1727.9
10	6.170± 0.034	5.479	90.6 ± 8.7	573.3	1939.9
11	6.283± 0.051	5.580	103.8 ± 7.9	392.7	2120.6
12	6.646± 0.092	5.901	103.6 ± 7.6	235.6	2277.7
13	6.855± 0.023	6.087	96.3 ± 8.0	196.3	2316.9
14	7.386± 0.020	6.558	87.1 ± 4.3	62.8	2450.4
15	8.133± 0.056	7.222	67.1 ± 3.0	0.0	2513.3

Nondimensional Form of Test Data

$K_l^* = 0.227$ $j_l^* = 0.117$ $Re_T = 475.0$ $V_c^* = 0.574$

	K_g^*	P^*	K_f^*	K_c^*	j_g^*	j_f^*	j_c^*
1	0.140± 0.029	0.033± 0.001	0.227	0.000	0.072± 0.015	0.117	0.000
2	0.333± 0.036	0.051± 0.006	0.227	0.000	0.172± 0.019	0.117	0.000
3	0.534± 0.009	0.044± 0.006	0.226	0.001	0.275± 0.005	0.116	0.001
4	0.757± 0.006	0.057± 0.001	0.188	0.039	0.391± 0.003	0.097	0.020
5	0.836± 0.013	0.058± 0.002	0.149	0.078	0.432± 0.007	0.077	0.040
6	0.914± 0.010	0.061± 0.004	0.131	0.096	0.472± 0.005	0.068	0.049
7	1.016± 0.010	0.073± 0.005	0.096	0.131	0.524± 0.005	0.049	0.068
8	1.071± 0.004	0.077± 0.004	0.082	0.145	0.553± 0.002	0.042	0.075
9	1.099± 0.010	0.079± 0.004	0.071	0.156	0.567± 0.005	0.037	0.081
10	1.192± 0.007	0.091± 0.009	0.052	0.175	0.615± 0.003	0.027	0.090
11	1.214± 0.010	0.104± 0.008	0.035	0.191	0.626± 0.005	0.018	0.099
12	1.284± 0.018	0.104± 0.008	0.021	0.206	0.662± 0.009	0.011	0.106
13	1.324± 0.004	0.096± 0.008	0.018	0.209	0.683± 0.002	0.009	0.108
14	1.427± 0.004	0.087± 0.004	0.006	0.221	0.736± 0.002	0.003	0.114
15	1.571± 0.011	0.067± 0.003	0.000	0.227	0.811± 0.006	0.000	0.117

Test Data for Two Phase Air Flow in Double Grid Rod Bundle
Q_l = 3700 cc/min T_l = 282 °K T_g = 280 °K

	Air Flowrate (1000 cc/sec)	Channel Velocity (m/sec)	Pressure Drop (mm-H2O)	Liquid Flowrate Downward (cc/min)	Upward (cc/min)
1	1.079± 0.317	0.959	59.4 ± 4.5	3691.4	0.0
2	1.661± 0.311	1.475	68.8± 10.7	3675.7	15.7
3	2.708± 0.039	2.405	55.5 ± 2.9	3495.0	196.3
4	3.199± 0.108	2.841	56.4 ± 2.1	2748.9	942.5
5	3.405± 0.038	3.023	56.6 ± 2.5	2434.7	1256.6
6	3.888± 0.021	3.452	58.7 ± 3.4	1885.0	1806.4
7	4.299± 0.076	3.818	60.5 ± 4.0	1570.8	2120.6
8	4.837± 0.028	4.295	68.7 ± 5.4	1335.2	2356.2
9	5.493± 0.074	4.878	76.7 ± 5.5	863.9	2827.4
10	5.809± 0.057	5.158	84.5 ± 4.3	706.9	2984.5
11	6.264± 0.030	5.563	108.6 ± 8.6	432.0	3259.4
12	6.798± 0.020	6.037	101.6± 10.1	235.6	3455.8
13	7.072± 0.037	6.280	98.1 ± 8.4	133.5	3557.9
14	7.438± 0.043	6.605	82.2 ± 4.8	55.0	3636.4
15	8.266± 0.045	7.340	98.8 ± 4.8	0.0	3691.4

Nondimensional Form of Test Data

$K_l^* = 0.333$ $j_l^* = 0.172$ $Re_T = 703.0$ $V_c^* = 0.424$

	K_g^*	P^*	K_f^*	K_c^*	j_g^*	j_f^*	j_c^*
1	0.209± 0.061	0.059± 0.004	0.333	0.000	0.108± 0.032	0.172	0.000
2	0.321± 0.060	0.069± 0.011	0.332	0.001	0.166± 0.031	0.171	0.001
3	0.523± 0.008	0.056± 0.003	0.316	0.018	0.270± 0.004	0.163	0.009
4	0.618± 0.021	0.056± 0.002	0.248	0.085	0.319± 0.011	0.128	0.044
5	0.658± 0.007	0.057± 0.003	0.220	0.113	0.339± 0.004	0.113	0.059
6	0.751± 0.004	0.059± 0.003	0.170	0.163	0.388± 0.002	0.088	0.084
7	0.831± 0.015	0.061± 0.004	0.142	0.191	0.429± 0.008	0.073	0.099
8	0.934± 0.005	0.069± 0.005	0.121	0.213	0.482± 0.003	0.062	0.110
9	1.061± 0.014	0.077± 0.005	0.078	0.255	0.548± 0.007	0.040	0.132
10	1.122± 0.011	0.085± 0.004	0.064	0.270	0.579± 0.006	0.033	0.139
11	1.210± 0.006	0.109± 0.009	0.039	0.294	0.624± 0.003	0.020	0.152
12	1.313± 0.004	0.102± 0.010	0.021	0.312	0.678± 0.002	0.011	0.161
13	1.366± 0.007	0.098± 0.008	0.012	0.321	0.705± 0.004	0.006	0.166
14	1.437± 0.008	0.082± 0.005	0.005	0.328	0.741± 0.004	0.003	0.169
15	1.597± 0.009	0.099± 0.005	0.000	0.333	0.824± 0.005	0.000	0.172

APPENDIX B. INPUT DECKS FOR CALCULATIONS

```
$$$
```

```
$$$
```

```
$$$
```

```
$$$
```

```
$$$
```

```
$$$
```

```
$$$
```

```
$$$
```

```
$$$
```

```
$$$
```

```
$$$
```

NRC FORM 335 (2-89) NRCM 1102, 3201, 3202

U.S. NUCLEAR REGULATORY COMMISSION

BIBLIOGRAPHIC DATA SHEET

(See instructions on the reverse)

1. REPORT NUMBER (Assigned by NRC, Add Vol., Supp., Rev., and Addendum Numbers, if any.)

NUREG/IA-0100

2. TITLE AND SUBTITLE

Assessment of CCFL Model of RELAP5/MOD3 Against Simple Vertical Tubes and Rod Bundle Tests

3. DATE REPORT PUBLISHED

MONTH	YEAR
June	1993

4. FIN OR GRANT NUMBER

L2245

5. AUTHOR(S)

S. Cho, N. Arne, Korea Electric Power Corp., Research Center
B.D. Chung, H.J. Kim, Korea Instittue of Nuclear Safety

6. TYPE OF REPORT

Technical

7. PERIOD COVERED *(Inclusive Dates)*

8. PERFORMING ORGANIZATION – NAME AND ADDRESS *(If NRC, provide Division, Office or Region, U.S. Nuclear Regulatory Commission, and mailing address; if contractor, provide name and mailing address.)*

Korea Electric Power Corporation, Research Center
Korea Institute of Nuclear Safety
117-15 Yongjeon-Dong, Dong-Gu, Taejon, Korea
P.O. Box 16, Daeduk-Danji, Taejon, Korea, 305-353

9. SPONSORING ORGANIZATION – NAME AND ADDRESS *(If NRC, type "Same as above"; if contractor, provide NRC Division, Office or Region, U.S. Nuclear Regulatory Commission, and mailing address.)*

Office of Nuclear Regulatory Research
U.S. Nuclear Regulatory Commission
Washington, D.C. 20555

10. SUPPLEMENTARY NOTES

11. ABSTRACT *(200 words or less)*

The CCFL model used in RELAP5/MOD3 version 5m5 has been assessed against simple vertical tubes and rod bundle tests performed at a facility of Korea Atomic Energy Research Institute.

The effect of changes in tube diameter and nodalization of tube section were investigated. The roles of interfacial drags on the flooding characteristics are discussed. Differences between the calculation and the experiment are also discussed.

A comparison between model assessment results and the test data showed that the calculated value lay well on the experimental flooding curve specified by user, but the pressure jump before onset of flooding was not calculated.

12. KEY WORDS/DESCRIPTORS *(List words or phrases that will assist researchers in locating the report.)*

ICAP Program
RELAP5/MOD3
CCFL Model

13. AVAILABILITY STATEMENT

Unlimited

14. SECURITY CLASSIFICATION

(This Page)
Unclassified

(This Report)
Unclassified

15. NUMBER OF PAGES

16. PRICE

NRC FORM 335 (2-89)

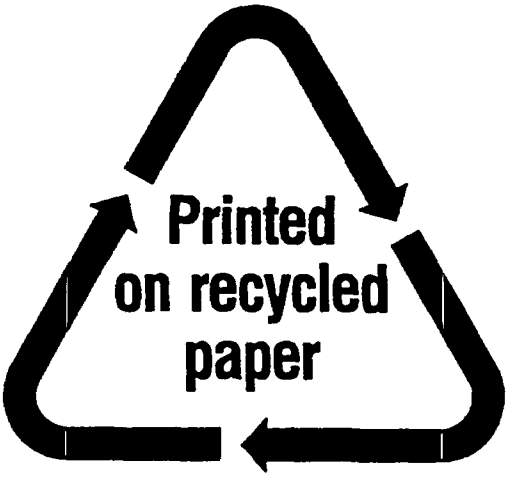

Federal Recycling Program

UNITED STATES
NUCLEAR REGULATORY COMMISSION
WASHINGTON, D.C. 20555-0001

OFFICIAL BUSINESS
PENALTY FOR PRIVATE USE, $300

SPECIAL FOURTH-CLASS RATE
POSTAGE AND FEES PAID
USNRC
PERMIT NO. G-67